ABSTRACT

Title of Dissertation:	RADIATION-INDUCED MODIFICATION OF ARAMID FIBERS: OPTIMIZING CROSSLINKING REACTIONS AND INDIRECT GRAFTING OF NANOCELLULOSE FOR BODY ARMOR APPLICATIONS
	Lorelis González López, Doctor of Philosophy, 2022
Dissertation directed by:	Professor Mohamad Al-Sheikhly, Department of Materials Science and Engineering

The goal of this dissertation was to design, synthesize, and analyze novel aramid fibers by covalently grafting nanocellulose through electron beam irradiation. These nanocellulose functionalized fibers showed enhanced strength and larger surface areas, which improves their performance and applicability in fiber-reinforced composites. Unmodified aramid fibers have smooth and chemically inert surfaces, which results in poor adhesion to many types of resins. Nanocellulose was chosen as the ideal filler to functionalize the fibers due to its reactive surface and high strength-to-weight ratio. Aramid fibers were further modified by radiation-induced crosslinking reactions as a means to avoid scission of the polymeric backbone and to further increase the fiber strength.

An indirect radiation-induced grafting approach was used for synthesizing these novel nanocellulose-grafted aramid fibers while avoiding the irradiation of nanocellulose. The fibers were irradiated using the e-beam linear accelerator (LINAC) at the Medical Industrial Radiation Facility (MIRF) at the National Institute of Standards and Technology (NIST). After the irradiation, the fibers were kept in an inert atmosphere and then mixed with a nanocellulose solution for grafting. The grafted fibers were evaluated by gravimetric analysis, Fourier-transform infrared spectroscopy (FTIR), scanning electron microscopy (SEM), and nuclear magnetic resonance (NMR) spectroscopy. The mechanical properties of the synthesized fibers were studied by single fiber tensile tests.

Aramid fibers were also irradiated at the MIRF in the presence of acetylene gas and triacrylate solution as a means to induce crosslinking reactions. These fibers were irradiated at both low doses and high dose rates at room temperature. A mechanism for the crosslinking of aramid fibers was proposed in this dissertation. Mechanical testing of the fibers after crosslinking showed an increase in the strength of the fibers of up to 15%.

Ultra-high molecular weight polyethylene (UHMWPE) fibers were also studied, but due to an issue of entanglement of the fibers during the grafting process, their mechanical properties could not be analyzed. Future work will focus on using a better set up to avoid entanglement of these fibers.

To complete the study of the radiation effects on polymers, this thesis explored the radiation-induced degradation of aromatic polyester-based resins. The composition of the resins studied included phenyl groups and epoxies, which complicate radiation-induced grafting and crosslinking reactions. Unlike aramid and polyethylene fibers, polyester-based resins have a C-O-C bond that is susceptible to degradation. The resins were irradiated at high doses in the presence

of oxygen. The scission of the polymeric backbone of the polymers was studied using Electron Paramagnetic Resonance (EPR) analysis. EPR showed the formation of alkoxyl radicals and C-centered radicals as the primary intermediate products of the C-O-C scissions. The degradation mechanisms of the resins in the presence of different solvents were proposed. Changes in the T_g of the polymers after irradiation, as an indication of degradation, were studied by Dynamic Mechanical Analysis (DMA). The results obtained from this work show that irradiation of these resins results in continuous free radical-chain reactions that lead to the formation of recyclable oligomers.

RADIATION-INDUCED MODIFICATION OF ARAMID FIBERS: OPTIMIZING CROSSLINKING REACTIONS AND INDIRECT GRAFTING OF NANOCELLULOSE FOR BODY ARMOR APPLICATIONS

by

Lorelis Enid González López

Dissertation submitted to the Faculty of the Graduate School of the
University of Maryland, College Park, in partial fulfillment
of the requirements for the degree of
Doctor of Philosophy
2022

Advisory Committee:
Professor Mohamad Al-Sheikhly, Chair
Professor Lawrence Sita
Professor Lourdes Salamanca-Riba
Professor Luz Martínez Miranda
Professor Robert Briber

Dedication

I would like to dedicate my dissertation to my mom, who I admire the most.

Acknowledgements

I would like to start by thanking my advisor, Dr. Mohamad Al-Sheikhly, for his guidance, feedback, and constant encouragement. All his advice, immense knowledge, and leadership allowed me to complete this work and become the researcher I am. He was always there for any concerns and treated me as part of his family, which I will be forever grateful for.

I would like to thank Dr. Amanda Forster, who was part of this work from the beginning. She guided and encouraged me, and helped me complete all sorts of experiments at NIST. I would like to acknowledge the members of my committee for their time spent reviewing this thesis, Dr. Lawrence Sita, Dr. Luz Martínez-Miranda, Dr. Lourdes Salamanca-Riba, and Dr. Robert Briber. I want to thank Dr. Fred Bateman for the use of the e-beam and his help with all the problems that arose during the irradiations.

I would also like to thank Dr. Zois Tsinas who always gave me his advice and provided immense technical assistance throughout my years in the lab. Thank you to Aiysha Ashfaq for your support, all the conversations, and friendship. Thank you to everyone who has been a part of the Al-Sheikhly lab, Dr. Azadeh Farzaneh, Dr. Najlaa Hassan, Dr. Salimeh Gharazi, and Steven Guerin. Thank you to the staff of the Materials Science and Engineering Department, especially N. Adaire Parker, for their expert guidance and assistance.

I would also like to thank my friends Pedro, and Karen, who kept me sane and in the loop of everything going on outside my research. I greatly thank my family, here in MD and back home in PR; special thanks to Ale whose hugs always made my weekends better. I would like to thank my amazing husband Angel, who never doubted I could do this and who was always willing to

listen to all my worries and doubts. I could not have done this without him. Thank you to my mom and dad, for all the love and support, and for always being there.

Table of Contents

List of Tables

List of Figures

1. Introduction to the field

1.1 High-Performance Polymer Fibers

High-performance fibers are engineered to have extraordinary mechanical and chemical properties. They are derived from materials with unique molecular structures that give them many attractive characteristics. These fibers are designed with a specific performance goal, usually with high strength, stiffness, and heat and chemical resistance.[1,2] Other outstanding properties of high performance fibers include high elastic modulus, strain to failure, and toughness.[3]

The beginning of the high-performance polymer fiber industry is often accredited to DuPont, where the first aromatic polyamide, or aramid fiber, was invented.[1] The commercialization of Kevlar, a para-aramid fiber, in the late 1960's led to the interest in producing several types of fibers, including ultrahigh molecular weight polyethylene (UHMWPE) fiber. In part due to their application in fiber-reinforced polymer composites, the growth of these fibers has been consistently increasing since their introduction. Significant advancement in their production has been driven by their use for both military and commercial applications. In terms of their military applications, it includes soft and flexible fiber panels for body armor, and as reinforcement in rigid polymer composites for lightweight vehicle armor.[3] The aerospace industry has also played an important part in the development of these fibers. There, the fibers are used in reinforced composite structural materials, including pressure vessels and satellites.[4]

Optimization of the structural and ballistic properties of high-performance fibers is of great interest.[1] Although the theoretical strength and modulus of these fibers is high, synthesized fibers usually do not exhibit values as high as predicted. For example, polyamide fibers have shown a maximum moduli only 1/20 of their theoretical value.[2] Figure 1 shows the tensile modulus of

various high performance fibers which are still below their theoretical values.[5] Further research on increasing these values is an attractive area of research that has gotten a lot of attention in recent times.

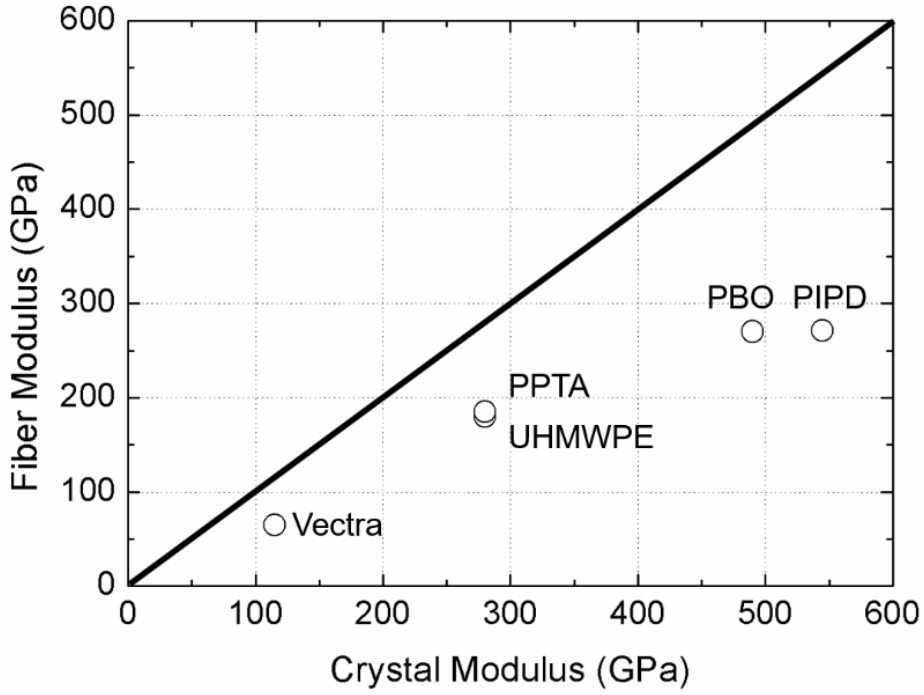

Figure 1. Measured fiber modulus versus the theoretical crystal modulus for several high-performance polymer fibers. Figure taken from Park.[5]

1.2 Fiber-Reinforced Polymer Composites

Fiber-reinforced polymer composites have been established as an important type of engineering material for high performance applications due to their excellent mechanical properties. Some of the attractive properties of these composites are a high strength to weight ratio, high toughness to weight ratio, and ease of fabrication.[6,7] These composites are typically made of high-strength fibers, such as aramid fibers, and a binder material, including but not limited to resins or elastomers. They have a vast number of applications including ballistic armor[8–10], wind turbine blades[11–13], and sports good[14–16]. Depending on their use, various aspects of the composite such as

the fiber orientation, ratio of fiber to matrix, and fiber-matrix adhesion can be tailored to meet these demands.[17–19]

The excellent mechanical properties of the composites are in part due to the use of high-performance fibers. However, effective attachment between the fibers and the resin is also a huge contributor to their attractive properties.[20,21] A strong interface is key to achieving the composite's theoretically expected properties which are based on the properties of its constituents. The main interactions that determine fiber-resin adhesion at the interface are mechanical interlocking and chemical bonding. Mechanical interlocking is a type of physical attachment between the fiber and the resin, while chemical bonding is due to the electrostatic attraction between their chemical groups.[17,22–26] To improve the properties of the composite, it is necessary to understand and increase these interactions.

The degree of mechanical interlocking can be increased by modifying the surface morphology of the fibers. Fiber roughness, or the existence of irregularities on the surface of the fiber, results in more contact points between the fiber and the resin, increasing the interactions at this interface. These irregularities act as a mechanical anchor, resulting in better physical contact or attachment between the fiber and the resin at the interface.[23,27] In terms of the chemical bonding, adding a nanomaterial such as nanocellulose, which has surface functional groups such as hydroxyl that are very reactive, allows for the possible formation of hydrogen bonding between the nanocellulose and the resin, creating a stronger fiber-nanocellulose-resin interface.[27–30]

1.2.1 Aramid fibers

Aramid, or aromatic polyamides fibers, are a class of high-strength synthetic fibers, first introduced by DuPont in 1965.[31] Their commercial product Kevlar remains one of the best-known aramids in the market. Aramids may be divided into two types: para- and meta-aramids, depending

on where the linkage is attached to the aromatic ring. Kevlar is a para-aramid, and its chemical structure consists of large phenyl rings, linked together by amide groups in a close and compact molecular structure. This gives them rigidity and low solubility (Figure 2). These polymer chains are held together by hydrogen bonds between adjacent chains, and π-π stacking of its aromatic rings, giving them high strength, high modulus, toughness, and thermal stability.[32] The term aramid will be used to refer to Kevlar fibers in this work.

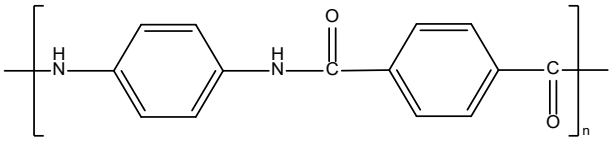

Figure 2. Poly(p-phenylene terephthalamide), chemical structure of Kevlar.

Aramid fibers are synthesized via the condensation reaction of the monomers 1,4-phenylene-diamine and terephthaloyl chloride. N-methyl pyrrolidone (NMP) and calcium chloride are used as solvents for the polymerization reaction, and calcium chloride acts as the ionic component to occupy the hydrogen bonds of the amide group. Hexamethylphosphorous triamide, a known carcinogenic, was originally used as solvent, but replaced by NMP for safety concerns. A schematic of this reaction is shown in Figure 3.

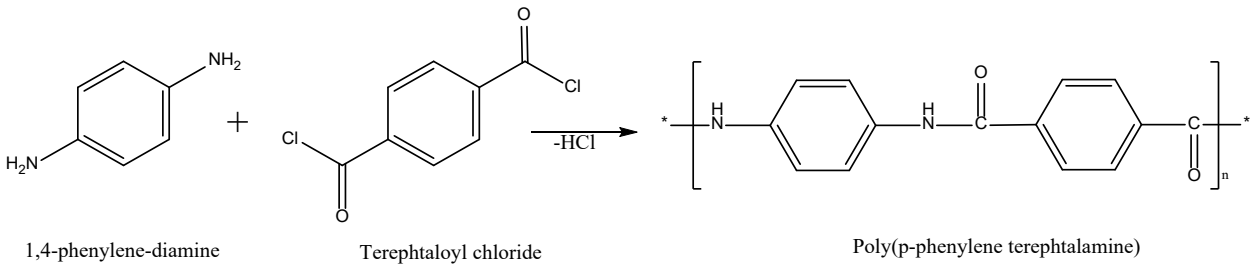

Figure 3. Schematic of the condensation reaction between 1,4-phenylene-diamine and terephthaloyl chloride to produce para-aramid.

Most synthetic fibers are made of flexible chain polymers that require their molecules to be in an extended chain configuration and largely crystalline packing, in order to achieve the best

mechanical properties. Because of this, the production of these fibers commonly involves mechanically drawing the fiber after melt spinning. However, the drawing process of flexible chain polymers requires disentanglement of the chains followed by their orientation in the solid phase. This affects the final mechanical properties of the produced fibers, making them less than theoretically predicted. In the case of aramid fibers, the polymer poly-p-benzamide forms a liquid crystalline solution which allows for the formation of a "rod-like" molecular structure, instead of the flexible-chains, when it's dissolved. As the concentration of the polymer is increased, the chains start to associate in a parallel alignment and produce highly oriented polymer chains. Figure 4 shows the difference in behavior between flexible and rigid polymers during the spinning process.

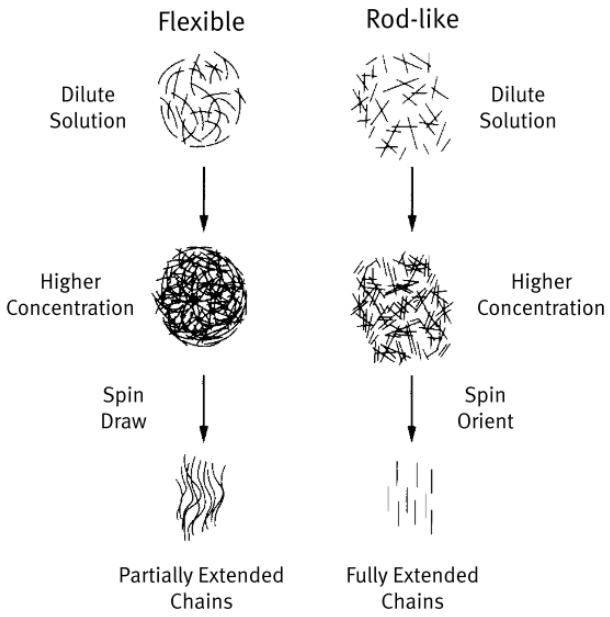

Figure 4. Representation of the difference in behavior between flexible and rigid polymers during the spin drawing process. Figure taken from Hancox.[32]

Since their introduction, one of the most important uses of the aramid fibers has been as a reinforcement in composite materials.[33] Application of these composites include bulletproof

vests[3,34], the aerospace and aircraft industry[35,36], and even as straighteners in fiber optic cables[37]. Unfortunately, the use of aramid fibers in composites is limited by their smooth and chemically inert surface, which results in poor adhesion to many types of resins. As a result, functionalization of the fibers must be done prior to their addition into the composites in order to enhance their overall performance and maximize their potential.

Attempts to modify the surface of aramid fibers by generating functional groups on their surface, and increasing its surface's roughness, include plasma treatment[38,39], acid chemical treatment[40,41], and fluorination[20,28]. The main challenge with these treatments is that they cannot be used in an industrial scale and usually result in an unwanted decrease in the intrinsic fiber strength due to backbone breaking of the polymer chains.[42] Another limitation of this type of approach is that it is based on creating functional groups in the fiber's surface that are specific to only one type of resin, making it unsuitable for application with other resins.[43] Improvements to the adhesion between the fibers and resins can be measured in terms of its interfacial shear strength (IFSS). For example, an increase of up to 42.07% in the IFSS of aramid/epoxy composites was observed by Zhao after treatment with phosphoric acid solutions.[44] However, even using low concentrations of the solutions resulted in a decrease of the mechanical properties of the fibers.

High energy irradiation of aramid fibers has also been studied as a way to enhance the interfacial properties in the composite, by improving aramid fibers' adhesion to resins.[45–48] Irradiating polymers with ionizing radiation such as γ-rays or accelerated electrons leads to the formation of very reactive intermediates, free radicals, and excited states.[47] Research has shown that irradiated fibers have a more uneven surface, which contributes to the degree of mechanical interlocking, and helps in the fibers' bonding with the resin. By controlling the irradiation parameters, such total dose and dose rate, the mechanical properties of the fibers are not

significantly reduced, making this one of the most efficient, clean, and energy-saving methods for fiber modification. Functionalization by irradiation is usually done at high doses (up to 2,200 kGy), but although improvement of up to 17.7% in the IFSS of aramid/epoxy composites has been accomplished[47], these high doses lead to damage in the tensile strength of the fibers. In terms of the chemical components, the formation of radicals on the surface of the fiber allows for the grafting of a nanometric filler onto the fiber. This nanometric filler is chosen to increase the chemical bonding at the fiber-resin interface. Lower doses, from 20 to 40 kGy, can also result in the generation of radicals[49], although no proposed mechanism, or radical formation information is found in the literature.

It is also of interest to increase the tensile strength of these fibers, and to make them more resistant to irradiation. As mentioned above, one of the main uses of these fibers is in the aerospace industry, where they are exposed to high doses of space radiation.[50] The grafting of various monomers onto aramid fibers have been reported to not only increase the mechanical properties of the subsequently made fiber-reinforced composites, but also the tensile strength of the fibers.[43,48,51] Zhang et al. successfully grafted hyperbranched polysiloxane onto aramid fibers through a chemical grafting procedure.[52] The study showed that grafted fibers were more resistant to UV irradiation, with their modulus and break extension staying at 95-97% after 168 h of irradiation. Also, the grafted fibers had higher tensile properties than the non-grafted fibers. The increased UV-resistance of the grafted fibers is attributed to the UV-resistant quality of the hyperbranched polysiloxane. An increase in the tensile properties was reported to be due to the hyperbranched polysiloxane mending the defects present on the surface of the fibers.

1.2.2 Ultra-high molecular weight polyethylene fibers

Ultra-high molecular weight polyethylene (UHMWPE) fibers are another important type of high-performance fibers. They are commercially produced by DSM under the name Dyneema, and by Honeywell under the name Spectra. Polyethylene is a polymer produced from the monomer ethylene. Depending on the polymerization conditions, the properties of the produced polyethylene can be tuned. A schematic of the chain polymerization of polyethylene from the ethylene monomer is shown in Figure 5.

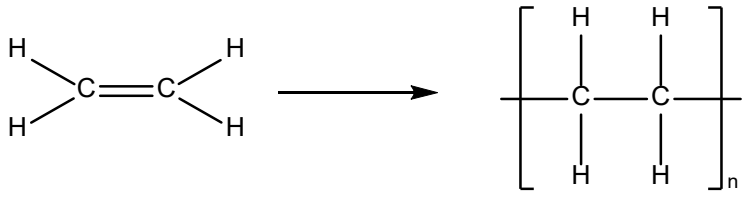

Figure 5. Schematic of the chain polymerization of ethylene, resulting in polyethylene. (n represents the degree of polymerization).

Coordination catalysts can be added to the reaction to produce linear polyethylene with a high molecular weight. The use of these catalysts leads to a living polymerization, where the polymerization continues until the ethylene is completely depleted. That is how UHMWPE, which has a molecular weight of at least 1 million g/mol, is produced.[53] Another benefit of incorporating the catalysts in the production of PE is that it produces highly crystalline polymers by preventing branching during the polymerization.[54] The crystallinity of linear PE produced by this method ranges from 70-90%.[55] This is a major factor to which the excellent physical and mechanical properties of UHMWPE fibers is attributed. UHMWPE fibers are produced through a gel spinning process in which UHMPE resin is dissolved and extruded through a spinneret into a water bath. After removing the solvent, the polymer goes through the drawing process discussed above.

UHMWPE fibers have a high strength to weight ratio, high chemical resistance, and good mechanical properties, including hardness and Young's modulus due to their high crystallinity. These properties make them ideal for use in fiber-reinforced polymer composites. Similar to aramid fibers, UHMWPE reinforced composites are used in a wide range of industries including ballistic protection, aerospace, and medical devices.[56–58] Despite their extensive use, these fibers exhibit certain drawbacks that limits their applications and overall performance. Some of these drawbacks include low surface energy, poor creep resistance, and lower thermal stability. As is the case for aramid fibers, UHMWPE fibers also show poor adhesion in composites due to their non-polar, inert nature.

UHMWPE fibers are commonly modified before their use in composites to improve the degree of adhesion between the fiber and the resin at the interface. Functionalizing the fiber by introducing polar groups is one way to achieve this. Li et al. observed that chromic acid modified UHMWPE fiber had not only an increased interfacial adhesion strength when preparing a composite, but also showed increased elongation at break and tear strength.[59] Characterization of the fibers showed a higher surface roughness and an increase in oxygen-containing groups on the surface of the fibers, which impact its behavior in the composite. The main issue with this technique is that the strength and tensile properties of the fibers are decreased with increasing treatment time. The introduction of nanomaterials as reinforcements has also become a common method for the functionalization of these fibers. The challenge is to have an even distribution of the nano-reinforcer in order to achieve good adhesion at the fiber-resin interface, and not affect the properties of the composite. When choosing a nano-reinforcement, materials with good mechanical properties, such as carbon nanotubes and nanoclays, are most attractive.[60] Mohammadalipour et al. reported that introduction of nanoclay onto the resin improved the tensile

strength, modulus, and overall adhesion of the composite.[61] Most of work reported on the introduction of nano-reinforcements onto FRPCs center on their addition to the resin, with less emphasis on the fibers.[60,62–64]

Radiation-induced grafting is an alternative to incorporate these nano-reinforcements onto the fiber surface. The high crystallinity of UHMWPE fibers makes it more difficult to graft nanoparticles when compared to bulk material, which has been previously explored.[65,66] Yakusheva et al. grafted acrylic monomers onto UHMWPE fibers after irradiating the fibers in a pulsed ion-beam installation at doses of up to 10^{-16} ions/cm^2.[67] A direct grafting approach was followed by Kondo et al. as they used a radiation-induced graft-polymerization technique to graft N-vinyl formamide monomer onto UHMWPE fibers.[68] Studies like this focus on the mechanical properties of the composite produced after fiber modification rather than on the effects of the modification on the fibers, which must be maintained in order to achieve the best performance. Xing et al. worked on the grafting of methyl acrylate (MA) monomer onto UHMWPE by a gamma-ray pre-irradiation induced graft polymerization technique.[69] They studied the effects of radiation dose on the mechanical properties of the fibers and observed a decrease in the tensile strength as a function of radiation dose. Although higher doses lead to a higher amount of monomer grafted, it also resulted in a lower tensile strength of the fiber. The low dose rate achieved by gamma-ray irradiation could be a significant issue causing this decrease in strength. The benefits of using electron beam irradiation over gamma-ray will be discussed in a following section.

1.2.3 Nanometric filler

The addition of nanomaterials, such as nanocellulose, to either part of a polymer composite can strengthen the interface by providing better contact between the fiber and the resin. Furthermore, this nanometric filler may enhance a property of the composite and add

multifunctionality. Attaching a nanometric filler as a reinforcement to the fibers improves the adhesion between the fibers and the resin by (1) creating irregularities on the fiber's surface, allowing for mechanical interlocking, and (2) introducing functional groups for chemical bonding. It also leads to a significant increase in the surface area for interactions, and increases the roughness of the otherwise smooth fibers.[17,22,43–46,70] This could widely improve the fibers' adhesion to many kinds of resins.

Nanomaterials commonly used to modify fiber-reinforced composites include nanocellulose[30], multi-walled carbon nanotubes (CNTs)[71,72], silica[43], and zinc oxide[73]. Research on the addition of CNTs to aramid fiber composites show an increase in the IFSS attributed to a high density of nanotubes distributed in the fiber surface, seen as surface irregularities, that provide more contact points between the resin and the fibers.[22,71] A challenge with using CNTs is their unreactive nature, which means they need to be treated in harsh conditions to functionalize, and the low purity of most available nanotubes.[74,75] This is also true for silica and zinc oxide nanoparticles, where labor-intensive methods are needed to manufacture the modified composites.[18,70,76] Nanocellulose, on the other hand, is a cleaner, more reactive, and highly available material that can be attached to the fibers by a simple immersion process.[23,77–79]

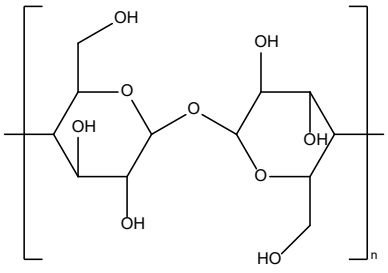

Figure 6. Chemical structure of cellulose. (n represents the degree of polymerization)

Cellulose is a homopolymer comprised of *β*-1,4-linked anhydro-*D*-glucose units (Figure 6), which can be derived from a wide variety of sources including wood, grass, algae, and fungi. Nanocellulose can be obtained from cellulose to produce two main types: (1) cellulose nanocrystals, usually produced by an acid treatment of the cellulose, and (2) cellulose nanofibers, commonly produced through mechanical disintegration. A schematic of these two processes is shown in Figure 7. This work will focus on cellulose nanofibers, and their grafting onto polymer fibers. Cellulose nanofibers, which will be referred to simply as nanocellulose in this work, are commercially available and have generated high interest for industrial applications, especially after the discovery of pretreatments methods that facilitate the mechanical disintegration process.[80] Because of their excellent mechanical properties, low cost, low toxicity, and renewable resource origin, nanocellulose is often regarded as an ideal candidate for reinforcing composites.[81–83] In addition to their high aspect ratio and strength, an attractive property of nanocellulose is their highly reactive, hydroxyl-full surface.[84–86] These functional groups would not only help the cellulose attach to the fibers, but also be a source of reactive sites for the resin to bond to.

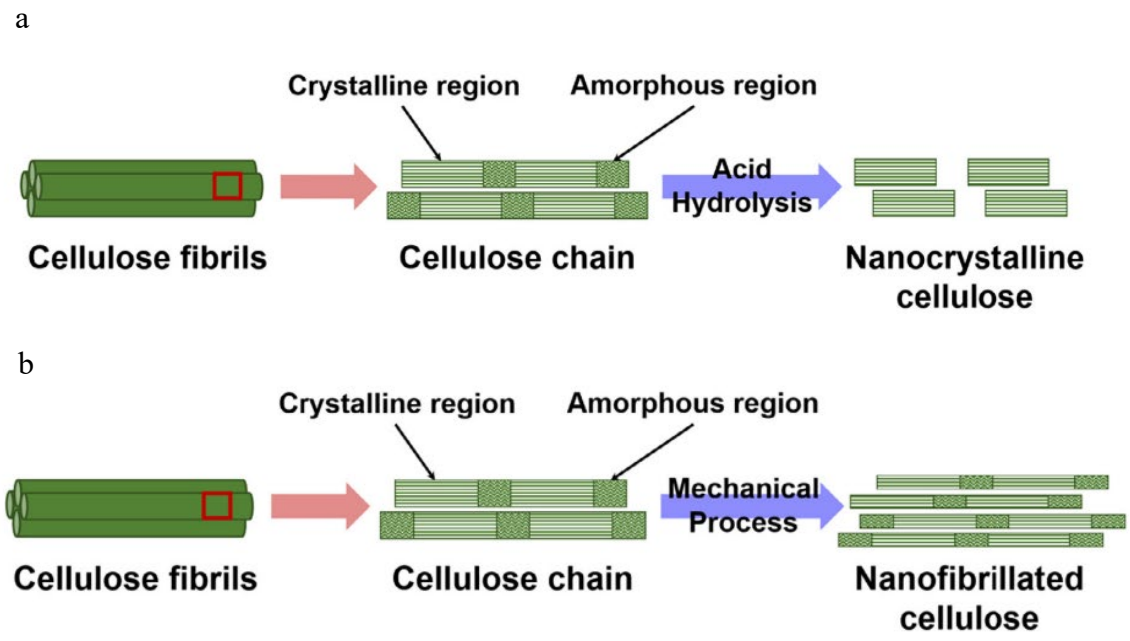

Figure 7. Schematic of (a) nanocrystalline, and (b) nanofibrillated cellulose, which can be extracted from cellulose fibrils using acid hydrolyzed amorphous regions, and mechanical processing, respectively. Cellulose nanofibers are also called nanofibrillated cellulose or cellulose nanofibrils. Figure taken and modified from Phanthong et al.[83]

Nanocellulose is prepared by mechanical disintegration of dry cellulose pulp or cellulose in an aqueous medium. To produce nanocellulose with a high degree of polymerization, crystallinity, and aspect ratio, aqueous solution is preferred. In this environment the interfibrillar hydrogen bonding of the cellulose is loosened, enabling the delamination of the fibrils instead of their chopping. The fibers used for this work were produced via a supermass colloider grinder. In this process, a cellulose slurry is passed between static and rotating grinding stones. The cellulose is separated into its elemental form of nanofibers by the shearing forces that are generated between the stones. During the process the cell wall is delaminated, and the nanofibers are individualized. The size of the nanofibers can be varied by adjusting the space between the stones.[87,88]

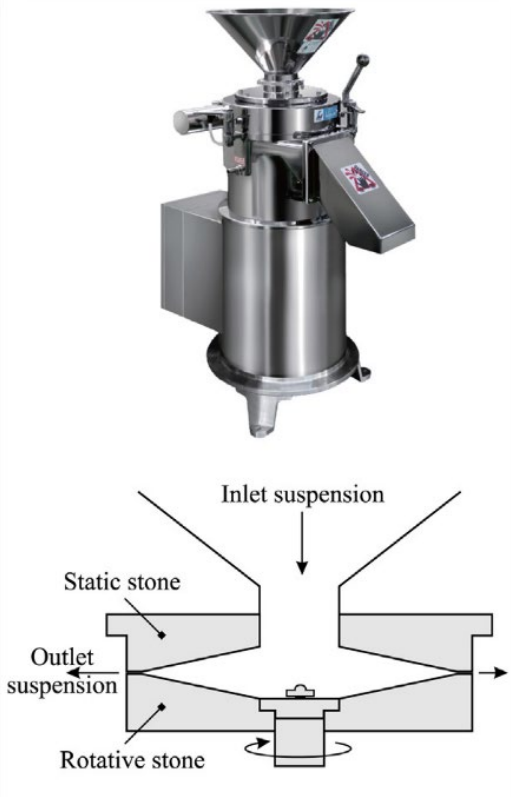

Figure 8. Schematic of supermass colloider in which the grinding process of cellulose to produce cellulose nanofibers takes place. Image taken and modified from Nechyporchuk.[87]

Nanocellulose has been used to improve the performance of composites both by attaching it to the fibers and by dispersing it in the resin.[82,89] As reported in a paper by Uribe, et al.[30], after incorporation of nanocellulose in carbon fiber-reinforced laminates, the composite's ultimate strength increased by 28, 20 and 86% under tensile, flexural, and shear strength testing, respectively. In the experiment, the nanocellulose was incorporated on the carbon fibers by a simple dipping process in a nanocellulose solution, which was followed by a vacuum-assisted liquid resin infusion to fabricate the laminates. The use of nanocellulose in composites was also demonstrated by Asadi, et al.[82] who immersed chopped glass fibers in an aqueous nanocellulose solution, and dried them at room temperature. They reported an improvement of 69% in the IFSS of coated fibers, and an improvement of 43% in their strength modulus.[82] Although nanocellulose

has been successfully incorporated in various fiber-reinforced composites, there is a missing gap in the literature about their incorporation onto the surfaces of high performance fibers, including aramid and UHMWPE, and the mechanisms by which they are attached.

1.2.3.1 Linker

One way to improve the attachment of the nanocellulose to the polymer fiber is by grafting a polymer linker to the nanocellulose. The linker is used to create covalent graft points between the nanocellulose and the fiber. Yatvin, et al.[90] used a sulfonyl azide monomer to covalently bond various copolymers to aramid fabric via thermal grafting. For this process, the material that is going to be grafted onto the aramid, the nanocellulose, is first bonded to a more reactive material. For example, a polymer such as 4-vinylbenzyl chloride (VBC) (Figure 9) contains carbon-carbon bonds that are more likely to react with radicals generated on the polymer fiber surface. Thus, a simple chemical grafting approach can be followed to attach the VBC to the nanocellulose, while separately, radicals are created on the fiber surface by irradiation. The two are then mixed, with the double bond in the VBC being suitable to react and covalently bond to the fiber via the produced radicals.

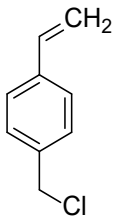

Figure 9. Chemical structure of 4-vinylbenzyl chloride.

1.2.4 Binder resin

The final part of the fiber-reinforced composite is the binding material that holds it together, in this case a thermoset resin. Epoxy resins are used in most aramid fiber-reinforced

composites, including in composite pressure vessels used in space shuttles[91], in high speed boats[92], and vehicle armor[3]. Epoxy resins are defined as having one or more epoxide groups in the molecule. Depending on their application, they can be reacted, or cross-linked with themselves or other reactants (curing agent) to make resins with specific properties. In addition to acting as a binder, the resin also acts as a stress transfer medium for the reinforcing fibers.

Typical epoxy resins used in aramid fiber reinforced composites include LRF 092, a highly crosslinked epoxy anhydride/tertiary amine resin, and E51 a bisphenol-A type epoxy resin (Figure 10).[42,46,47,91]

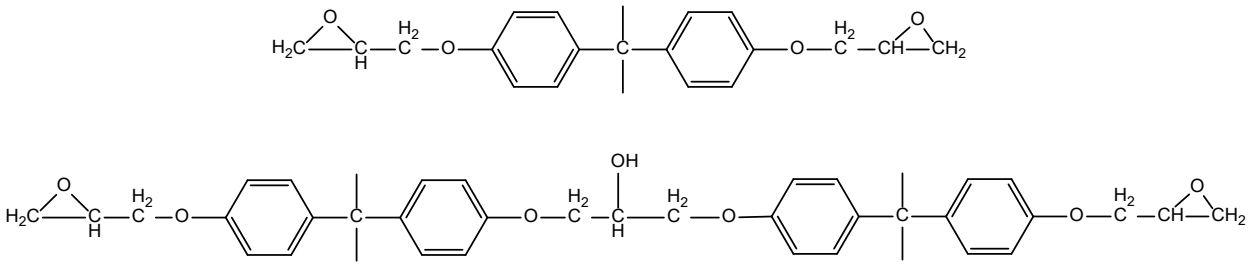

Figure 10. Chemical structure of LRF 092 (top) and E51 (bottom) epoxy resins.

1.3 Effect of Radiation on Polymers

The effects of electromagnetic radiation on any material depends on the power and frequency of the applied radiation. Radiation types with a low frequency, such as microwave and infrared radiation, are considered non-ionizing radiations. Non-ionizing radiations only have enough energy to excite the electrons of the material, without ionizing them.[93,94] Ionizing radiation, such as gamma ray (γ-ray) and electron beam (e-beam), has enough energy to modify the chemical, physical, and biological nature of the material. When the material is irradiated, if the energy is higher than that of a particular orbital electron, an electron is ejected, resulting in ionization. Ionizing radiation is currently used for the sterilization of medical equipment, disinfestation and

pest control of food and agricultural products, and materials modification.[95] This dissertation will focus on the use of ionizing irradiation to modify and improve the mechanical properties of polymers. The use of ionizing irradiation with the goal of polymer recycling will also be investigated.

To describe the interaction of ionizing radiation with matter it is important to define the following parameters: dose, dose rate, and radiation chemical yield. The dose is the amount of energy absorbed per unit mass of matter and it's expressed with the SI unit gray (Gy); 1 Gy is the amount of radiation required to deposit 1 Joule (J) of energy per 1 kg of matter $\mathrm{Gy} = \frac{\mathrm{J}}{\mathrm{kg}}$. The dose rate is the absorbed dose per unit time (Gy/s), and the radiation-chemical yield represents the number of moles produced or destroyed per unit of absorbed energy (mol/J).[96,97]

1.3.1 Types of ionizing radiation

The main types of ionizing radiation are high energy electrons (e-beam), gamma (γ) rays, and x-rays.[96,97]

1.3.1.1 Interactions of gamma (γ) and x-rays with matter

In most gamma irradiation facilities, a radioactive isotope, commonly cobalt-60 (^{60}Co), is used as a power source. γ-rays are high energy photons emitted when an electron in the valence shell drops to a lower energy state, a process known as radical decay. One of the issues with gamma irradiation is that once that radical decay is started, it will continue until the atom reaches a stable state. At this point, the source will need to be replaced. ^{60}Co for example, has a half-life of 5.3 years. Additionally, in comparison with the electron beam, gamma irradiation can achieve only low dose rates on the order of 10^{-3} kGy/s. In terms of the penetration depth, gamma rays have the

advantage of achieving high penetration, which is useful when irradiating bulk materials. The absorbed dose decreases exponentially with penetration, according to Beer-Lambert's law:

$$\mathrm{I_t} = \mathrm{I_0 e}^{-at} \tag{1.1}$$

where I_t is the radiation intensity after passing through thickness t, I_0 is the initial radiation intensity, and a is the coefficient of linear absorptivity.

The interactions of γ and x-rays can be categorized into the following:

1. Photoelectric effects:

In this type of interaction, the γ photons lose all of their energy upon interacting with the electrons of atoms or molecules. The electron is then ejected, and its kinetic energy (E_{Ee}) is equal to the energy of the incident photons (E_γ) minus the binding energy of the electrons with the nucleus of the atom (B_{Ee}).

$$\mathrm{E_{Ee}} = \mathrm{E_\gamma} - \mathrm{B_{Ee}} \tag{1.2}$$

Figure 11 illustrate the photoelectric interaction.

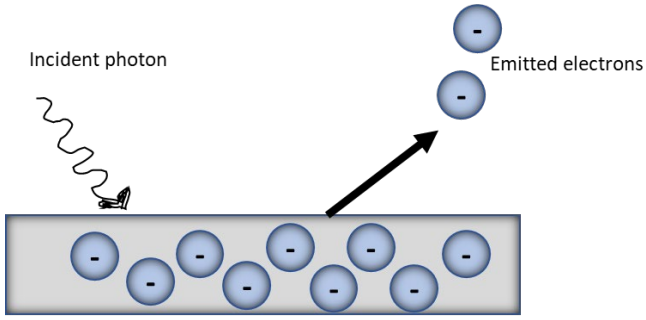

Figure 11. Schematic of the photoelectric interaction.

2. Compton scattering

In the Compton scattering interactions, the incident γ photons do not lose all of their energy upon interactions with the electrons of matter. The energy of the scattered γ photons and the energy of the ejected electron can be determined with the following equations:

$$E' = \frac{E}{1 + \frac{E}{m_0 c^2}(1 - \cos\theta)} \tag{1.3}$$

where E is the initial photon energy (MeV), E' is the scattered photon energy (MeV), $m_0 c^2$ is the electron rest mass energy (0.511 MeV), and θ is the angle of the scattered photon.

If the photon scattering angle is known, the energy of the recoil electron (KE_{e^-}) can be calculated as:

$$KE_{e^-} = \frac{E}{m_0 c^2} \frac{E(1 - \cos\theta)}{1 + \frac{E}{m_0 c^2}(1 - \cos\theta)} \tag{1.4}$$

3. Pair Production

In regions of high atomic numbers (Z) and higher energies, pair production interactions begin to dominate. In this mechanism, an atom emits a positron/electron pair upon absorption of an incoming photon in the nucleus. After the individual particles attenuate and lose a significant amount of energy, the two will then recombine to produce two photons each of energy 0.511 MeV. These photons are called annihilation radiation and are characteristic of pair production. In compliance with the conservation of energy, the pair production interaction has a low-energy threshold of 1.022 MeV – the rest mass energy of the positron and electron. A schematic of the process is shown in Figure 12.

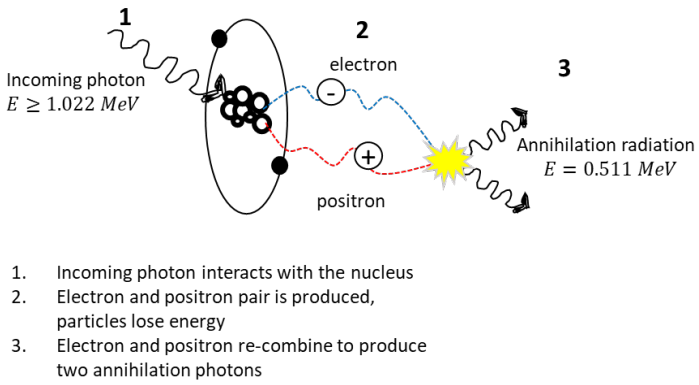

Figure 12. Schematic of pair production interactions.

Conservation of mass for the pair production is as follows:

$$E_\gamma = 2m_0c^2 + E_{e^+} + E_{e^-} \quad (1.5)$$

The pair production interaction coefficient (κ) is proportional to the square of Z of the attenuating material and increases rapidly for E ≥ 1.022 MeV.

1.3.1.2 Interactions of high-energy electrons with matter

E-beam technology was originally developed in the 1950s and had the ability to produce electrons with an energy up to 2.3 MeV.[97,98] During e-beam irradiation fast electrons, with the energy to excite and ionize other molecules, are generated in a vacuum usually by a heated cathode or a radio frequency (RF) ion source. [97,99] Particle accelerators are used for this process. The fast electrons generated are then accelerated and shaped by an electrostatic field formed between the anode and cathode. An electron optical system is commonly used to focus the accelerated electrons to the window plane. The electrons with high enough energy can then exit the accelerator through a 10 – 15 μm thick titanium window foil, towards the target. In addition to avoiding the handling of radioactive isotopes, the advantages of the e-beam over gamma irradiation include the possibility of higher dose rates, in the order of 10 kGy/s, and the ability to control the emission of electrons through the use of magnets.

As a high-energy particle traverses through a medium, a fraction of its initial energy is lost through each interaction with an electron or nucleus in the medium. As these particles collide, electrons are knocked free of their orbit to produce an ion pair, a positively-charged ion and a negatively-charged free electron.

$$M \xrightarrow{e^- p^+ a} M^+ + ne^- \tag{1.6}$$

Charged particles interact via charged Coulombic interactions represented by Coulomb's Law. This law takes into account both charge (higher charge yields a stronger force) and distance (force decreases as $1/r^2$).

$$F = k\frac{q_1 q_2}{r^2} \tag{1.7}$$

where F is the electric force acting on $q_1$and q_2, $q_1$and q_2 are the charge of particles 1 and 2, respectively, and r is the distance between the charges.

Rate of Energy Loss

As a charged particle travels through a medium, Coulomb forces between the moving particle and the electrons of the stationary atoms result in millions of interactions before the particle is completely stopped. Because the particle is scattered through many angles and each interaction has a distinct probability of occurring, it is impossible to calculate the exact total energy loss of the particle. For this reason, an average energy loss per unit distance or stopping power (dE/dx) will be defined for several types of charged particles. Stopping power may also be used to calculate the energy loss rate (-dE/dx) through various media. Depending upon the mass of the particle, the track may be jagged (for small, charged particles such as electrons and positrons) or relatively straight (for heavy ions such as alpha particles).

While an electron travels through the medium, a significant portion of the energy released will be in the form of bremsstrahlung radiation which is deposited some distance away from the particle track.

1. Stopping power for electrons:

$$\frac{dE}{dx}\left(\frac{MeV}{m}\right) = 4\pi r_0^2 \frac{mc^2}{\beta^2} NZ \left\{ \ln\left(\frac{\beta\gamma\sqrt{\gamma-1}}{I} mc^2\right) + \frac{1}{2\gamma^2}\left[\frac{(\gamma-1)^2}{8} + 1 - (\gamma^2 + 2\gamma - 1)\ln 2\right]\right\} \quad (1.8)$$

2. Stopping power for p, d, t, a:

$$\frac{dE}{dx}\left(\frac{MeV}{m}\right) = 4\pi r_0^2 z^2 \frac{mc^2}{\beta^2} NZ \left[\ln\left(\frac{2mc^2}{I}\beta^2\gamma^2\right) - \beta^2\right] \quad (1.9)$$

3. Stopping power for positrons:

$$\frac{dE}{dx}\left(\frac{MeV}{m}\right) = 4\pi r_0^2 \frac{mc^2}{\beta^2} NZ$$
$$\left\{\ln\left(\frac{\beta\gamma\sqrt{\gamma-1}}{I} mc^2\right) - \frac{\beta^2}{24}\left[23 + \frac{14}{\gamma+1} + \frac{10}{(\gamma+1)^2} + \frac{4}{(\gamma+1)^3}\right] + \frac{\ln 2}{2}\right\} \quad (1.10)$$

where $r_0 = \frac{e^2}{mc^2} = 2.818 \times 10^{-15} m$ (electron radius), $4\pi r_0^2 = 10^{-28} m^2 = 10^{-24} cm^2$, $mc^2 = 0.511$ MeV (electron rest mass energy), $\gamma = \frac{T+mc^2}{mc^2} = \frac{1}{\sqrt{1-\beta^2}}$, $WT = (\gamma-1)mc^2$ (kinetic energy), $\beta = \frac{v}{c}$, c is the speed of light in m/s, N is the number of atoms per m^3 in a material, Z is the atomic number of the material, z is the charge of incident particle, and I is the mean excitation potential of the material.

For Z > 12, I can be approximated as:

$$I(eV) = (9.76 + 58.8Z^{-1.19})Z \quad (1.11)$$

1.3.2 Irradiation in aqueous solution

When dilute aqueous solutions are irradiated, the radiation interacts with the water and produces various reactive species. The observed chemical changes are the indirect result of the reactions of the radicals generated from the water, with the material. The following species are the product of exposing water to ionizing radiation:[100]

$$H_2O \xrightarrow{\text{Irradiation}} {}^{\bullet}OH, e_{aq}^{-}, H_3O^{+}, H^{\bullet}, H_2, H_2O_2 \tag{1.12}$$

During the irradiation of aqueous solutions, the ionized molecules react rapidly to form hydroxyl radicals (${}^{\bullet}OH$), while the electrons become hydrated (e_{aq}^{-}).[100,101] These radical species react together or with the hydrogen ion (H_3O^{+}) to form smaller amounts of hydrogen radical ($H^{\bullet}$), hydrogen molecules (H_2), and hydrogen peroxide (H_2O_2). The radiation-chemical yield, or yield (G), of these species have been established for electrons with energies in the 0.1 – 20 MeV range and are shown in Table 1.

Table 1. Radiation chemical yield of species formed after the irradiation of aqueous solutions.[100]

Species	*Yield (μmol/J)*
H_2	0.04
H_2O_2	0.08
e_{aq}^{-}	0.29
$H^{\bullet}$	0.064
${}^{\bullet}OH$	0.29
H_2O_2	0.08
H_3O^{+}	0.29

These radical species are of great importance in the use of radiation for grafting. They promote the generation of radicals on the substrate and facilitate the grafting of the selected monomer. The hydroxyl radical (${}^{\bullet}OH$) is the most important since it will readily abstract hydrogen

or attach to a C-C double bond and initiate the polymerization process. It has been shown that the generation of hydroxyl radicals can be enhanced by the use of nitrous oxide.[102–104]

1.3.3 Radiation-induced crosslinking and degradation in polymers

Ionizing radiation can result in either crosslinking or degradation of polymers, caused by the reactive species generated. Chemical crosslinking is the process in which two or more polymer chains form bonds between themselves and see an increase in their molecular weight. When polymer chains are broken, that process is known as chain scission. The polymer undergoes degradation and a reduction in its molecular weight is observed. The mechanisms for both processes are shown in Figure 13.

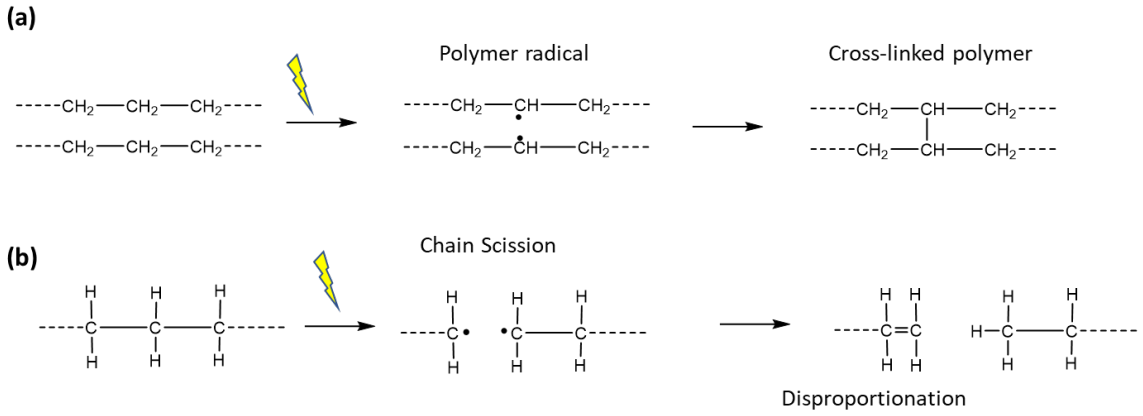

Figure 13. Mechanisms for radiation-induced (a) crosslinking, and (b) degradation.

The G-value, or radiation chemical yield, is used to quantify the polymer's response to irradiation in terms of crosslinking (G(X)) or chain scission (G(S)). In this case the G-value represents the chemical yield of crosslinking or degradation from radiation by the number of molecules per 100 eV of energy dissipated in the material. Polymers are commonly classified depending on their response to ionizing radiation, whether they exhibit predominantly crosslinking or chain scission. Table 2 shows the G-values of a variety of polymers.

Table 2. G-values for selected polymers. Table taken from Andrew. [97]

Polymer	*G*(*X*) Value	*G*(*S*) Value	Ratio *G*(*X*)/ *G*(*S*)
Polybutadiene	5.3	0.53	10
Natural rubber	1.3–3.5	0.1–0.2	7.4
High-density polyethylene	0.96	0.19	5.05
Low-density polyethylene	1.42	0.1–0.2	2.95
Polyvinylidene fluoride	0.6–1.0	0.3–0.6	3.33
Polymethyl methacrylate	0.45–0.52	0.05	6.6
Polyamide 6/6	0.5–0.9	0.7–2.4	0.71
Atactic polypropylene	0.4–0.5	0.3–0.6	0.91
Isotactic polyethylene	0.16–0.26	0.29–0.31	0.67
Butyl rubber	<0.5	2.9–3.7	0.18
Polyisobutylene	0.05–0.5	5	0.05
Polytetrafluoroethylene	0.1–0.3	3.0–5.0	0.05

The structure of the polymer influences its response to ionizing radiation. It has been observed that polymers with an α-hydrogen, like PE, favor crosslinking. While vinyl polymers with two side chains attached to the backbone carbon, such as polymethylmethacrylate, tend to degrade. Aromatic polymers, such as aramid, are usually resistant to ionizing radiation.[97] The effects of quaternary C-atoms are shown in Table 3.

Table 3. Effects of quaternary C-atoms for irradiation of polymers.[105]

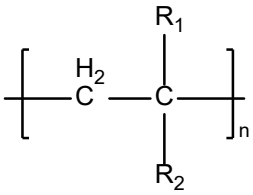 **Polymer**	**R_1**	**R_2**	**Radiation-induced change**
Polyethylene	H	H	Cross-linking
Polypropylene	CH_3	H	Cross-linking
Poly(vinyl chloride)	Cl	H	Cross-linking
Polyacrylonitrile	CN	H	Cross-linking
Polyacrylates	CO_2R	H	Cross-linking
Polystyrene	C_6H_5	H	Cross-linking
Poly(vinylidene chloride)	Cl	Cl	Degradation
Polyisobutylene	CH_3	CH_3	Degradation
Polymethylstyrene	C_6H_3	CH_3	Degradation
Poly(methyl methacrylate)	CO_2CH_3	CH_3	Degradation
Natural rubber			Cross-linking
Cellulose and derivatives			Degradation

1.3.3.1 Radiation-induced crosslinking

As discussed above, depending on the irradiation conditions and the properties of the polymer being irradiated, crosslinking can occur when the radicals generated on the polymer preferably react with each other. This creates new permanent intermolecular bonds between molecules that were previously separate. In addition to the chemical structure and chain mobility of polymers, the association between its molecules have a huge effect on its mechanical properties. Some advantages of radiation-induced crosslinking over chemically-induced crosslinking include little to no temperature dependence, no unwanted chemical residue, and a quick turnaround period.[106]

Electron beam irradiation is commonly used for the radiation-induced crosslinking of many polymers, with the goal of improving their chemical and physical properties including the

polymer's Young's modulus, hardness, and heat and chemical resistance.[107] High radiation dose rate tends to favor crosslinking over chain scission reactions. However, it is important to note that even for polymers in which crosslinking is dominant, some degradation is still observed.[108,109] This is due to the radiation still breaking some bonds along the backbone of the polymer, thus reducing their properties. For semi-crystalline polymers, crosslinking occurs in the amorphous phase of the polymer. The crosslinking 'strengthens' the polymer and reduces mobility of the chains in the amorphous phase.

The degree of degradation can be minimized, by the addition of certain chemicals that enhance the crosslinking of the polymer.[110–112]. For example, the addition of a mediating alkyne gas during irradiation prevents degradation of polymeric material and enables the introduction of additional molecular and functional characteristics. Furthermore, keeping the polymer system in an inert atmosphere will protect the radicals from reacting with oxygen, which often leads to oxidative degradation.

Crosslinking enhancement

The effect of e-beam irradiation on PE fibers in an acetylene environment was reported by Klein et al. in 1993. They found that the degree of crosslinking achieved was dependent on the crystallinity of the fibers and concluded that crosslinking provided an effective mechanism for stress to be transmitted through the polymer.[113] However, a study on the gamma irradiation of UHMWPE fibers in various environments found that even in acetylene, the tensile strength and elongation of the fibers decreased substantially.[114] It is to be expected that the higher crystallinity of the UHMWPE fibers would make crosslinking harder to achieve. Also, the low dose rate of gamma irradiation may play a big role in these results. Deng et al. also studied the mechanical and thermal effects of irradiation environment (air, nitrogen, and acetylene) on UHMWPE fibers. They

found an initial increase in the tensile strength for samples irradiated in the acetylene environment, but saw a decrease after 160 days.[114] This could be a result of the radicals, which promote cross linking and chain scission, staying on the fibers after the initial irradiation. These radicals could cause oxidation and thus damage of the fibers. One solution to this is to anneal the fibers after irradiation and thus removing any unreacted radicals.[115]

The e-beam irradiation of aramid fibers in acetylene gas has been scarcely reported. It has been found that coating a layer of acetylene on aramid fibers and cords, increases the adhesion to various polymers and epoxy resins.[116] The same group reported that plasma polymerization of acetylene on aramid cords increased their adhesion to rubber compounds.[117] Benzoic acid has been used as a crosslinker for aramid fibers, with the goal of increasing their adhesion to epoxy resins and increasing their compressive strength.[118]

1.3.3.2 Radiation-induced degradation

Although radiation-induced degradation might be an undesired reaction in most cases, it can lead to the optimization of recycling processes. Polymer recycling is an important issue, since polymer waste is a daunting challenge being faced all over the world.[119–123] Ionizing radiation can be used to modify the chemical structure and the overall properties of all types of polymers. There are three main ways in which ionizing radiation can aid in dealing with the polymer waste problem: (1) enhancing the mechanical properties and performance of the recycled polymers, (2) degrading or increasing the degradability of polymers, and (3) producing advanced polymer materials with better environmental compatibility.[121,124–127] For this work, the focus will be on using e-beam irradiation for the degradation of polymer resins, which are an important part of fiber-reinforced polymer composites. As discussed above, the main effects of polymer irradiation are crosslinking

and scission of the polymeric backbone. In this case, scission of the polymer is the desired outcome of the process.

One common approach for recycling polymer waste is chemical recycling. Chemical recycling is based on the decomposition or conversion of the large macromolecular structure of polymers into smaller molecules. The concept is based on the depolymerization of the material, where the size of the molecule is reduced, but the monomer unit remains unchanged. Thus, the resulting polymer can be used for the production of new materials. The main issue with chemical recycling is that it requires high temperatures and the use of catalysts to drive the reaction. This leads to large energy consumption, which would also be an environmental issue. The pre-treatment of polymers by irradiation before chemical recycling results in a decrease in the energy consumption and promotes the chemical recycling reactions.

Zhao (1996) et al. found that chain scission caused by irradiation of polypropylene results in the polymer being more susceptible to thermal degradation, as observed by a decrease in its thermal degradation temperature. As a result of the irradiation, a decrease in the molecular weight of the polypropylene was observed, which they attribute to chain scission of the backbone of the polymer. Additionally, since the polymer was irradiated in air it also led to the formation of polar groups on the surface of the polymer, increasing its oxidative degradability. After irradiation, the temperature needed for pyrolysis of the polypropylene was greatly reduced.[128] In another case, a decrease in the onset temperature for mass loss of butadiene-containing polymers was achieved after irradiating copolymers in the presence of air.[129] Their comparison between the irradiation in the presence and absence of oxygen, shows that scission and polymer degradation may be promoted by conducting the irradiation in the presence of air.

In addition to lowering the energy required for further chemical recycling of these polymers, irradiation of polymer waste can also be used for creating new and better materials. High density polyethylene (HDPE) waste was recycled into filler by first irradiating the HDPE via the e-beam and then grinding it into a powder. This powder was used as a filler for low density polyethylene, creating a HD/LD polyethylene material with improved mechanical properties when compared to LDPE.[130] Vignon et al. made a polymer blend (representing thermoplastic waste) with polycarbonate, to synthesize a polycarbonate-based extruded thermoplastic.[131] The samples were exposed to gamma irradiation, in the range of 0 – 150 kGy and the mechanical properties of the product were studied. It was found that irradiating the material led to more homogeneous blends with higher thermal stability.

Unsaturated polyester resin

One of the most widely used types of thermosetting polymers are unsaturated polyester resins (UPRs).[132,133] UPRs have a relatively low cost, and good mechanical, electrical, and chemical properties.[133–135] It is expected that the global UPRs market will grow from $ 9.6 billion in 2021 to $ 12.9 billion by 2026.[136] This makes UPRs an interesting candidate in the search for polymer recycling methods.[137] Polyester resins are produced by the condensation of a polyol with a combination of saturated and unsaturated anhydrides, and their properties can be tuned by the proportion and choice of the starting materials.[138–142] As thermoset resins, they are thermally and chemically stable, which complicates their recycling process.[143,144] Current efforts to recycle thermoset resins include mechanical methods, which involve a grinding process of the material, thermal methods where the resin is decomposed by heating it up to high temperatures, and chemical methods, which mostly concentrate on depolymerization of the resin.[145–147] The advantages of ionizing irradiation over these methods include: (1) high rates of radical formation,

which influence the degradation process, (2) no need of initiators or additives, and (3) can be done at room temperature.[148]

Promoting polymer degradation

As previously discussed, the effect of irradiation on the polymer depends heavily on the environment in which the polymer is irradiated and the chemical structure of the polymer. Irradiation of the polymer in air leads to the formation of peroxyl radical species and results in a major enhancement effect on the radiation degradation of most polymers.[149] Dispersing the polymer in a solvent prior to irradiation will result in the absorption of the high-energy radiation by both the polymer and the solvent, and in the generation of radicals from both. All the radicals generated will then induce reactions in the polymer and influence its degradation.

The physicochemical characteristics of the polymer in combination with the irradiation environment, e.g., presence of oxygen, proximate solvents, irradiation temperature, total dose, and dose-rate, can either induce scissions, crosslinking, or both in the irradiated pure polymers.[96] The distinctive backbone bonds in polyesters, comprised of the C-O-C bond sequence is highly sensitive to ionizing radiation and generally favors scission.[109] The mechanism of radiation-induced scissions is complicated by the presence of additional moieties common in representative polyesters including double bonds, phenyl, and carbonyl groups. While the presence of the C-O-C bonds enhance scissions, the π structure of the phenyl groups provides protection via the reaction of the electron with the π structure, ultimately reducing effective bond breakage. The presence of double bonds plays an important role in the structures of the radiation-induced free radicals, their kinetics, and the mechanisms by which they decay. As for polyester resins used in industry to prevent corrosion, which contain unsaturated vinyl monomers such as vinyl toluene, styrene, and other additives, the radiation effects become even more complicated since these residual vinyl

monomers undergo radiation polymerization, which contribute to an increase to the T_g of the polyester-resins. These challenges in the use of ionizing radiation to degrade the unsaturated resins can be overcome by tuning the irradiation conditions such as high dose rate to impede the radiation polymerization of these residual vinyl monomers. In addition, the presence of O_2 during the irradiation is critical to inhibit the radiation polymerization of the vinyl monomers present in the resins, and also to prevent the crosslinking reactions of the radiolytically produced polyester radicals.[109]

1.3.4 Radiation-induced polymerization

Ionizing radiation can also induce polymerization reactions, which are initiated when a monomer or oglomer is irradiated. There are two main types of polymerization reactions: free radical and cationic polymerization.[150] Radiation-induced free-radical polymerization reactions usually follow the chain addition mechanism. As excited species, such as free radicals, are produced on the irradiated material, they can initiate the chain polymerization mechanism. This technique enables the initiation of polymerization reactions at conditions in which conventional initiation methods do not work to start the reaction.

The polymerization process can be divided into 4 steps: initiation, propagation, termination, and chain transfer. The chain initiation reactions start when the material is irradiated, and the initiator decomposes into a free radical (X^*). The rate of reaction of this step is controlled by the decomposition of this initiator. The chain initiation ends when the free radical adds to the first monomer unit and produces the chain initiating species (M^*). This initiating species, or initiating monomer, starts the propagation reactions. It goes through an iterative growth and after successive addition of monomer molecules, macroradicals are formed. Both steps are shown in Figure 14.

Initiation

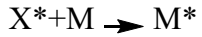

Propagation

Figure 14. Schematic of the initiation and propagation steps in the polymerization mechanism.

The active free radical species are highly unstable and tend to self-annihilate through two termination reactions: combination and disproportionation. Combination reactions occur when two macroradicals react resulting in the formation of a polymer comprised of the two species. On the other hand, in disproportionation reactions one of the species abstracts a H-atom from the other which results in a H saturated macromolecule together with its omega unsaturated counterpart.[150] Chain transfer reactions compete with the propagation reactions as the reactive macromolecule ($M - M^*$) may react with a component present in the experiment, that is not the monomer. In this case the active site is transferred to that other non-monomer species, terminating the polymerization of that specific chain, but starting a new chain polymerization. A schematic of these two steps is shown in Figure 15.

Termination

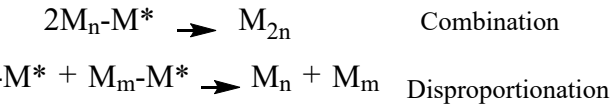

Chain Transfer

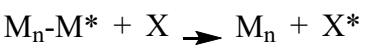

Figure 15. Schematic of the termination and chain transfer steps in the polymerization mechanism.

In cationic polymerization reactions, an electrophile reacts with the monomer which has a π bond. The reaction is initiated by adding the electrophile which results in cleavage of that double bond, and a cation is left on one end of the original double bond. For example:

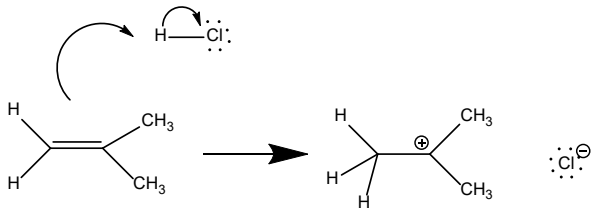

Propagation then proceeds with the reaction of the monomer with the active species.

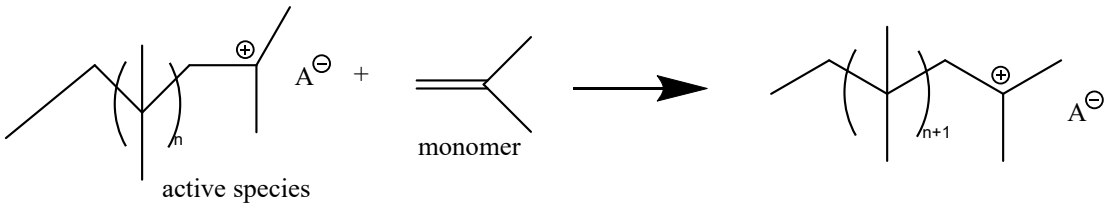

The polymerization is terminated generally by combination the nucleophilic anion with the cationic chain. Another way in which the chain is terminated is by chain transfer. In this case, hydrogen can be abstracted by the counterion or by the monomer.

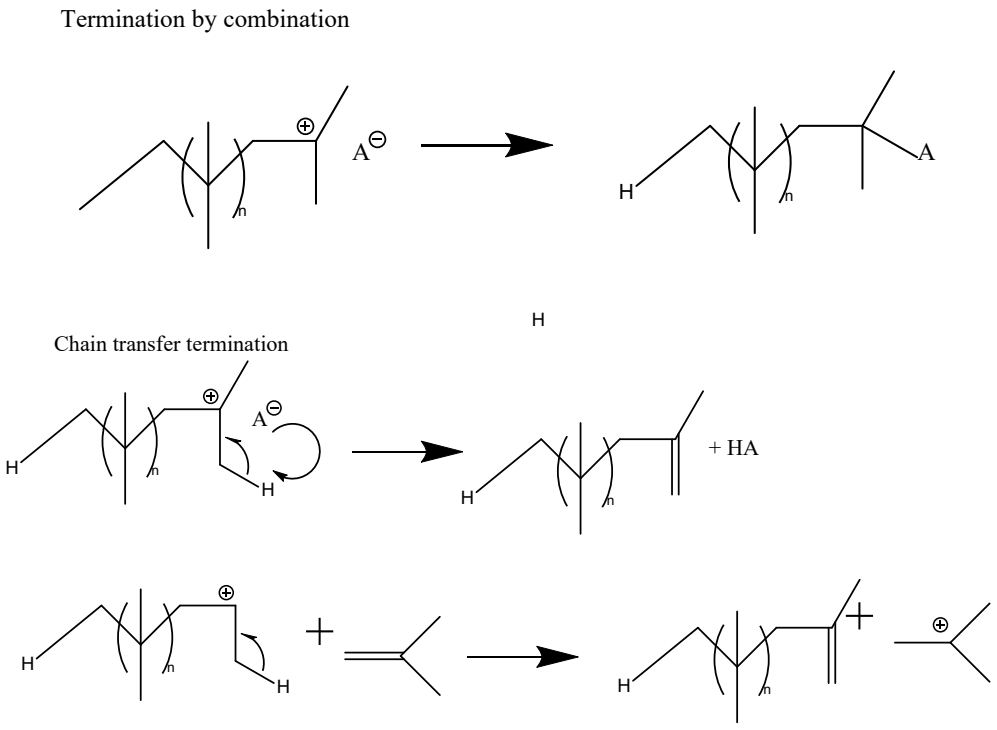

1.3.5 Radiation-induced grafting

Radiation-induced grafting refers to the process in which a functional monomer may be covalently bonded to a polymer substrate with the use of radiation. This is a rapid method that allows for the functionalization of a variety of polymers, and that can be upgraded from the laboratory to the industrial scale.[96] Some of the advantages of radiation-induced grafting over chemical grafting include, not requiring any hazardous reactants, and no limitations in the polymer shape. The degree of grafting (DoG) is used to quantify the amount of grafting achieved through the following equation:

$$\text{DoG}\ (\%) = \frac{m_f - m_i}{m_i} \times 100 \qquad (1.13)$$

where m_f is the mass of the sample after grafting, and m_i is the mass of the sample before grafting.

There are two main ways to graft monomers onto a substrate: direct and indirect grafting. These will be discussed in the following sections.

1.3.5.1 Indirect Grafting

In the process of indirect grafting the polymer substrate is irradiated first in a vacuum or in an inert atmosphere, to protect the radicals formed during the irradiation. The substrate is kept in that inert atmosphere until it is mixed with the monomer that will be grafted onto it. At that moment the radicals generated will start the reaction with the monomer or polymer that is being grafted. Radicals are then generated on the monomer, through which a covalent bond between the monomer and the substrate is formed. In the case of using a monomer, polymerization grafting can also be achieved. One of the advantages of this type of grafting is that there is a low degree of homopolymerization of the monomer since the radicals are formed through a chain transfer mechanism. This in turn leads to an easier process of washing the grafted material, since less homopolymer will need to be removed. In addition, this allows for the grafting of virtually any monomer, since it would not be subjected to any irradiation that may damage it. The disadvantage of indirect grafting involves the need to maintain the irradiated substrate in an inert atmosphere and at cold temperatures to conserve the radicals before the monomer is introduced. If kept at room temperature, the radicals generated will quickly begin to decay by recombination.

1.3.5.2 Direct Grafting

The process of direct grafting is that in which both the polymer substrate and the monomer are irradiated together. Grafting is achieved through the simultaneous generation of radicals in the substrate and in the monomer, which then react to form covalent bonds between the two. The irradiation may be done in air, in inert atmosphere, or in an environment that promotes the generation of a specific kind of radical, i.e., nitrous oxide. The main disadvantage of this method is that it is limited to certain substrate-monomer pairs. A similar number of radicals is desired for both the substrate and the monomer. However, if they have different radiation-chemical yields (G)

more radicals of one will be generated over the other. This is especially concerning if the monomer has a higher yield since it will lead to a high degree of homopolymerization and a low DoG. Ways to promote grafting and avoid homopolymerization include: (1) polymerization inhibitor in the monomer solution, (2) high temperature environment, and (3) lower dose rates.[151]

1.3.6 Radiation grafting under different atmospheres

As discussed above, it is of outmost importance to control the type and yield of radicals formed during the irradiation to achieve high degrees of grafting. In this section, the effect of different types of irradiation atmospheres on the final product will be discussed.

1.3.6.1 Presence of oxygen

When a polymer is irradiated under a natural atmosphere, the presence of oxygen around it will have significant effects on the type of radicals formed. The result is the oxidation of the polymer from the reaction of the polymer molecule with the peroxyl radicals generated from the oxygen molecules. The following chain reaction scheme describes the oxidative degradation of polymers (RH) in air:[152]

Initiation

Propagation

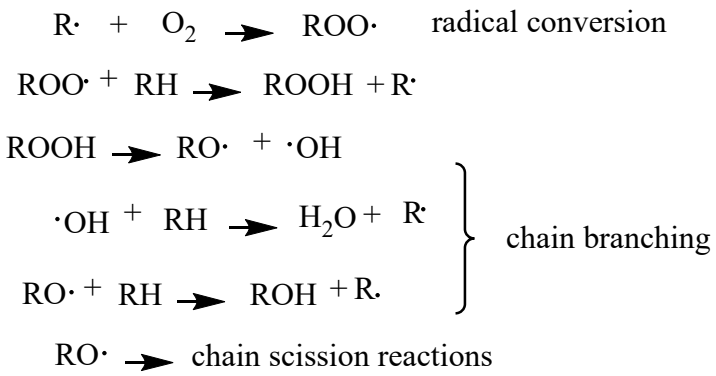

Termination

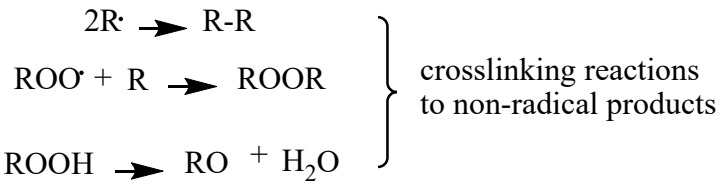

During e-beam irradiation the presence of oxygen not only increases the rate of degradation of the polymer, but also increases the possibility of cross-linking.[109] For the purpose of the grafting experiments done in this work, the irradiations were conducted in the absence of oxygen.

1.3.6.2 Absence of oxygen

Irradiations under vacuum or in an inert atmosphere allow for the formation of radicals in the polymer without the interference of oxygen molecules. In the case of indirect grafting procedures, the absence of oxygen slows the decay of the radicals generated on the polymer until the monomer is introduced. If direct grafting is done in non-aqueous solution, the absence of oxygen will also be beneficial to achieve a high DoG because it will avoid the reaction of the radicals with species other than the polymer.

1.3.6.3 Nitrous oxide environment

As discussed previously, during the irradiation of the polymer in aqueous solution the hydroxyl ($^{\bullet}OH$) radical plays an important role in the formation of radicals on the backbone of the polymer. These radicals are generated when the $^{\bullet}OH$ radical abstracts hydrogen atoms from the backbone of the polymer or adds to a C-C double bond. Thus, it is beneficial to have a high concentration of hydroxyl radicals in the solution. In 1960 Dainton and Peterson[104], showed that the addition of nitrous oxide into an aqueous solution led to the increase in concentration of hydroxyl radicals. When nitrous oxide is introduced to the solution the aqueous electrons react with it which leads to the generation of more hydroxyl radicals trough the following reaction:

$$e_{aq}^{-} + N_2O \xrightarrow{H_2O} N_2 + {}^{-}OH + {}^{\bullet}OH \qquad (1.14)$$

This reaction is very fast ($k = 9.1 \times 10^9\ M^{-1}s^{-1}$) which allows for the majority of the aqueous electrons to be converted to hydroxyl radicals, before reacting with the other species.[153]

1.3.7 Additional parameters affecting radiation-induced grafting yield

The DoG can be controlled by various irradiation parameters including dose, dose rate, and linear energy transfer (LET). The irradiations done in this work were completed with the use of an e-beam accelerator. In general, a higher irradiation dose leads to a larger number of radicals generated and thus a higher DoG. However, the effects of high doses on the polymer substrate must be taken into account when selecting the irradiation dose for grafting. In terms of the dose rate, the inverse is observed; a high dose rate leads to a decrease in the DoG. This is due to high dose rates increasing the density of radicals which promotes their recombination and the formation of gels.[154]

Other conditions that affect the DoG are the chemistry of the polymer substrate, monomer concentration, and grafting temperature. The substrate chemistry is important because it determines the reactivity of the radicals produced during irradiation. The nature of the radical is usually determined by electron paramagnetic (EPR) spectroscopy to determine its reactivity with the monomer. The presence of functional groups that can either stabilize or quench the radicals generated must also be considered. Mostly, a higher concentration of the monomer leads to a higher DoG. However, an increase in the monomer concentration might lead to an increase in the viscosity of the solution and thus a decrease in the diffusion of the monomer to the polymer substrate which might reduce the DoG. Finally, an increase in the temperature can increase the DoG for both direct and indirect grafting procedures. Heating the sample above the glass transition temperature (T_g) of the polymer increases the mobility of the chain segments which promotes active site migration to the surface and thus increasing the concentration of radicals. It can also help by decreasing the viscosity of the solution leading to better diffusion of the monomer to the polymer. However, high temperatures can also promote the recombination of radicals which would be counterproductive for the indirect grafting approach.

2. Materials and Experimental Methods

The main objective of this work was to design and produce a new aramid fiber with improved mechanical properties, through grafting and crosslinking. The first approach focused on the radiation-induced grafting of nanomaterials onto the fiber, both direct and indirectly, a schematic of which is shown in Figure 16. The specifics of both methods will be discussed in the following sections. The second approach was focused on the irradiation of the fibers in an atmosphere that would enhance their crosslinking. A similar effort was made to produce an improved UHMWPE fiber, following a parallel approach.

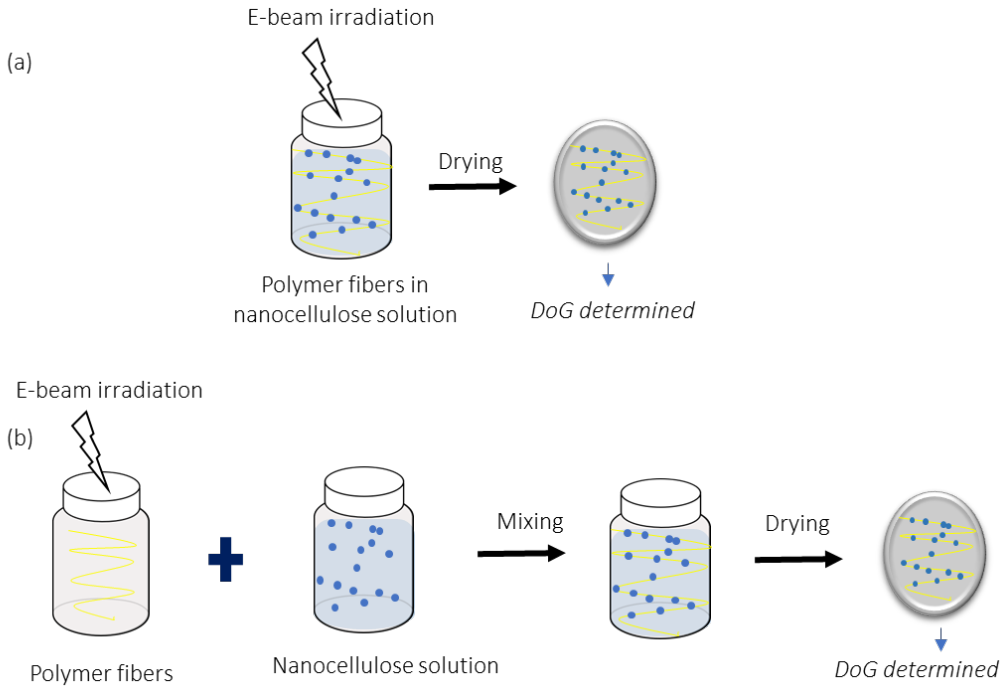

Figure 16. Schematic of the processing steps for the radiation-induced grafting, (a) direct, and (b) indirect, of nanocellulose onto aramid fibers and the subsequent testing procedure.

After becoming an e-beam operator at NIST, this thesis moved to include another project, which will be discussed here as well. This second project is closely related to the polymer fiber modification one and focuses on the use of irradiation of polymer resins with a different goal: to

degrade the resin and increase its recyclability. Polymer resins are an important part of fiber-reinforced composite; thus, it is of interest to understand the effects of irradiation on them. All the work in this part of the project was done in collaboration with groups from Oak Ridge National Laboratory (ORNL) and Brookhaven National Laboratory (BNL).

2.1 Materials

Aramid and UHMWPE fibers were selected for this study because of their importance in many fields, including the military and defense industry. A previous grant of the Al-Sheikhly group with the Department of Defense (DoD) and NIST had directed research on functional fibers used in body armor, including aramid and UHMWPE fibers. With the goal of improving the interfacial strength between fibers and resins used in composites, and the total strength of the fiber, irradiation-induced grafting and irradiation-induced crosslinking processes were studied. Unsaturated polyester resins contribute largely to the polymer waste problem currently faced in the world. In this work, radiation was explored as a tool to reduce the high-energy expenditure process of recycling, by inducing radiation scission and degradation of the resin.

2.1.1 Polymer Fibers

The aramid fibers studied in this project were produced by DuPont under the commercial name Kevlar® 49. The fibers have an average diameter of 9.3 μm. The measured tensile strength and modulus are approximately 3.1 and 95.3 GPa, respectively. A spool of UHMWPE fibers produced by DSM under the commercial name Dyneema SK76 was also used in this project. These fibers have an average diameter of 18.54 μm.

2.1.2 Nanocellulose

Cellulose nanofibrils (referred in this work as nanocellulose) were purchased from Cellulose Lab. Two types of nanocellulose were studied in this work: (1) nanocellulose slurry, and

(2) freeze dried nanocellulose. Both consisted of nanocellulose with a nominal width from 30-80 nm and several hundred microns in length. In the case of the slurry, it was a 3 wt% aqueous solution. A styrene-containing linker was grafted onto freeze dried nanocellulose to enhance the grafting of the modified nanocellulose onto the polymer fibers. Nanocellulose has been used previously to enhance the interface adhesion between fiber and resin in polymer composites.[23,30,86,155] However, no studies on the incorporation of nanocellulose on aramid or UHMWPE fibers, or its effect on the fibers, has been published. Nanocellulose would not only act as a mechanical anchor between the fiber and the resin, but also introduce functional groups that can facilitate bonding in the composites.

2.1.3 Polymer resin

Four unsaturated polyester resins were provided by AOC Resins, Collierville, TN. The 4 resins studied were: (1) Marine use dicyclopentadiene (DCP)-based, (2) VipelF701®, (3) VipelF013®, and (4) VipelF774®. All resins share the ester bond shown in Figure 17. They were irradiated in two states: (1) bulk solid slabs, and (2) powder form. A variety of solvents were used to determine the best environment to achieve degradation. The solvents used were dimethyl sulfoxide (DMSO, ACS reagent, ≥99.9%) and isopropyl alcohol (IPA, ACS reagent, ≥99.5%) which were purchased from Sigma Aldrich and used as received. A water purification system (Milli-Q type 3) was used to obtain purified water.

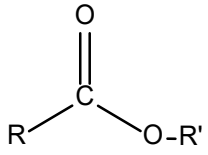

Figure 17. Ester bond - common bond in all the resins studied.

Table 4 shows the approximate structure of the resins used and the sample names used in this thesis for simplification.

Table 4. Polyester-based resins and their composition.

1R: Marine use DCPD based resin 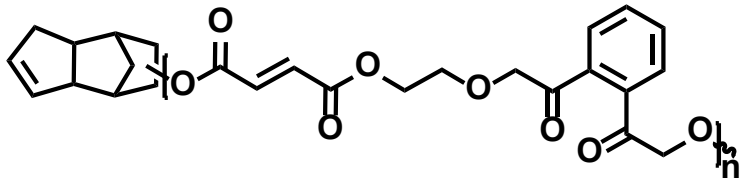 **Main Components**: Dicyclopentadiene (DCPD), Maleic Anhydride, phthalic anhydride, glycols, small amount of vinyl monomers (methyl methacrylate, vinyl toluene)
2R: VipelF701® 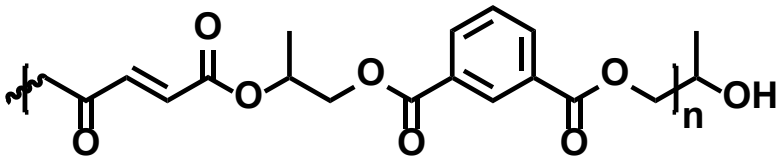 **Main components**: Maleic anhydride, isophthalic acid, propylene glycol **Description**: Corrosion resistant isophthalic polyester resin
3R: VipelF013® 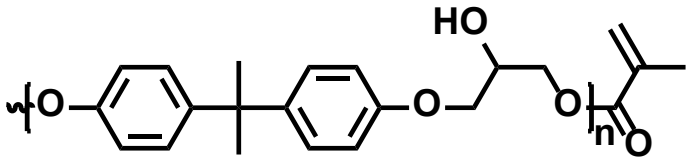 **Main components**: Bisphenol-A (BPA) diglycidyl ether, maleic anhydride, styrene, small amounts of polyols and acrylate monomer **Description**: Bisphenol-A, Epoxy Vinyl Ester Resins (Higher Styrene Content)
4R: VipelF774® 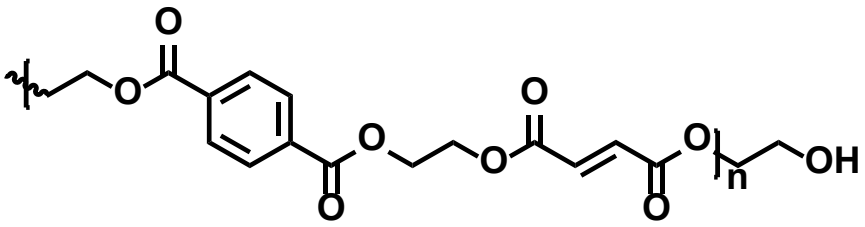 **Main components**: Maleic anhydride, phthalic anhydride, terephthalic acid, propylene glycol **Description**: High Cross-linked Terephthalic Polyester Resin

2.2 Sample preparation

In this section the general procedure followed for preparing the samples before irradiation will be discussed. A spool of aramid fibers was kept wrapped in a plastic bag inside a black container to keep the fibers clean and protect them from extended exposure to light. The UHMWPE spool was kept in dark ambient conditions. This first section will focus on the samples used for the nanocellulose grafting experiments, the following section will deal with the samples used for the crosslinking experiments, and the last one focuses on the polyester resin samples.

2.2.1 Preparation of samples for grafting

Ceramic scissors were used to cut threads of fiber from the spool and obtain pieces with a mass between 0.069 – 0.070 g. This range was selected to reduce the impact of sample size on the grafting. The initial mass was originally chosen based on the size of the vials used for the first experiments, in which 7 mL of water could be added to irradiate the fibers in a 100:1 water to fiber ratio. After cutting the fibers and placing them in septum vials, aramid fibers were placed in an oven at 100 °C for 3 h to remove any moisture that was absorbed from the laboratory environment. The fibers were then weighed and placed inside a vacuum desiccator until the morning of the irradiation. The septum vials enable the purging of the atmosphere inside the vial with inert gas, or with nitrous oxide when the sample was submerged in water. All the vials were purged for 20 minutes in the morning before the irradiation and sealed with parafilm to avoid diffusion of oxygen inside the vials. For the purging, two needles were inserted into the septum vial: the first needle is connected to the gas and is used to introduce inert gas or nitrous oxide to the sample and as the oxygen is displaced, it escapes the vial through the second needle.

There were two grafting solutions used in the experiments: (1) unmodified nanocellulose, and (2) styrene-grafted nanocellulose. For the first solution, the 3 wt% nanocellulose slurry in

water obtained from Cellulose Lab was used. The slurry was diluted to obtain the same mass of fiber and nanocellulose in each vial. The initial grafting experiments of nanocellulose onto aramid fibers were not successful (DoG < 5%) and thus the styrene-nanocellulose solution was synthesized. Freeze-dried nanocellulose was obtained from Cellulose Lab and modified by introducing a styrene group to its structure. This styrene group has a double bond that facilitates bonding between the radicals generated on the fiber and the nanocellulose. In general, the procedure for the grafting of the styrene onto the nanocellulose was based on the Williamson ether synthesis procedure and is presented here. The nanocellulose was first dispersed in DMSO, and 4-(chloromethyl) styrene was added and mechanically stirred into the mixture. A small scoop of sodium hydride (NaH) was added to start the reaction. The mixture was left stirring on a stir plate, at room temperature, overnight. The product was then centrifuged and thoroughly washed with ethanol. A schematic of the proposed mechanism for the grafting of 4-(Chloromethyl) styrene onto nanocellulose is shown below (Figure 18). After the synthesis of this modified styrene-nanocellulose, an aqueous solution was prepared.

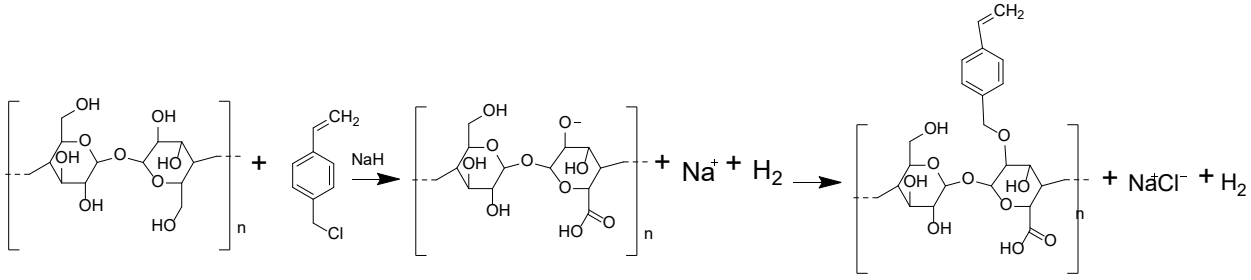

Figure 18. Schematic of the proposed mechanism for the grafting of 4-(chloromethyl)styrene onto nanocellulose.

2.2.2 Preparation of fiber samples for crosslinking studies

For the crosslinking experiments, three 7” pieces of polymer fibers were placed in 7 mL vials with septa caps. This was done to facilitate the subsequent mechanical tests that would be

done on the fibers. A total of 30 samples were sent to Dr. Mark Driscoll at the SUNY College of Environmental Science and Forestry. Of these, 15 samples were purged with acetylene gas, and 15 were dipped in a glycol/trimethylolpropane triacrylate (TMPTA) solution. The samples were then sent back to UMD, where the irradiation and characterization experiments were conducted. The acetylene gas samples were sealed with parafilm before irradiation. TMPTA samples were rinsed with acetone to remove excess solution and irradiated after drying.

2.2.3 Preparation of polyester-based resins for degradation

The polyester resins were used as received from ORNL. The powder samples were placed in 20 mL vials and the bulk samples were placed in 7 mL vials, as shown in Figure 19. Five different environments were studied for each resin: (1) dry at ambient conditions, (2) in water, (3) in DMSO, (4) in a water/DMSO mixture, and (5) in IPA. The powders were soaked overnight in their corresponding solutions before irradiation. All vials were uncapped, and the samples exposed to environmental air during the irradiation.

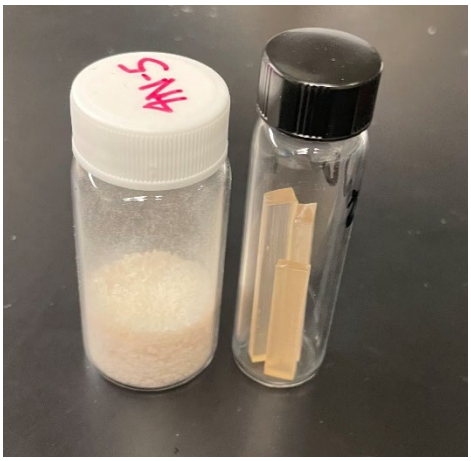

Figure 19. Example of powder and bulk resin samples.

2.3 E-beam irradiation

Irradiation experiments were conducted in the electron beam (e-beam) linear accelerator (LINAC) at the Medical Industrial Radiation Facility (MIRF) at NIST. The MIRF is a radio frequency-powered, traveling wave electron LINAC that provides energies from 7 to 32 MeV. Currently, its optimal operation is reached at an energy of 11 MeV. It has a pulse rate of 120 pulses/sec and an average beam current of 0.1 mA. A schematic of the MIRF is shown in Figure 20.

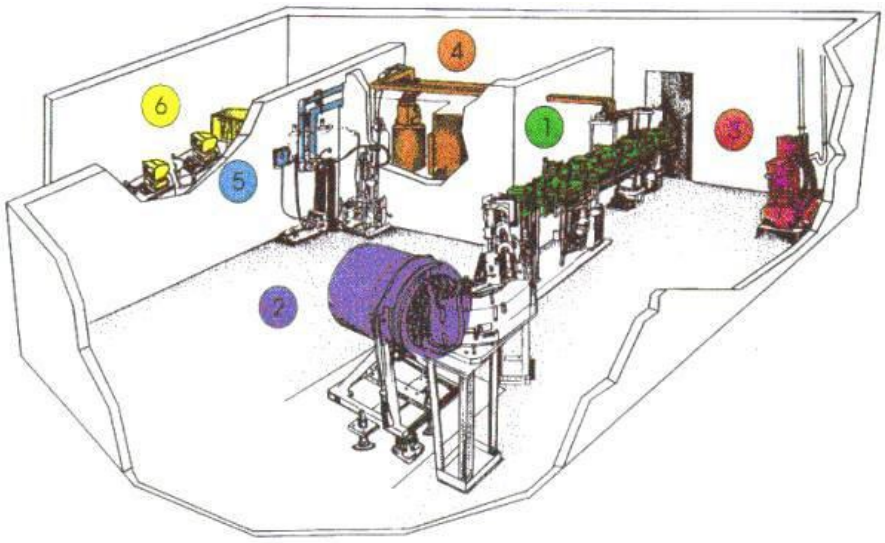

Figure 20. Schematic of the MIRF. In the figure the following are highlighted: (1) two -stage traveling wave rf LINAC, (2) collimator head for medical treatment beam, (3) 380 V motor generator to convert to 50 Hz, (4) 8 MW Klystron and waveguide for 3000 MHz rf, (5) water cooling system, and (6) operator's console and data acquisition system.

2.3.1 Irradiation set-up

Samples were irradiated at a constant dose rate. This can be modified by either changing the current of the e-beam or the position of the sample. Different irradiation set ups were investigated to achieve the highest DoG, and each will be discussed in the next sections. In general, the set up for both the grafting and crosslinking experiments consisted of a foam block positioned 100 cm away from the beam exit window, on which two samples were placed next to each other.

Figure 21 shows the positioning of the samples in front of the beam. Temperature has a significant effect on the radiation-induced grafting process.[156,157] The set-up was adjusted to irradiate the samples at three different temperatures: (1) room temperature with samples irradiated as shown in Figure 21, (2) high temperature where samples were placed in a "hot box" connected to a hot air supply, and (3) sub-ambient temperature where samples were placed in a cooler filled with dry ice.

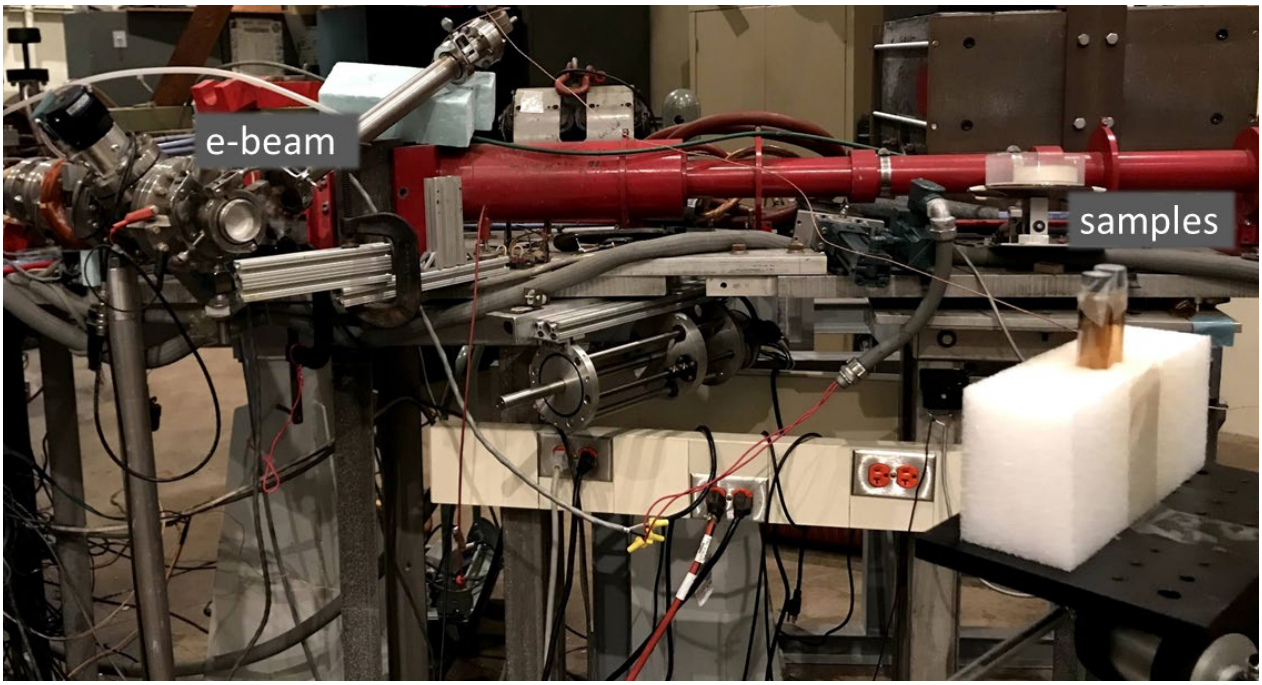

Figure 21. Set-up of sample irradiation in front of the e-beam.

2.3.1.1 Room temperature set-up

The first approach to graft nanocellulose onto the aramid fibers was made by conducting room temperature irradiations of either the fibers by themselves (indirect grafting) or the fibers and the nanocellulose solution (direct grafting). Conducting the irradiations at room temperature has the advantage of requiring less time, as the samples do not need to reach a set temperature before irradiation, and allowing for the grafting of temperature-sensitive monomers for which other grafting techniques might not work.[156] Irradiating the fibers at room temperature and below

their T_g means that the polymer chain is rigid, and the nanocellulose can bond to the radiation-produced free radicals on the outer layer of the material.

2.3.1.2 High temperature set-up

The second approach for the grafting experiments was heating up the polymer fiber inside a "hot box" set up during the irradiation. This set up configuration can be seen in Figure 22. The "hot box" consists of an insulated foam box with two holes cut in the front and back to avoid interference of the foam with the electron beam. Similarly as in the room temperature set-up, the samples were placed on top of a foam block in pairs. To heat the box, a copper pipe attached to a source of pressurized air was connected to the box. A heating tape was wrapped to the outside of the copper tube and the temperature adjusted as desired. As the pipe was heated, hot air was pushed into the box, heating the samples. The temperature was monitored by using two thermocouples, one at the hot air inlet and the other one close to the samples. The samples were placed inside the box and kept at the desired temperature for 5 minutes to reach equilibrium before irradiation.

Figure 22. The inside of the "hot box" insulated irradiation chamber used for high temperature irradiations.

Irradiations performed at high temperature, and above the T_g of the polymer, have the advantage of creating more active sites for the grafting material to attach to. This is the result of the chains having more mobility and the free radicals migrating to the surface, increasing the population of sites available for grafting.[156] It has been reported that high temperature irradiation can maximize the total grafting onto polymer substrates and improved resistance to wear.[158–160]

2.3.1.3 Low temperature set-up

The third approach consisted of placing the samples inside a small cooling box, which could be filled with dry ice. Two holes were cut in the front and back of the box, to avoid interference with the beam. A photo of this set up is shown in Figure 23. This set-up was used to continue the indirect irradiation grafting experiments. In this case a temperature of around -40 °C could be reached and maintained as the irradiation took place. Again, the temperature was monitored using a thermocouple placed inside the box, and the samples were allowed to reach equilibrium before the irradiation started.

Figure 23. The inside of the cooler used as an insulated irradiation chamber for conducting the irradiation experiments at sub-ambient temperature.

For indirect grafting, this low temperature approach was the most successful. Its benefits rely on restricting the mobility of the radicals created after irradiation. The produced radicals are less likely to react, either with each other or with the molecules in the environment, at low temperature. Then, after irradiating and storing the sample, when the nanocellulose is introduced, there are more radicals present in the fibers to which the nanocellulose can attach to. This method has also been shown to be successful for the grafting on a variety of polymers.[161]

2.3.1.4 Crosslinking studies set-up

Samples in acetylene or triacrylate environments were irradiated at room temperature at different doses. The set-up is the same as the one used for the irradiation of fibers at room temperature described in section 2.3.1.1 and shown in Figure 21.

2.3.1.5 Resin degradation set-up

The set-up used for the polymer resin irradiations is shown in Figure 24. In this case, since the experiments consisted of a large number of samples irradiated at the same conditions, a circular, rotating turntable was used as the base. The experiments were conducted in the presence of oxygen, and none of the samples were capped for this experiment. Around 15-20 samples, depending on the size of the vial, could be irradiated at the same time. The rate of rotation was around two turns per minute. A mechanical motor underneath the turntable was used to operate it with an external voltage supply.

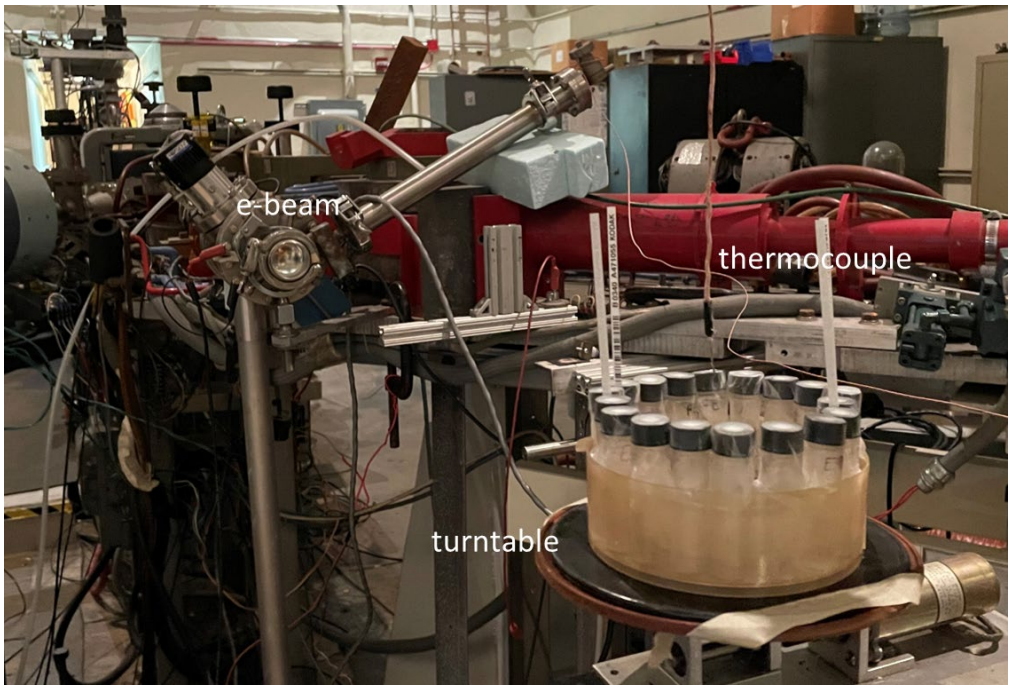

Figure 24. Turntable set-up used to irradiate polymer resin samples at the same time. Picture was taken during the dosimetry measurements and the caps and alanine strips were removed prior to starting the experiments.

Since these samples were irradiated to high doses, the temperature of the solution inside the vials was monitored by placing an additional vial filled with water next to the sample vials and inserting a thermocouple in it. The temperature was kept below 80 °C, to assure that no boiling of the solvents would occur. This was achieved by fractionating the dose; the samples were irradiated continuously until the temperature reached 80 °C at which point the irradiation was stopped. After the temperature decreased to approximately 30 °C, the irradiation was restarted.

2.3.2 Dosimetry

An important aspect of radiation chemistry is the determination of the total dose absorbed by the sample during irradiation. Factors that affect the dosimetry include the sample geometry (type of vial used), physical state of the sample (dry or in solution), and the configuration set-up. Dosimetry was performed only when these conditions were altered. Calibration vials, at the same

conditions, environment, and set up as the main experimental vials, were used for the dosimetry measurements. This entailed one calibration of the vials with only the fibers inside (indirect grafting) and one calibration of the vials with the fibers and the nanocellulose aqueous solution (direct grafting) for the grafting experiments. The same dosimetry was used for the crosslinking experiments, where the fibers are irradiated by themselves. A final dosimetry experiment for the polyester resin samples was also done. Due to a change at the MIRF facilities, two dosimetry methods were used and will be explained in this next section.

2.3.2.1 Alanine-EPR dosimetry system

Kodak BioMax Alanine Dosimeter Films were placed in the front and back of both samples before irradiation as shown in Figure 25. Since the fibers were placed along the length of the vials, the alanine strips were taped vertically on the calibration sample. It was assumed that the total dose received by the sample could be estimated from the average dose received by the front and back strips. The range of the alanine strips allows for calibration between 3 to 80 kGy. Thus, based on previous calibration experiments, the calibration vials were irradiated for a set amount of time (2-3 minutes).

Figure 25. Alanine strips placement for dosimetry measurements.

After irradiation, the alanine strips were taken to an EPR equipped with a dosimeter reader (Figure 26). This EPR is capable of reading the signal from the unpaired electrons generated on the strips during the irradiation. The software integrates the area under the absorption peak obtained, compares it to a standard value, and determines the dose absorbed by the strip. The dose received by the four strips is measured and averaged to determine the total dose received by the sample.

Figure 26. Bruker Alanine Dosimeter Reader. Alanine strips were inserted into the middle cavity after irradiation.

The dose administered to the samples can be adjusted by relating this calculated total dose to the number of counts received by a Faraday cup that is placed behind the samples (Figure 27). A Faraday cup is a metal cup that catches the charged particles leaving the e-beam, which are proportional to the current from the electron beam. The Faraday cup is connected to a current integrator in which 1×10^{-10}C is equal to one single "count", where the particles can be counted as the irradiation is done. Both the total number of counts collected by the Faraday cup and the irradiation time are collected using a counter-timer linked to the current integrator. The counts are then compared to the total dose administered to the sample, calculated through the dosimetry.

Figure 27. Faraday cup in reference to the sample placement.

2.3.2.2 Radiochromic films system

The second dosimetry calibration was done using radiochromic films (Figure 28). Similarly to the alanine strips, the radiachromic films were taped to the front and back of the calibration vials before irradiation. These films contain a dye that is sensitive to ionizing radiation. As the film is irradiated, the color changes, and the dose received can be determined. The energy absorbed by the films was measured using a Thermo Scientific GENESYS 20 Visible Spectrophotometer (Figure 29) and converted into absorbed dose following a calibration graph previously generated at the MIRF. The average dose measured from the films was determined to be the dose received by the sample. After obtaining this value, it was related to the total number of counts determined by the Faraday cup, to get a charge-to-dose measurement with which the total dose administered to the sample can be selected.

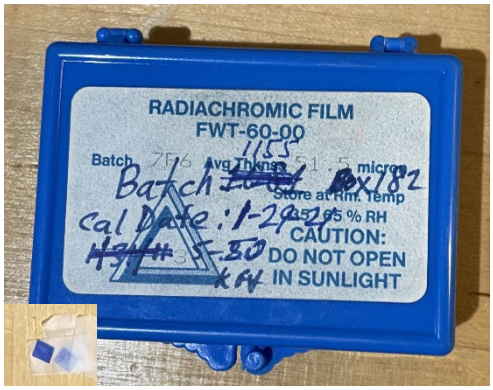

Figure 28. Radiochromic films used for dosimetry.

Figure 29. Visible Spectrophotometer used for radiochromic film dosimetry.

2.4 Post-radiation process

After irradiating the samples, the fibers were processed through a number of steps to complete the grafting process, and in the case of the crosslinked fibers, to avoid degradation. The polyester resins were prepared for characterization. This section will go over the steps taken to study each of these sets of samples.

2.4.1 Samples for direct grafting

Samples used for the direct grafting experiments were washed with DI water to remove excess nanocellulose that had not been grafted. This consisted of using a total of 600 mL of water to rinse the fibers 6 times. UV-Vis Spectroscopy was used to corroborate that all the excess nanocellulose was extracted from the fibers. After washing, the nanocellulose-grafted fibers were dried in a vacuum desiccator for 72 h, until there were no changes in the weight of the samples. After drying, the final mass of the sample was obtained with the use of a mass balance.

2.4.2 Samples for indirect grafting

The samples that were prepared for indirect grafting, and thus consisted of fibers irradiated in an inert atmosphere, were placed in dry ice immediately after irradiation to conserve the free radicals produced. These samples were then transferred to a glove box, or a glove bag, purged with inert gas. Aqueous solutions of nanocellulose or styrene-nanocellulose were also purged with inert gas and transferred into the glove box or glove bag. There, the aqueous solutions were mixed with the fibers, shook thoroughly to ensure complete mixing of the nanocellulose through the fibers, and left mixing overnight. These samples were mixed at three different conditions: (1) room temperature where samples were left inside the glove box, (2) high temperature for which an oil bath was prepared inside the glove box, and (3) low temperature in which the glove bag was placed in a fridge. Similar to the irradiation temperature, the grafting temperature is a crucial parameter in radiation-induced grafting. A temperature of 80 °C was selected to favor the mixing of the nanocellulose onto the fibers. Low temperature grafting (~20 °C) was studied to avoid possible homopolymerization of the styrene-nanocellulose solution.

2.4.3 Samples for crosslinking studies

Fiber samples that were irradiated in an acetylene or triacrylate (TMPTA) environment were annealed following irradiation to avoid the reaction of the radicals created with oxygen. The samples were then kept sealed until characterization.

2.4.4 Polyester resin samples

After irradiating the polyester resin samples, the solvents were removed first through decantation. Then, all the samples were placed in a vacuum desiccator for a week until all the remaining solvent was evaporated. A small amount of each powder sample was then placed in EPR tubes for characterization. These were kept at ambient conditions for follow up measurements up to 6 months after irradiation. The rest of the samples were sent to ORNL for further characterization.

2.5 Sample Characterization

The irradiated samples were characterized at different stages during the experimental process. First, the effects of irradiation on the fibers were analyzed. This entailed looking at the radicals generated through irradiation, the mechanical effects of the irradiation, and the morphology of the fibers. After the grafting process several characterization techniques were used to determine the amount of monomer grafted, to examine the morphology of the sample after grafting, and to study its mechanical properties. In the case of the crosslinking experiment samples, the crosslinking degree achieved was investigated and its effect on the fibers' mechanical properties. The radicals generated after irradiation of the polyester resins were also investigated.

2.5.1 Electron Paramagnetic Resonance (EPR) spectroscopy

The radicals present in the fibers after irradiation were studied by analyzing a batch of irradiated, non-grafted, samples. The principle of EPR spectroscopy is based on the interactions

between unpaired electrons and a magnetic field. This is known as the Zeeman effect. When this interaction happens, the unpaired electron has two allowed energies states, a lower energy state when the moment of the electron (μ) is aligned with the magnetic field ($m_s = +1/2$), and a higher energy state when the μ is aligned against it ($m_s = -1/2$). A schematic of this is shown in Figure 30. The energy difference between the two states, and the energy required for transition between the states is:

$$\Delta E = g\mu_B B_0 \tag{2.1}$$

where g is the g-factor, which helps identify the molecule studied, μ_B is the Bohr magneton (9.274 $\times 10^{-24}$ J/T), and B_0 is the magnetic field.[162]

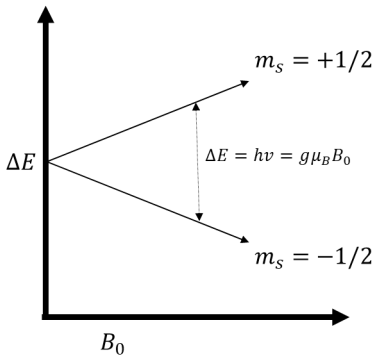

Figure 30. Absorption of energy by the spins, or resonance, occurs when the magnetic field is scanned and the energy difference between the states is equal to the energy of the spectrometer.

A magnetic field, which "tunes" the 2 electron spin states (m_s), and a microwave frequency (ν) are simultaneously applied to the sample. When the energy of the applied radiation (E) is equal to the energy difference between the two states, absorption of energy occurs. The intensity of the energy absorption is recorded by the EPR, usually derived by the software, and the EPR spectrum is obtained. Absorption occurs, and EPR data is collected, when:

$$\Delta E = h\nu = g\mu_B B_0 \tag{2.2}$$

where h is Plank's constant (6.626×10^{-34} J·Hz^{-1}) and v is the frequency at which the signal was recorded.[162]

At a given frequency, the g-factor, which is independent of frequency, can be used to get information about the sample. For example, C-centered radicals have a g-factor close to the g-factor of the free electron (g~2.0023). Nitroxide radicals have been found to have a g-factor ~ 2.006, while the g-factor of metal ions can vary greatly.[163]

The EPR spectra provides more information about the sample in terms of the hyperfine interactions, which are the interactions between the magnetic moments of the electron and the nuclei of the molecules. When the free radical is located near the nuclei, the nuclei produce a magnetic field (B_1) on the free radical, which either adds or subtracts from the magnetic field applied by the EPR (B_0). Depending on the alignment of the moment of the nucleus (parallel on antiparallel) B_1 can be either positive or negative. The total magnetic field is then defined as:

$$B = B_0 \pm B_1 \tag{2.3}$$

If, for example, the electron spin interacts with 1 Hydrogen atom, which has a spin (I) of ½, the absorption signal splits into two identical peaks. If there are 2 H atoms, it would further split into two more peaks, resulting in a spectrum with a quartet signal. This splitting follows Pascal's triangle. Thus, the number and the manner in which the signal is split provides information about the environment of the free radical present in the sample. The more nuclei in the vicinity of the free radical, the more signals present in the spectrum. If the number is too high, signals may overlap resulting in a broad number of signals observed.[163] The number of lines in the EPR spectrum, or total number of hyperfine splittings can be calculated with the following formula:

$$\prod_i (2M_i I_i + 1) \tag{2.4}$$

where M is the number of the adjacent H atoms, and I is spin number of the nuclei.[164]

EPR spectroscopy measurements were carried out in a Bruker EMX EPR spectrometer at room temperature (Figure 31). The instrument was calibrated before each set of measurements with a 2,2-diphenyl-1-picrylhydrazyl (DPPH) stable free-radical sample. The spectra were acquired at X-band frequency, a microwave power of 5.0 mW, a frequency modulation of 100 kHz, and a modulation amplitude of 3.12 G. Spectra was collected with 600 G sweep width centered at 3500 G and represents the average of 4 scans.

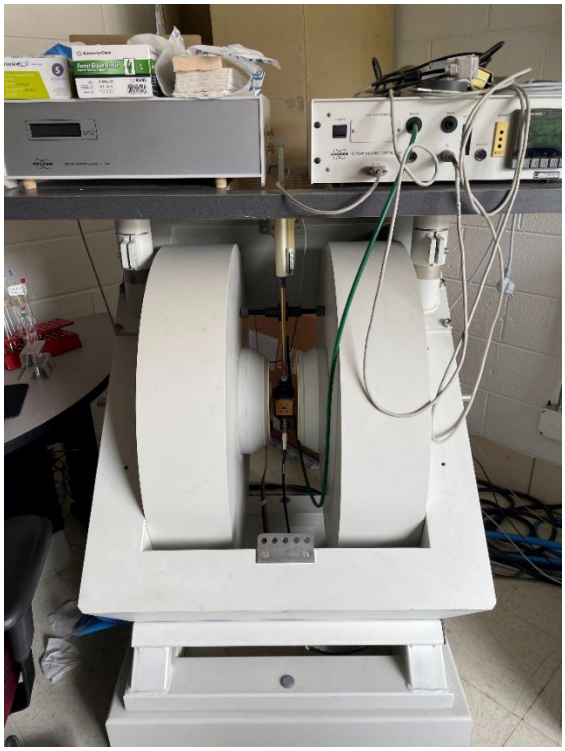

Figure 31. Bruker EMX EPR spectrometer

After irradiating the polymer fiber samples in an inert atmosphere and at sub-ambient temperature, they were placed in a cooler filled with dry ice and moved to a glove box purged with

inert gas. In the glove box, the samples were transferred from the irradiation vials to EPR tubes and sealed with parafilm to limit the presence of oxygen. Then the samples were brought to the EPR and analyzed.

In the case of the polyester resin samples, powder samples were transferred to EPR tubes at ambient conditions and characterized. The samples were left in ambient conditions for 6 months, with measurements taken at different time intervals.

The concentration of radicals in each sample can be determined by using a standard sample with a known number of spins per gram, and calculating the concentration by proportion using the following equation:

$$[x] = \frac{[std]A_x R_x (scan_x)^2 G_{std} M_{std} (g_{std})^2 [s(s+1)]_{std}}{A_{std} R_{std} (scan_{std})^2 G_x M_x (g_x)^2 [s(s+1)]_x} \tag{2.5}$$

where [ ] is the concentration of radicals (spins/g), A is the area under the absorption curve obtained by EPR, R is the degeneracy of the spectrum, g is the g-value of the radical, also known as the fingerprint of the radical, s is the electron spin quantum number, and the instrument parameters: G is the signal amplifier gain (Hz), M is the amplitude of the modulation (G), and $scan$ is the sweep width (G). The subscripts std and x refer to the standard manganese sulfate monohydrate ($MnSO_4 \cdot H_2O$) sample, and the experimental sample, respectively.

2.5.2 UV-Vis Spectroscopy

For the samples that went through the grafting process, UV-Vis spectroscopy was done to confirm that all non-grafted nanocellulose had been removed from the fiber surface. The absorbance of the DI water rinsing solution was measured in a Cary 300 Bio UV-Vis

Spectrophotometer between 200 to 800 nm. A DI water sample was used as the standard for comparison.

2.5.3 Fourier transform infrared (FTIR) attenuated total reflection (ATR) spectroscopy

FTIR-ATR was used to confirm the grafting of the styrene-containing linker onto the nanocellulose and as an initial probe of the grafting of the nanocellulose onto the fibers. In this technique, IR light travels through a crystal and into a sample. As the light travels into the sample, in the regions of the IR spectrum where the sample absorbs energy, the evanescent wave is attenuated. This attenuated beam is reflected back to the crystal, towards the detector. Depending on the covalent bonds of the molecule, radiation can be absorbed or transmitted. Since different bonds absorb at different energies, the IR spectrum is used to identify these bonds. All FTIR-ATR measurements were carried out using a Thermo Scientific Nicolet iS50 FTIR equipped with a Nicolet iTX Diamond attenuated total reflectance (ATR) accessory. Samples were run from 525 to 4000 cm^{-1} with a resolution of 8 cm^{-1} with 96 scans per sample. The surface of the ATR attachment was cleaned with acetone, ethanol, methanol, and water, and dried prior to every measurement. Background spectra was collected before each sample. Each sample was measured twice, at two different locations chosen randomly. A comparison of the spectrum of the nanocellulose sample before and after grafting, was used to show the changes in the chemical structure after grafting the styrene-containing linker.

2.5.4 Gravimetric Analysis

The total amount of grafting achieved was quantified through gravimetric analysis. The weight of the fibers was first taken prior to irradiation. After the grafting procedure, the fibers were washed with DI water as describe in section 2.4, and dried. The final weight of the fibers was then re-taken. A MS205DU Mettler-Toledo scale was used to determine the mass of the fibers before

and after grafting. These measurements were then used to calculate the final Degree of Grafting (DoG) achieved (eq. 1.13).

2.5.5 Scanning Electron Microscopy (SEM)

The morphology of the fibers before and after irradiation, and after grafting, was studied through SEM. Irradiation of the fibers results in the formation of divots and irregularities on the surface of the fibers which can be observed by SEM. After nanocellulose grafting, its distribution on the fiber surface can be analyzed in terms of homogeneity and density. The characterization was conducted in a Tescan XEIA Field Emission Gun (FEG) SEM. The fibers were taped to the specimen holder using conductive double-sided carbon tape and coated with a thin (<20 nm) conductive gold and platinum layer using a Hummer X Sputtering System.

2.5.6 Solid-state nuclear magnetic resonance (ssNMR) spectroscopy

Grafted samples were characterized with ssNMR in order to identify the bonding between the styrene-nanocellulose and the aramid fibers. Solid-state natural abundance ^{13}C and ^{15}N NMR spectra of magic angle spinning (MAS) samples were acquired on a Bruker AVANCE NEO 500 MHz NMR spectrometer using the combination of standard cross-polarization (CP) with proton spinal-64 decoupling. Samples were packed in 3.2 mm o.d. rotors and run in Bruker 3.2 mm H/F-X double resonance probe. Proton 90° pulse widths of 2.5 μs and contact times of 2 ms were used to acquire both ^{13}C and ^{15}N NMR spectra. The pulse delays of 5 s and 4 s were used to acquire both ^{13}C and ^{15}N NMR spectra, respectively. Carbon-13 chemical shifts were referenced with respect to TMS by setting $\delta(^{13}C) = 0$ ppm and nitrogen-15 chemical shifts were referenced with respect to α-glycine by setting $\delta(^{15}N) = 33.4$ ppm. Spectra of MAS samples were acquired at ambient temperature with spinning frequency of 8 to 15 kHz and spinning sidebands were confirmed by running experiments with a different spinning rate. ^{13}C CP/MAS NMR experiment

was acquired with a total scan of 2k to 30k and ^{15}N CP/MAS NMR experiment was acquired with a total scan of 18k to 60k depending on the sample amount.

2.5.7 Single fiber testing

The effects of the irradiation and grafting on the fibers were analyzed by conducting single fiber tensile tests. Three sets of samples were studied (1) fibers irradiated in inert atmosphere at different total doses, (2) nanocellulose-grafted fibers at different doses and different post-irradiation conditions, and (3) fibers irradiated in acetylene or triacrylate environments. Single fiber tensile tests were carried out in a FAVIMAT tester (Figure 32) equipped with a 210 cN load cell, at a gauge length of 20 mm and a test speed of 2.0 mm/min. Irradiated yarns of fiber were cut to approximately 30 mm and single fibers of aramid were chosen randomly and separated with a mini spring clamp. After separating the single fibers, a pair of tweezers was used to place the unclamped end of the fiber on the top grip of the FAVIMAT. The mini clamp hung off the end of the bottom grip, keeping the fiber taut. The bottom grip was then closed, gripping the fiber at the bottom edge, and starting the testing. To achieve high confidence results, at least 50 specimens of each treatment condition were tested.

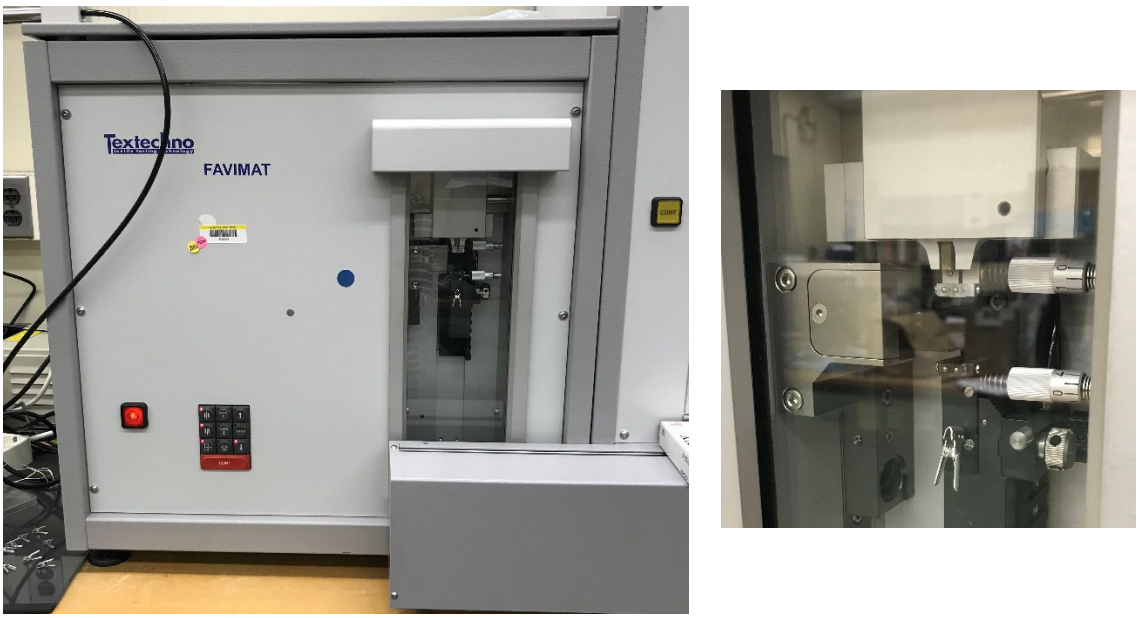

Figure 32. FAVIMAT single-fiber tester used for the mechanical testing of aramid fibers. Inset on the right shows the set-up, with a mini spring clamp placed on the end of the fiber which kept them taught.

Weibull statistics are generally used for the analysis of the tensile strength of single fibers. Weibull combined the weakest link theory, which indicates that overall failure of the fiber happens when the segment with the lowest individual strength fails, with the two-parameter power law. Thus, the failure probability of the fibers can be described by the following distribution:[165,166]

$$F_l(\sigma) = 1 - \exp\left\{-\left(\frac{l}{l_0}\right)\left(\frac{\sigma}{\sigma_{l_0}}\right)^{\rho}\right\}, \sigma \geq 0 \tag{2.6}$$

where l is the length of the fiber, l_0 is an arbitrary reference length, σ is the stress, σ_{l_0} is the Weibull scale parameter at length l_0, and ρ is the Weibull shape or flaw dispersion parameter.

The Weibull distribution was applied to determine how irradiation affects the mechanical properties of the fibers. A Weibull probability plot, showing 99% confidence bounds, was analyzed in order to see how irradiation affected the distribution. This plot compares the distribution of the data to the Weibull distribution. The Weibull shape and scale parameters also

offer information about the fiber strength. The shape parameter shows how the values are distributed, whether in a clustered or dispersed manner, and is inversely related to the standard deviation. The scale parameter gives information about how the strength of the fibers varies with irradiation.

Through tensile tests, the Favimat measures the following fiber parameters: elongation (%), force (N), tenacity (g/den), and work (g*cm). It also determines the linear density (den) of the single fibers by using a vibration method; following the ASTM D 1577, the resonance frequency of the fiber is measured at a set gauge length and known pre-tension. The software presents the data as a typical tenacity (N) as a function of the elongation (%) curve.

2.5.8 Gel Content

The crosslinking degree of the samples was determined based on swelling experiments conducted on the fibers before and after grafting. After irradiating the fibers in acetylene and triacrylate (TMPTA) environments and annealing them, fibers were dissolved in sulfuric acid (H_2SO_4). The fibers were left stirring inside a glove box purged with inert gas overnight. Then, the fibers were washed with DI water and the undissolved fiber was weighted. The change in weight is proportional to the degree of crosslinking of the fibers.

2.5.9 Dynamic Mechanical Analysis

The changes in the glass transition temperature of the polyester resins were investigated through Dynamic Mechanical Analysis (DMA). The bulk irradiated samples were placed in the DMA in single cantilever mode. An oscillatory strain amplitude of 0.1 % at a frequency of 1 Hz was applied to the samples and the temperature was changed at a rate 3 °/min. The glass transition temperature of the resins was reported as the peak of the plot of the tan δ as a function of temperature.

$$tan\delta = \frac{G"}{G'} \tag{2.7}$$

where G" is the loss modulus and G' is the storage modulus.

3. Results and Discussion

A variety of irradiation-induced grafting techniques were studied to achieve the objectives of this project and to produce a new material – nanocellulose-grafted polymer fibers. Preliminary studies focused on the effects of e-beam irradiation on aramid fibers both dry in N_2 environment and in a N_2O saturated water system. The next phase of the project dealt with the grafting of unmodified nanocellulose onto the aramid fibers, by direct and indirect grafting. However, low degrees of grafting were initially obtained under several different conditions for both the direct and indirect grafting experiments. Thus, a styrene-containing linker was introduced to the nanocellulose through chemical grafting to provide a double bond to which the free radicals generated on the aramid after irradiation could bond to. After achieving the synthesis of this styrene-nanocellulose, the following phase focused on grafting this material onto aramid fibers. The samples were evaluated for free radical generation, degree of grafting, morphology, chemical structure, and its mechanical properties.

The conditions in which irradiation could be used to promote crosslinking in polymer fibers by modifying its irradiation environment were also investigated. The results presented in this work show successful crosslinking and the subsequential effect on the fibers' mechanical properties. However, due to the presence of C-O-C bonds in the backbone of the chains of certain polymers, radiation induced grafting or crosslinking cannot be achieved for these types of materials. Rather the radiation induces scissions (not crosslinking) on the backbone of these chains. Radiation-induced scission of the polyester-based resins were also consequently examined in parallel. These radiation-induced scission reactions may facilitate the recycling of polyester waste. The following sections include the results obtained from the experiments conducted for each of these three projects and their respective discussions.

3.1 Effects of irradiation on aramid fibers

As a first step towards radiation grafting on aramids fibers, the main preliminary experiments for this project focused on the study of the effects of irradiation on aramid fibers. Two sets experiments were conducted: (1) aramid fibers irradiated in the presence of water, at a ratio of 100:1 water to fiber, and (2) aramid fibers irradiated dry in an inert environment. At first, both sets were irradiated at lower (50-80 kGy) irradiation doses. Larger doses were then studied to maximize the generation of free radicals on the fibers. Since the nanocellulose solution is aqueous, it was important to study the effects of water radiolysis during the irradiation. These effects would be significant when conducting direct grafting experiments, where the nanocellulose aqueous solution and the fibers were irradiated together. As the experiments continued, it was decided that indirect grafting was the most promising approach, and the studies on irradiation of aramid dry in inert atmosphere were expanded. In this section the data collected for these studies will be presented.

3.1.1 Determining the structures of the radiolytically produced free radicals of aramid fibers under anaerobic conditions using EPR spectroscopy

The first step to understanding the effect of irradiation on the fibers was to take EPR measurements of the fibers after irradiation. The type and concentration of the free radicals generated after irradiation was measured with EPR. Aramid fiber samples were irradiated at doses of 50, 100, 150, and 300 kGy, at a dose rate of approximately 400 kGy/h using the MIRF e-beam. The first experiments were done without water and in an inert atmosphere that was achieved after purging the vials containing the fibers with N_2 gas. The samples were kept in dry ice during and after the irradiation and transferred to EPR tubes as described in section 2.5.1. All measurements were taken at room temperature.

The EPR spectrum of non-irradiated aramid fiber is shown in Figure 33. There is a small peak at 3349.6 G and a wider peak at 3483.2 G, with g-factors of 2.0878 and 2.0081, respectively. These background free radicals have been previously reported in literature and have been ascribed to trapped radicals and paramagnetic impurities introduced during the manufacturing process.[167–169] However, their concentration is more than an order of magnitude less than the concentration of radicals in the fiber after irradiation. Thus, they were determined to not be large enough to affect the detectability of the free radicals generated during the irradiation.

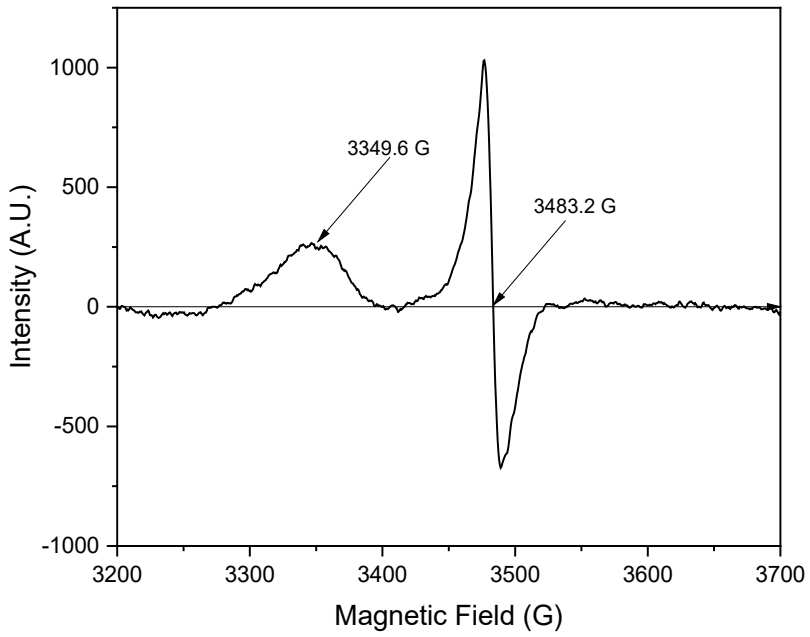

Figure 33. 1st derivative EPR spectrum of non-irradiated aramid fiber purged with inert gas.

Figure 34 (left) shows the EPR spectra of the fibers irradiated at 50, 100, and 150 kGy in the absence of oxygen, as well as a non-irradiated fiber for comparison. Although the intensity of the signal increases with dose, the peak stays at around 3488 G, consistent with a g-factor of 2.0052 which is reported for C-centered radicals.[170,171] Slight shifts in the x-axis are related to the change

in frequency, which the instrument tunes for each sample. The expected mechanism for the generation of free radicals after irradiation, and the hyperfine prediction, will be discussed below. The concentration of radicals for the different irradiation doses was calculated using equation 1.18 and the results are shown in Figure 34 (right). As expected, with an increase in irradiation dose there is more scissions of the C-N aramid bonds which results in an increase of the free radicals. Radical concentration is expressed in terms of spins per gram and a concentration of 6.17 x 10^{19} spins/g was achieved on the samples irradiated at 300 kGy. This signifies a high concentration of free radicals available for grafting. Even at the lowest dose studied of 50 kGy, the concentration of the free radicals is at least an order of magnitude larger than the concentration before irradiation which was 4.12 x 10^{18} spins/g.

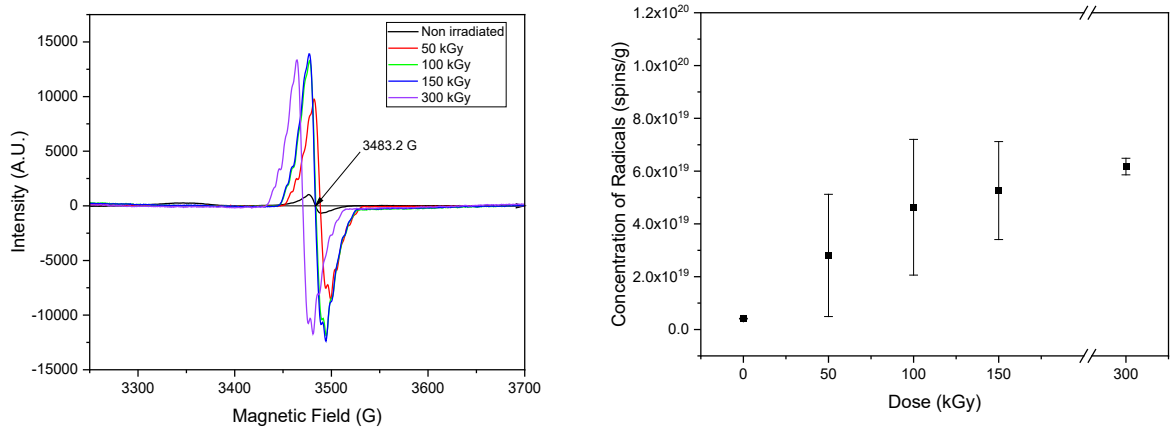

Figure 34. 1st derivative EPR spectra of non-irradiated and irradiated aramid fibers treated at 50, 100, and 150 kGy in inert conditions (left), and the concentration of radicals generated at the different irradiation doses (right).

As mentioned before, the EPR measures the intensity of the energy absorbed when a magnetic field is applied to a sample. Although the 1st derivative of the absorption spectrum is commonly shown as EPR, it is interesting to look at both the absorption spectrum and at the second derivative. Figure 35 shows the absorption spectrum (Fig. 35a), the first derivative of the

absorption spectrum (Fig. 35b), and the second derivative of the absorption spectrum (Fig. 35c) obtained from EPR measurements. The concentration of radicals is obtained by calculating the area under the absorption curve by integration. As described in section 2.5.1, EPR spectra is commonly displayed as the 1st derivative because of the detection method of the instrument, in which the signal to noise ratio is optimized. The second derivative can be used for easier visualization of the peaks detected. Looking at the 2nd derivative can be useful for identifying both slight changes in the slope of the spectrum and its center. The high number of peaks centered at around 3483 G are consistent with the generation of a broad number of free radicals. The high number of radicals generated causes an overlap of the signals.[163] This makes it more complicated to identify individual radicals present in the sample. The 2nd derivative shows the same information as the 1st derivative, but it enhances the features at the expense of broader peaks.[172]

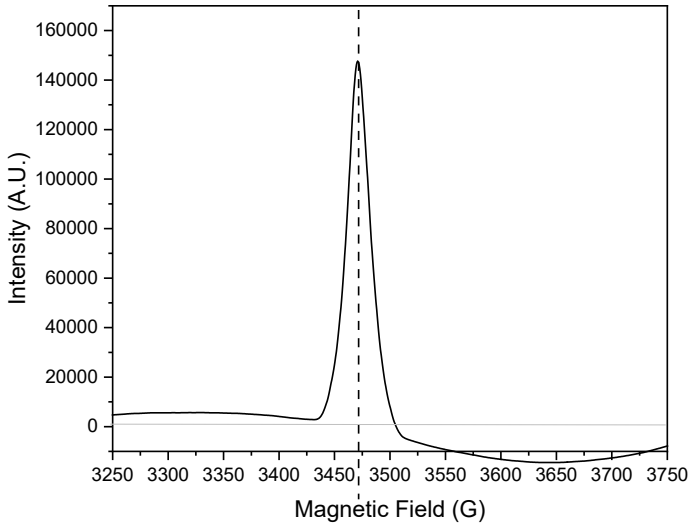

(a)

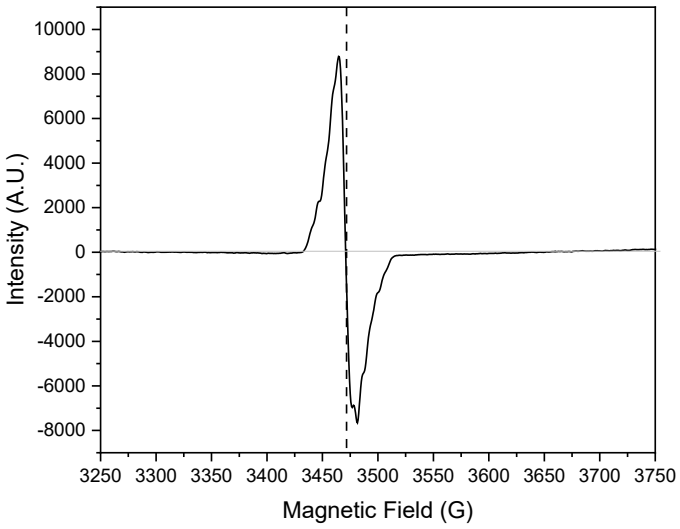

(b)

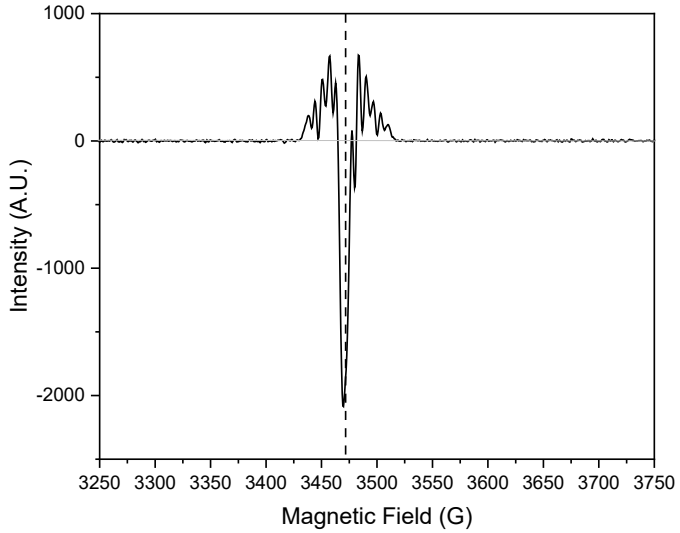

(c)

Figure 35. (a) Absorption, (b) first derivative, and (c) second derivative EPR spectrum of aramid fibers irradiated dry in N_2 environment at 150 kGy.

Figure 36 depicts possible mechanisms and the resulting free radicals produced by irradiation-induced scission of aramid fibers. Chain scission of the C-N bond has been accepted as the most likely result of irradiation of aramid fibers in inert environments.[173,174] It is important to note that the aramid samples were irradiated in a completely inert atmosphere and precautions were taken to prevent O_2 diffusion into the samples. As shown in the schematic, oxygen reacts very rapidly with the radiolytically produced C-centered free radicals of the aramid molecules leading to the impeding of the grafting reactions.

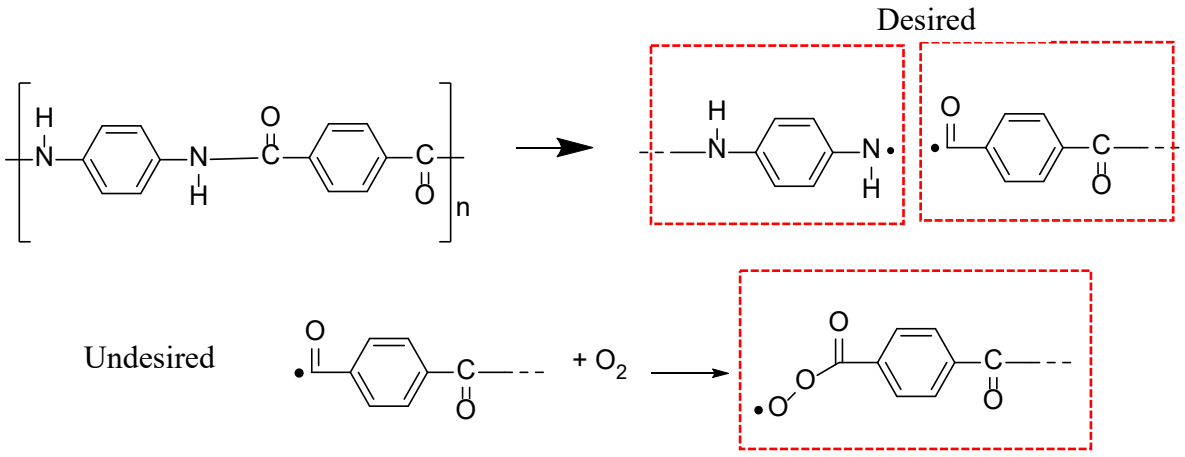

Figure 36. Proposed mechanisms for the formation of radicals after irradiation of aramid fibers in inert atmosphere.

3.1.2 Determining the structure of the radiolytically produced free radicals of aramid fibers in the presence of N_2O-saturated H_2O using EPR Spectroscopy

Preliminary studies on the effects of the irradiation of aramid fibers in the presence of water were also conducted. For this part, the fibers were irradiated at 50, 100, and 200 kGy, in the presence of water and in vials saturated with N_2O. Figure 37 shows the 1st derivative EPR spectra for these samples. Since these samples had to be dried prior to irradiation at room temperature, the concentration of radicals cannot be correctly calculated. However, it is clear that the shape and centering of the peak is similar to the samples irradiated dry in inert atmosphere. In this case, the

center was identified to be at 3451 G and the g-value at that point is 2.0045. The slight decrease in g-value is a result of the positioning of the C-centered radical in the aramid structure. Instead of the discussed scission of the C-N bond after irradiation of the dry fibers in inert atmosphere, aramid fibers irradiated in water and saturated with N_2O gas are expected to generate radicals at different positions. This will be discussed next.

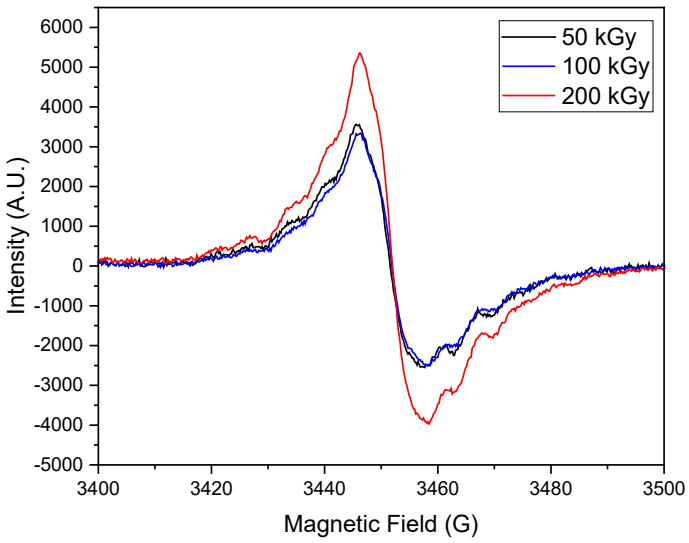

Figure 37. 1st derivative EPR spectra of irradiated aramid fibers treated at 50, 100, and 150 kGy in an aqueous environment and saturated with N_2O.

In these irradiation experiments, the mass ratio of aramid fiber to water was 100 to 1. Under these experimental conditions, water absorbed most of the energy from the accelerated electrons resulting in the formation of the following active species with their radiation chemical yields in micromole per joule:

$$G(^{\bullet}OH) = G(e_{aq}^{-}) = G(H_3O^{+}) = 0.29,\ G(^{\bullet}H) = 0.062,\ G(H_2) = 0.042,\ G(H_2O_2) = 0.082$$

Hydroxyl radicals ($^{\bullet}OH$) constitute a powerful oxidant, and they are highly reactive (through addition, abstraction, or electron transfer).[175] On the other hand, hydrated electrons (e_{aq}^{-})

are very strong reducing radicals and can be converted to •OH radicals through the following reaction:

$$N_2O + e_{aq}^- + H_2O \rightarrow {}^{\bullet}OH + N_2 + OH^- \quad (3.1)$$

The above reaction is very fast, with a reaction rate constant of $9.1 \times 10^9\ M^{-1}s^{-1}$.[153] Thus, saturating the system with N_2O prior to irradiation would double the •OH yield to G(•OH) = 0.56 micromole per joules. Under these experimental conditions, and in the absence of oxygen, •OH radicals are expected to undergo the following competing reactions on the backbone of the aramid polymer chains, abstraction of H atoms from NH or addition reaction onto the phenyl group (Figure 38).

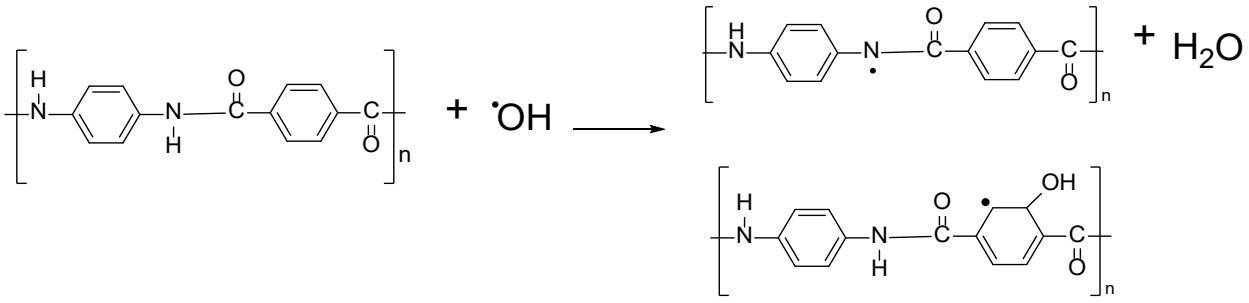

Figure 38. Proposed mechanisms for the formation of radicals after irradiation of aramid fibers in water and saturated with N_2O.

These reactions lead to the immediate formation of N-centered radical ((-H) Aramid-N•) and C-centered radicals (OH-Aramid•). Both, the addition and abstraction reactions are very fast with reaction rate constants of 5-6 $x10^9$ $M^{-1}s^{-1}$.[176] It is expected that the immediate concentrations of [((-H) Aramid-N •)] and [OH-Aramid•] are comparable due to the almost equivalent •OH abstraction and addition reaction rate constants, and the ratio of the NH group to the phenyl group on the backbone of the aramid chain being one. It should also be mentioned that, in addition to •OH, H-atoms (•H) with G(•H) = 0.062 micromole per joule, also add to the phenyl group and

abstract H from NH group. Figure 38 shows a schematic of the proposed mechanism after irradiation of aramid fibers in water. The main advantage of this approach is the possible avoidance of backbone scission of the C-N bond.

These studies on the irradiation of aramid in water are significant for the direct grafting experiments. The procedure for direct grafting consists of a one-step process where the fiber is placed in the nanocellulose aqueous solution and both the fiber and the nanocellulose are irradiated together. Thus, the radicals generated in both the fiber and the nanocellulose are a result of the water radiolysis. For indirect grafting, the fiber is irradiated by itself. The fiber cannot be immersed in water during the irradiation as it would freeze over from the use of dry ice. This would then require waiting for the fibers to thaw before starting the grafting process. However, that would expose the generated radicals exposed to air and decrease the total amount of grafting.

3.1.3 Determining the radiation-induced chemical changes of aramid fibers using FTIR spectroscopy

FTIR analysis after irradiation of aramid fibers both in a dry state in a N_2 environment and in water saturated with N_2O was conducted to look at possible changes in the chemical structure of the aramid caused by the irradiation. Figure 39 shows the FTIR of non-irradiated aramid fiber and highlights the main IR peaks of the aramid. The data was normalized based on the aromatic deformation peak at 820 cm^{-1}, which is unaffected by aramid irradiation.[177–179] A C-H stretching vibration of the aromatic rings occurs at 820 cm^{-1}. The Amide III (C-N stretch and C-H) characteristic peaks occurs at 1254 cm^{-1}, the Amide II (N-H bend and C-N stretch) occurs at 1514 cm^{-1}, and the Amide I (C=O) stretch occurs at 1656 cm^{-1}. At the start of the spectrum, 3302 cm^{-1}, the Amide A (N-H stretch) is observed.[179–181]

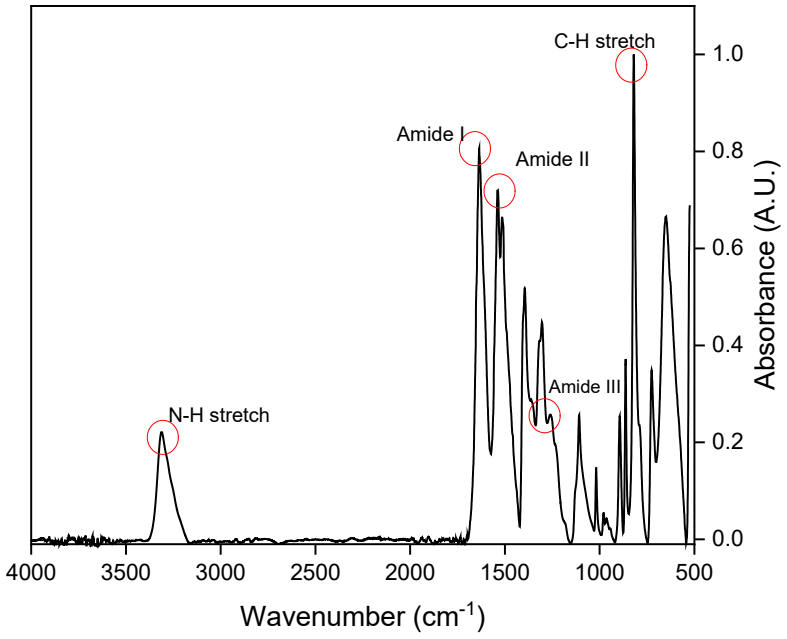

Figure 39. FTIR spectrum of non-irradiated aramid fibers and assigned IR peaks.

Figure 40 shows the FTIR spectra of aramid fibers irradiated at 200 kGy dry in N_2 atmosphere and in the presence of water saturated with N_2O. The high dose was selected because higher doses are expected to result in the most damage to the fiber, but similar analysis was done of the samples irradiated at all doses. It can be seen that there were no changes in the bonds present in the aramid fiber, before and after the irradiation, detected by the FTIR. Although not definite proof that there was no damage to the chemical structure of the aramid, this is the first step in determining any degradation of the structure of the fiber, which could lead to a decrease in its mechanical properties.

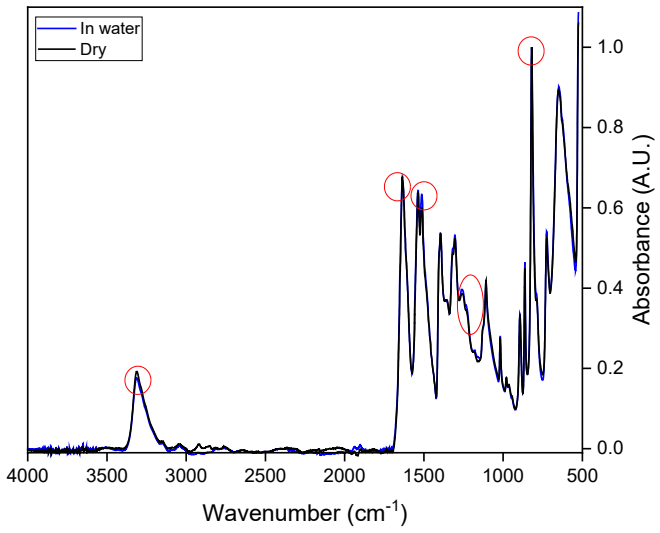

Figure 40.FTIR spectrum of aramid fibers irradiated at 200 kGy, dry in N_2 atmosphere (black) and in the presence of water saturated with N_2O (blue) and assigned IR peaks.

3.1.4 Single fiber testing of irradiated aramid fibers

Tensile tests of the aramid fibers, irradiated both dry in N_2 atmosphere and in the presence of water saturated with N_2O, at different irradiation doses, were conducted to look at the effects of the irradiation on their mechanical properties. As discussed in the previous section, the strength of the fibers can be described by the weakest link Weibull model. Weibull probability plots of the collected data with 99% confidence intervals were analyzed to see how irradiation affected the distribution. To achieve relatively high confidence intervals, at least 100 tests were run for each condition. Figure 41 shows the Weibull probability plots, where the failure distribution is plotted for the samples irradiated dry in N_2 atmosphere at the different irradiation doses, and the 95% confidence interval are shown by the dashed lines. The general positioning of the curve which does

not shift left or right, and the overlapping of the data, shows that there is no degradation of the tensile strength of the fiber after irradiation.

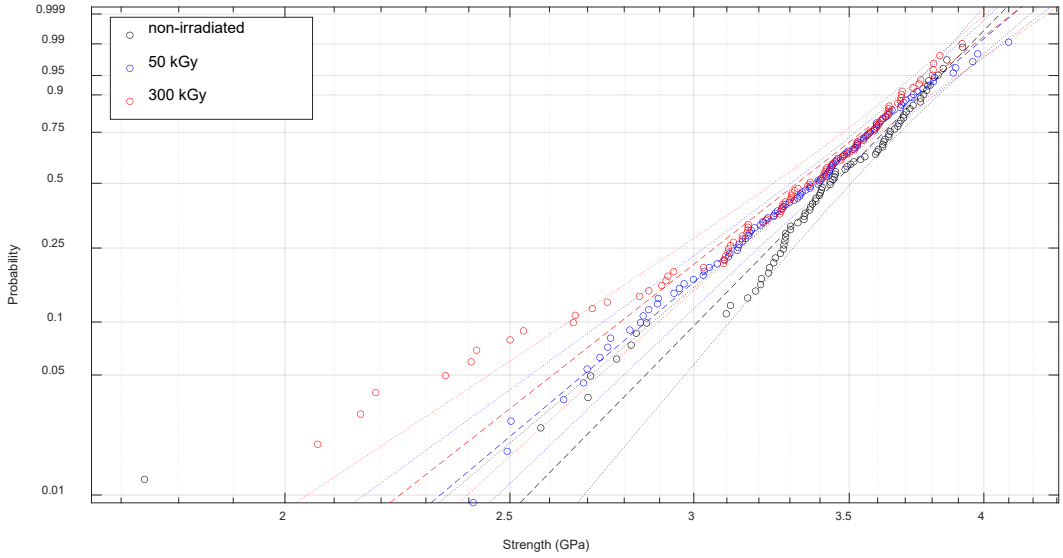

Figure 41. Weibull probability plots of failure strength for fibers irradiated to 0, 50, and 300 kGy dry in N_2 atmosphere, tested with a 20 mm gauge and at 0.75 mm/min.

The Weibull distribution scale and shape parameters for the samples irradiated dry in N_2 atmosphere at different doses are shown in Table 5. The scale parameter has a generally downward trend, which could show some degradation as the dose is increased. However, there are no big changes when comparing with the nonirradiated sample. In the case of the shape parameter, a decrease signifies that there is more variability in the strength of the fibers as irradiation dose increases.

Table 5. Weibull scale and shape parameters for fibers irradiated dry in inert atmosphere at different doses.

Dose (kGy)	Weibull scale parameter	Weibull shape parameter
0	3.53906	13.9436
50	3.48126	11.4965
100	3.49387	10.0673
150	3.47641	10.2517
300	3.4386	10.7523

Single fiber tensile tests were also conducted on fibers irradiated in the presence of H_2O at 50 and 80 kGy during the preliminary studies. Similar behavior to the fibers irradiated dry was observed (Figure 42). The data points are agglomerated and there are no significant shifts in the plot. The Weibull parameters also follow the same trend as the samples irradiated dry (Table 6).

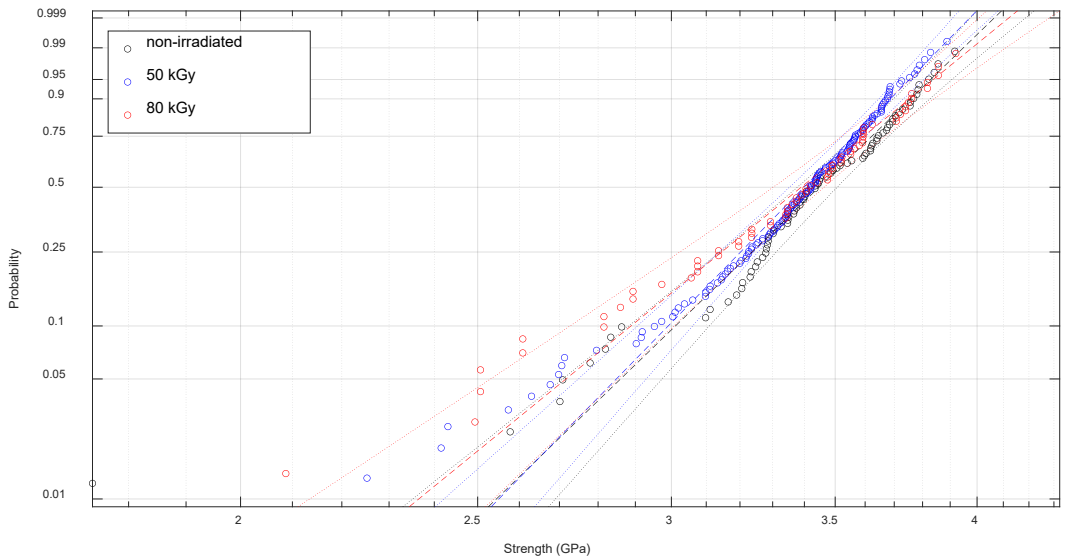

Figure 42. Weibull probability plots of failure strength for fibers irradiated to 0, 50, and 80kGy in the presence of water, tested with a 200 mm gauge and at 2 mm/min.

Table 6. Weibull scale and shape parameters for fibers irradiated in water saturated with N_2O at different doses.

Dose (kGy)	Weibull scale parameter	Weibull shape parameter
0	3.53906	13.9436
50	3.48433	14.743
80	3.49691	11.766

From these studies, it was concluded that e-beam irradiation of the aramid fibers can be pursued for further fiber modification. There was no significant damage to the strength of the fibers caused by the irradiation. Since the aim of the thesis was to improve the mechanical properties of the aramid fibers, it is important for the fibers to not be damaged during the irradiation process. The Weibull plot is widely used to display and visualize strength distributions. The results from all the tested fibers show a narrow distribution, in which the data points collected all agglomerate in the same position for the untreated and the irradiated fibers. This is a result of the aramid's high resistance to radiation as will be discussed in the conclusion. In terms of the positioning of the curves, drastic changes in the strength of the fibers can be observed by shifting of the curves to the left, such as what was seen for aged aramid fibers by Engelbrecht-Wiggans, et al.[182] They showed that degradation can be demonstrated by shifts between the curves in the probability plots. In this case, there is no shifting identified after irradiation, which could signify that no significant damage was done to the fibers during the irradiation. Since the goal is to increase the strength of the fibers, damage by irradiation should be minimized. These are promising results for the subsequent irradiation modification of aramid fibers.

3.1.5 SEM Morphological changes after irradiation

The effects of the irradiation on the morphology of the aramid fibers were analyzed by SEM. After irradiation of the fibers at 150 kGy dry, in inert conditions slight differences between the fibers can be observed. In Figure 43 the nonirradiated fibers show a smooth surface which is the main reason for the fiber's poor adhesion in composites. The smooth surface of the fibers becomes more irregular after irradiation with the e-beam. The appearance of these irregularities and grooves on the surface of the fiber may be interpreted as physical damage to the fibers. More work is needed to completely identify these results and the cause of the changes. Looking at the fibers at a higher magnification would give more insight into this. In this case, the bombardment of the surface with the electrons influence the directionality of the etch profiles.[183] If these irregularities were present in a significant region of the fibers they could act as a mechanical anchor and increase the fiber-resin interactions at the interface. In terms of the width of the fibers, it remains unchanged after the irradiation.

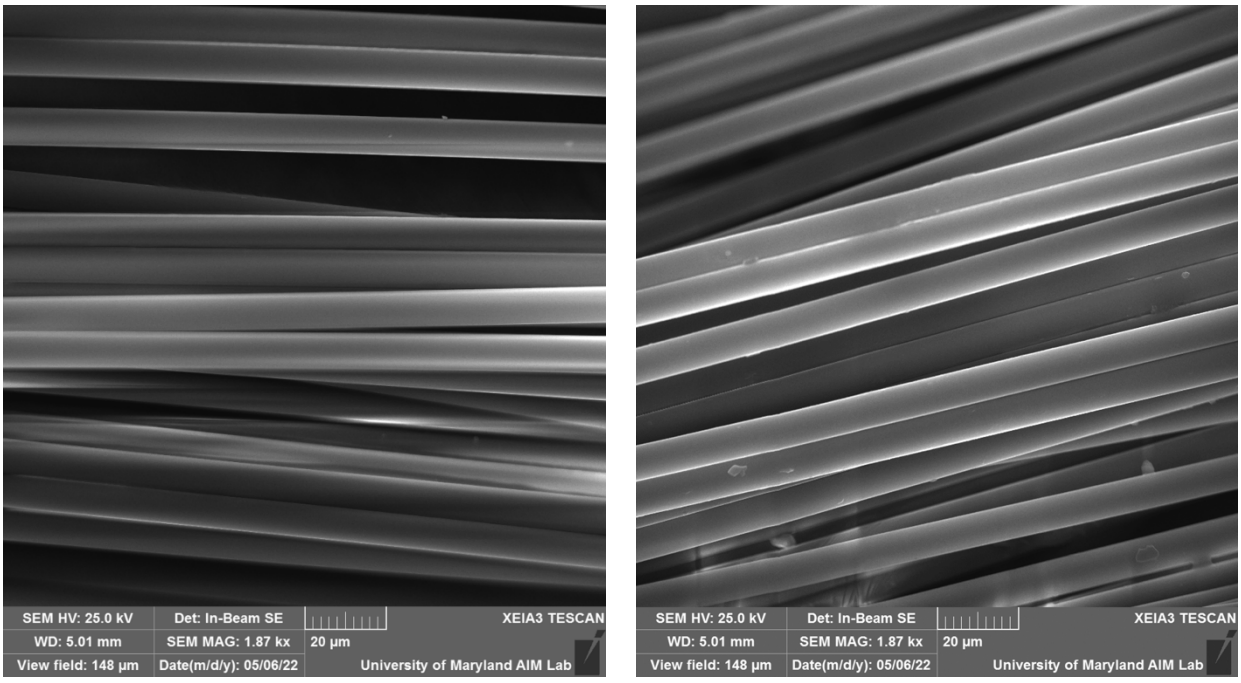

Figure 43. SEM images of (left) unirradiated, and (right) 100 kGy irradiated aramid fibers

3.2 Chemical grafting of styrene-containing linker onto nanocellulose

Before discussing the results from the experiments on grafting nanocellulose onto the fibers, this section will discuss the nanocellulose modification experiments which were done to improve its grafting onto the aramid fibers. Although the structure of nanocellulose is very reactive, it does not have any C=C double bonds which complicates the radiation induced grafting process. These C=C double bonds are commonly used for grafting since they preferentially react with free radicals generated through irradiation. An unsaturated monomer was grafted onto the nanocellulose by following a wet chemistry-based grafting approach.

3.2.1 Confirmation of synthesis of styrene-nanocellulose

After following the Williamson ether synthesis procedure for the grafting of 4-(Chloromethyl)styrene onto the nanocellulose, the samples were characterized based on the degree of grafting (DoG) and FTIR results. FTIR analysis is commonly used to confirm the successful grafting of different materials onto nanocellulose.[184–186] Figure 44 shows the IR spectra of nanocellulose before and after grafting. The peaks that confirm grafting are highlighted in the figure and correspond to the CH_2 and CH bending vibrations at 1427 cm^{-1}, and the p-distributed benzene ring at 827 cm^{-1}.[184,186] For the DoG results, the styrene-nanocellulose was dried in a desiccator after synthesis and then weighed. This measurement was compared to the weight of the nanocellulose before the synthesis. After adjusting the parameters to guarantee good mixing of the solution and homogeneous grafting, a DoG of 153.5% was achieved.

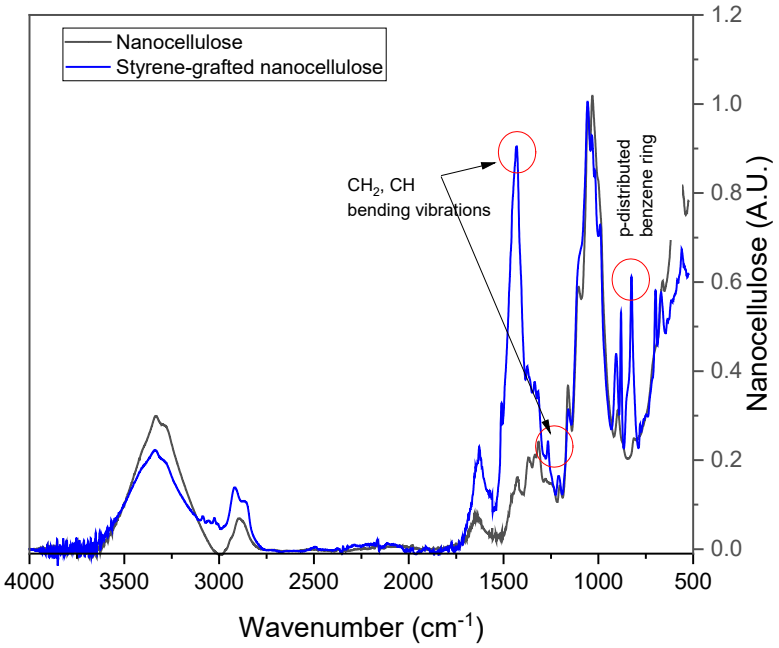

Figure 44. FTIR spectrum of nanocellulose (black) and styrene-grafted nanocellulose (blue) and assigned IR peaks.

3.3 Radiation grafting of styrene-nanocellulose onto aramid fibers

After looking at the effects of irradiation of the aramid without nanocellulose, the next step was to attempt the grafting of nanocellulose onto the fibers. Throughout this work, two grafting approaches were studied: indirect and direct grafting. Furthermore, two different types of cellulose, one in its natural state and one modified with a styrene-containing linker, were used. This section focuses on the characterization methods used to confirm the successful grafting of nanocellulose onto aramid fibers, and the effects of this grafting on the fibers' mechanical properties.

3.3.1 Gravimetric Analysis (DoG calculation)

After the fiber grafting procedure was completed, the fibers were washed with DI water to remove any homopolymerized and non-grafted nanocellulose. Then the fibers were dried in a

vacuum desiccator and weighted. The results presented here are divided into two sections based on the grafting approach followed.

To confirm that all non-grafted nanocellulose was removed after washing, the rinse solution as analyzed by UV-Vis spectroscopy. In the analysis, the absorbance of the solution was measured at wavelengths between 200 to 800 nm.[187] The results from one of the samples, before and after washings, was chosen at random and are shown in Figure 45. In the range between 300 and 600 nm, the sample measured from the first rinse of the fiber after grafting shows an absorbance higher than 80%. After washing the fiber with a total of 600 mL of DI water, which corresponds to 6 total washing cycles, the absorbance goes to 0%. By the end of the washing, all of the un-grafted nanocellulose had been removed from the fiber.

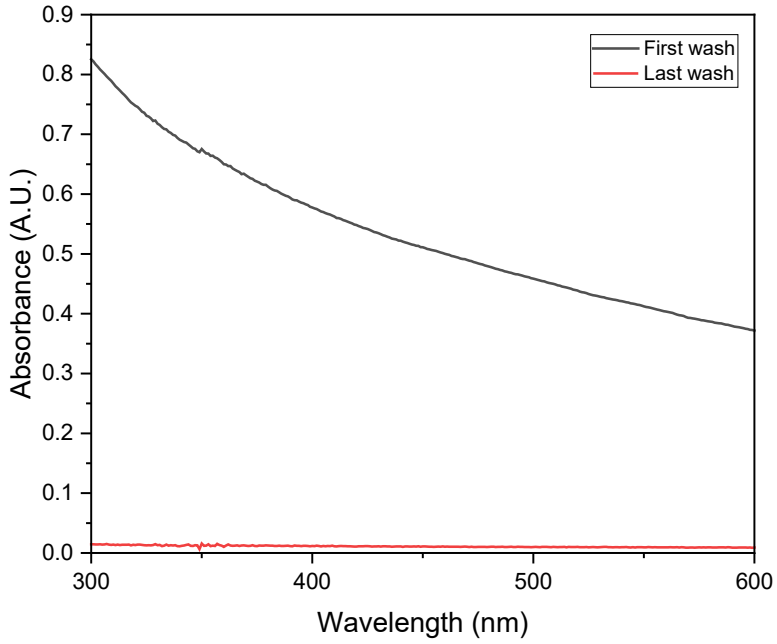

Figure 45. UV-Vis spectrum of rinsing solution after first (black) and last (red) wash with DI. Samples were washed multiple times after the grafting procedure, before DoG measurements were taken.

3.3.1.1 Direct Grafting of nanocellulose onto aramid fiber

The first approach followed for the grafting of nanocellulose onto the fibers was a direct grafting method. The samples were prepared as described in section 2.4.1. These first experiments were only conducted on the aramid fibers, since this was the original focus of the thesis. This method provides a simple procedure which consists of only one step and allows for the quick screening of various irradiation conditions. First, the experiments were conducted with the as-received nanocellulose solution, which was diluted to obtain a 1:1 nanocellulose to fiber ratio. These direct grafting experiments were repeated, at the same conditions, with the styrene-nanocellulose synthesized in the lab. Table 7 shows the summarized results of the DoG for both sets of experiments. Neither procedure showed a significant increase in weight (<5%) after grafting.

Table 7. Direct radiation grafting results of nanocellulose onto aramid fibers, varying type of nanocellulose, irradiation temperature, and total dose. All samples were purged before irradiation with N_2O.

Sample description	Total dose (kGy)	Irradiation temperature (°C)	Average degree of grafting (%)	Number of samples
Aramid fiber suspended in 1 wt% nanocellulose aqueous solution	*5*	*RT*	*0.26*	*3*
	10	RT	0.25	3
	5	80	0.14	3
	10	80	0.47	3
	50	RT	2.74	6
	100	RT	3.75	6
	50	80	0.20	3
	100	80	0.03	3
Aramid fiber suspended in 1 wt% styrene-nanocellulose aqueous solution	5	RT	0.71	3
	10	RT	0.77	3
	5	80	1.01	3
	10	80	0.74	3
	50	RT	0.35	3
	100	RT	0.34	3
	50	80	0.35	3
	100	80	0.19	3

As discussed above, these direct grafting experiments were done by irradiating the fibers in the aqueous nanocellulose solution. As shown in Table 7, these initial irradiation experiments resulted in negligible degrees of grafting. The first issue that was identified about this approach was incomplete mixing of the nanocellulose in the aqueous solution. Although the solution was mixed for a week before combining it with the fibers and sealing the vials, some of the nanocellulose visibly settled at the bottom of the vial in the time it took to start the irradiation. This could have led to the fibers not being completely covered with the nanocellulose, impeding the grafting during the irradiation. Another reason for the failure of this approach is due to the effects of high irradiation doses on the nanocellulose. One of the ways nanocellulose can be produced is through irradiation of cellulose.[188] When applied to the material in the nano-scale, high irradiation doses lead to degradation. As the nanocellulose-fiber mixture is being irradiated, the nanocellulose can degrade and no grafting occurs.

Additional experiments were conducted with the goal of improving the DoG for the direct grafting approach. Various other parameters were investigated, including varying the concentration of nanocellulose, the dose rate, and the state (dry or in solution) of the sample. Increasing the concentration of the nanocellulose in the solution brought out the problem of particle agglomeration, resulting in a non-homogeneous mixture that could not be used for grafting. Another technique tried was to immerse the fibers in the nanocellulose solution and dry them prior to irradiation. However, the fibers were not able to adsorb enough nanocellulose, which meant that not enough nanocellulose could be grafted during the irradiation. After continuing to achieve only low DoG these experiments were paused, and the indirect grafting approach was further investigated.

3.3.1.2 Indirect Grafting of nanocellulose onto aramid fiber

The indirect grafting approach focuses on irradiating the fibers by themselves and introducing the nanocellulose in an inert environment. The samples were prepared as described in section 2.4.2. After understanding the effects of high irradiation doses on the nanocellulose, this approach was pursued since it allowed for irradiating the strong fibers without exposing the nanocellulose. These experiments were conducted for both the aramid and UHMWPE fibers, the UHMWPE results are presented in a separate section. Similarly, to the previous method, the two types of nanocellulose solution, in a 1:1 fiber to nanocellulose ratio, were grafted onto the fibers: as-received nanocellulose, and styrene-nanocellulose. Samples were irradiated dry, in an N_2 atmosphere and at a temperature of around -40 °C. Parameters varied included: type of nanocellulose, total dose, and post-irradiation grafting temperature. Table 8 shows the results from these experiments. Experiments on the samples of fiber irradiated in water were not continued since the water freezes after being kept in dry ice, and it is not possible to avoid radical decay before mixing with the nanocellulose solutions.

Table 8. Indirect radiation grafting results of nanocellulose onto aramid fibers varying type of nanocellulose and total dose. All irradiations were done in sub-ambient temperatures.

Sample description	Total dose (kGy)	Nanocellulose	Average degree of grafting (%)	Number of samples
Dry aramid fiber, inert environment	150	As-received nanocellulose	0.3	3
	300		0.72	3
	150	Styrene-nanocellulose	0.46	3
	300		7.73	3
Aramid fiber in water, N_2O environment	150	As-received nanocellulose	0.04	3
	300		0.66	3
	150	Styrene-nanocellulose	0.44	3
	300		0.70	3

With the exception of the samples irradiated at 300 kGy and mixed with the styrene-nanocellulose solution, low DoG were achieved for all the initial samples grafted through the indirect method. The first issue determined was a lack of complete purging of the vials prior to irradiation. In order to remove oxygen from the vial, the samples must be purged with N_2 gas for at least 20 minutes and completely sealed before irradiation.

Efforts to improve the results also focused on possible problems with the styrene-nanocellulose solution. The original procedure with the nanocellulose included stirring the solution for 1 week before the grafting procedure. However, in the case of the styrene-nanocellulose 1 wt% aqueous solution, it was concluded that this process leads to homopolymerization of the styrene-nanocellulose. This results in the elimination of the unsaturation of the monomer, which are the possible grafting sites to which the aramid would bond to. To avoid this, after synthesizing the styrene-nanocellulose, it was kept in the freezer until the day of the irradiation-grafting experiment. The styrene-nanocellulose solution was prepared after the fibers were irradiated, and it was stirred for an hour before it was mixed with the irradiated aramid. Solutions were well-mixed, and no visible agglomeration of the particles was seen after combining with the fibers. Additionally, since the nanocellulose does not have the double-bond needed to promote grafting by forming a covalent bond with the radicals generated after fiber irradiation, unmodified nanocellulose was discarded as a possible filler for the fibers. The results shown in Table 9 show the improvements in the DoG obtained after making these changes.

Table 9. Indirect radiation grafting results of styrene-nanocellulose onto aramid fibers varying the total dose. Main change was preparing fresh styrene-nanocellulose solution to avoid homopolymerization before grafting. All irradiations were done at sub-ambient temperature, while the grafting temperature refers to the temperature at which the samples were mixed after irradiation.

Sample description	Total dose (kGy)	Grafting temperature (°C)	Average degree of grafting (%)	Number of samples
Dry aramid fiber	150	RT	5.64	6
	300		8.38	6

After these promising results, the effects of grafting temperature on the DoG of the indirectly grafted samples were further investigated. Due to its active sites, and presence of the double bond in its structure, styrene-nanocellulose was selected for the rest of the experiments. As shown above, homopolymerization of the styrene-nanocellulose greatly affected the ability of the nanocellulose to graft onto the aramid. Thus, to avoid any possible homopolymerization that might occur during the grafting process, the post-irradiation grafting procedure was conducted inside the fridge. This corresponds to the low temperature experiments, for which the temperature was kept at around 4 °C. The effect of high temperature was also investigated by placing the samples on an oil bath at 80 °C for this post-irradiation grafting process. This temperature was chosen from previous research conducted in this lab, where DoG was shown to be optimized. Figure 46 shows the results of the indirect grafting approach experiments conducted at different temperatures. For these experiments, the aramid was irradiated dry in an inert environment, at sub-ambient temperature, and mixed with the styrene-nanocellulose at different temperatures overnight.

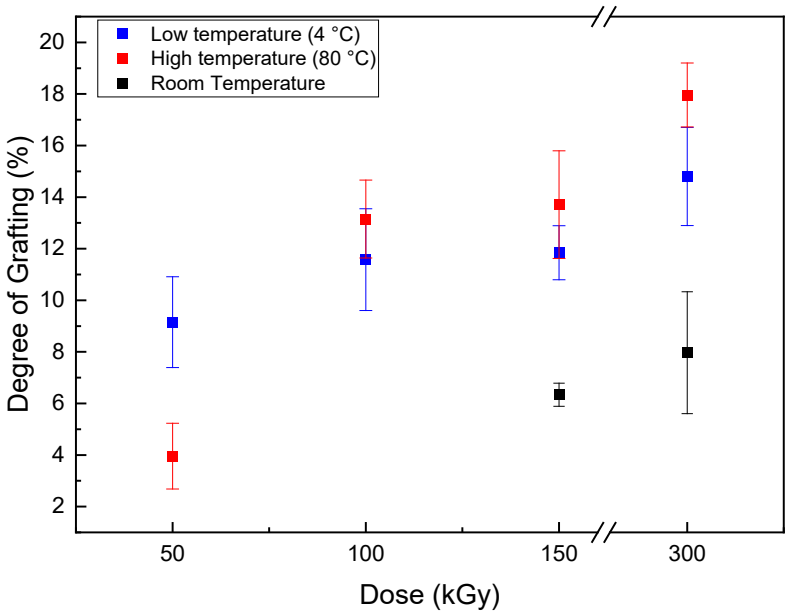

Figure 46. Indirect radiation grafting results of styrene-nanocellulose onto aramid fibers varying the total dose and grafting temperature. All irradiations were done at sub-ambient temperature.

It was observed that increasing the total dose resulted in an increase of the total DoG for all samples. This result is consistent with the concentration of radicals increasing with dose. For the reasons discussed above, the room temperature grafting experiments were only studied for the samples irradiated at 150 and 300 kGy, for which between 6 and 8 % DoG was achieved. For both high and low temperature, irradiating the samples at 50 kGy resulted in lower degrees of grafting. This is related to the concentration of free radicals generated at this dose. 50 kGy was determined to be too low of a dose to result in any meaningful grafting onto the fibers. The increase in DoG is most pronounced in the samples mixed at high temperatures. At higher temperatures there is better diffusion of the solution, which influences the final DoG. Setting the irradiation temperature to 40 °C ensures good mixing of the fiber and the cellulose, while keeping the grafting time short prevents excessive homopolymerization of the nanocellulose. A similar trend is observed for the

low temperature grafting, but with a smaller DoG. In this case, the grafting was done inside a glove bag instead of a glove box. Although precautions were taken to ensure that there was no oxygen present before combining the irradiated fiber and the nanocellulose, such as purging the bag multiple times, the glove bag does not have an oxygen monitor. Lower degrees of grafting can also be a result of this issue. However, this is still a significant improvement when comparing to the samples mixed at room temperature.

This gravimetric analysis was the first step in confirming a successful grafting procedure. However, it is important to see how this grafting step affected the mechanical properties of the fibers. This was studied by single fiber tensile tests. Additionally, the extent and uniformity of the grafting was studied using SEM, FTIR, and NMR.

3.3.2 Mechanical testing

Based on these DoG results, the next step was to look at how the grafting temperature and irradiation dose affected the tensile strength of the fibers. Single fiber testing was done for all the samples grafted and presented in the results from Figure 46. At least 30 to 50 strands of each sample were randomly tested to acquire statistically significant results. Figure 47 shows the results obtained from the single fiber tests conducted.

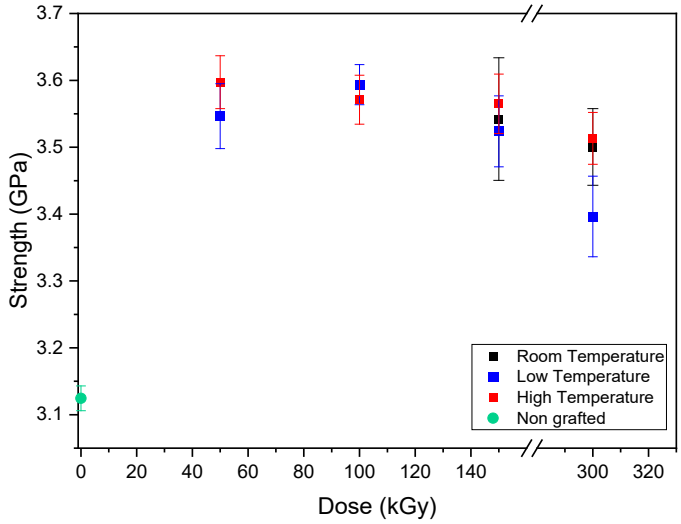

Figure 47. Strength as a function of irradiation dose for the styrene-nanocellulose onto aramid fiber at the different grafting temperatures.

An increase of up to 15 % in the tensile strength of the nanocellulose-grafted fibers was observed when compared to the nonirradiated, nongrafted fiber. The highest increase was seen in the samples grafted at high temperatures, but the behavior was similar for all the grafting temperatures studied. As the irradiation dose was increased, there was a slight decrease in the strength of the fibers. This is expected, since it was previously observed that just irradiating the fibers at high total doses resulted in slight decreases in its strength. Thus, the strength of the fibers can be initially affected by the irradiation, but after grafting the nanocellulose it increases to values higher than the strength of the nontreated fibers. This shows that grafting nanocellulose onto aramid fibers leads to a significant improvement of the strength of the fibers.

In terms of the temperature effect, this is most likely related to the different degrees of grafting obtained for the various grafting temperatures. The samples grafted at low temperatures (inside the fridge, 4 °C) had lower DoGs when compared to the higher temperature samples, at the same dose. This is reflected in a lower strength for these samples. Additionally, there is also a decrease

in the strength of low temperature samples when compared to the samples grafted at room temperature. The room temperature samples showed strengths comparable to those of the high temperature ones, even after achieving lower degrees of grafting. This behavior can be better observed in Figure 48, where the strength of the fibers is plotted as a function of the degree of grafting.

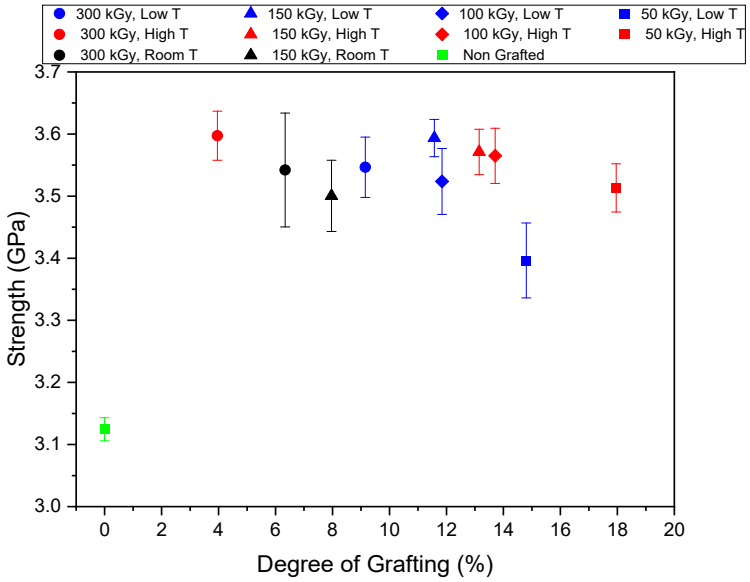

Figure 48. Styrene-nanocellulose onto aramid fiber: Fiber strength as a function of degree of grafting for the samples grafted at various temperatures. The strength of the nongrafted samples is shown for comparison.

In this figure, we can see that an increase in the fiber's strength was achieved even for the samples with the lowest degrees of grafting. As was mentioned before, this is consistent with lower doses leading to lower DoGs, but also less initial damage to the fibers. Looking at this plot, it is concluded that the best results are found in the samples irradiated to intermediate doses in the range of 100 to 150 kGy. These samples show both a significant increase in the fiber strength and high degrees of grafting, at all the grafting conditions. Based on this, the sample irradiated at 150 kGy and had a low grafting temperature, had the best results. These samples showed a DoG of

11.57 % and a strength of 3.59 GPa. Thus, they were selected as an example in the thesis to show the results from the additional characterization techniques done to investigate the chemical bonding and extent of the grafting.

3.3.3 SEM Morphological changes after grafting

Figure 49 shows the SEM images of the aramid fibers before treatment and after grafting the nanocellulose. The fibers irradiated at 150 kGy and grafted at low temperature were selected as an example to show the presence of nanocellulose on the fibers. On the left image, the fiber appears to have a smooth surface with no irregularities. On the right image, the fiber is no longer smooth and there are spots on the surface, which was expected after grafting the nanocellulose. This nanocellulose grafted on the fibers is significant to improve the physical interactions between the fibers and the resin in composites. Figure 50 shows a bundle of grafted fibers and it can be seen that the grafting is not completely uniform. However, it can be observed that nanocellulose was grafted in all regions of the fibers.

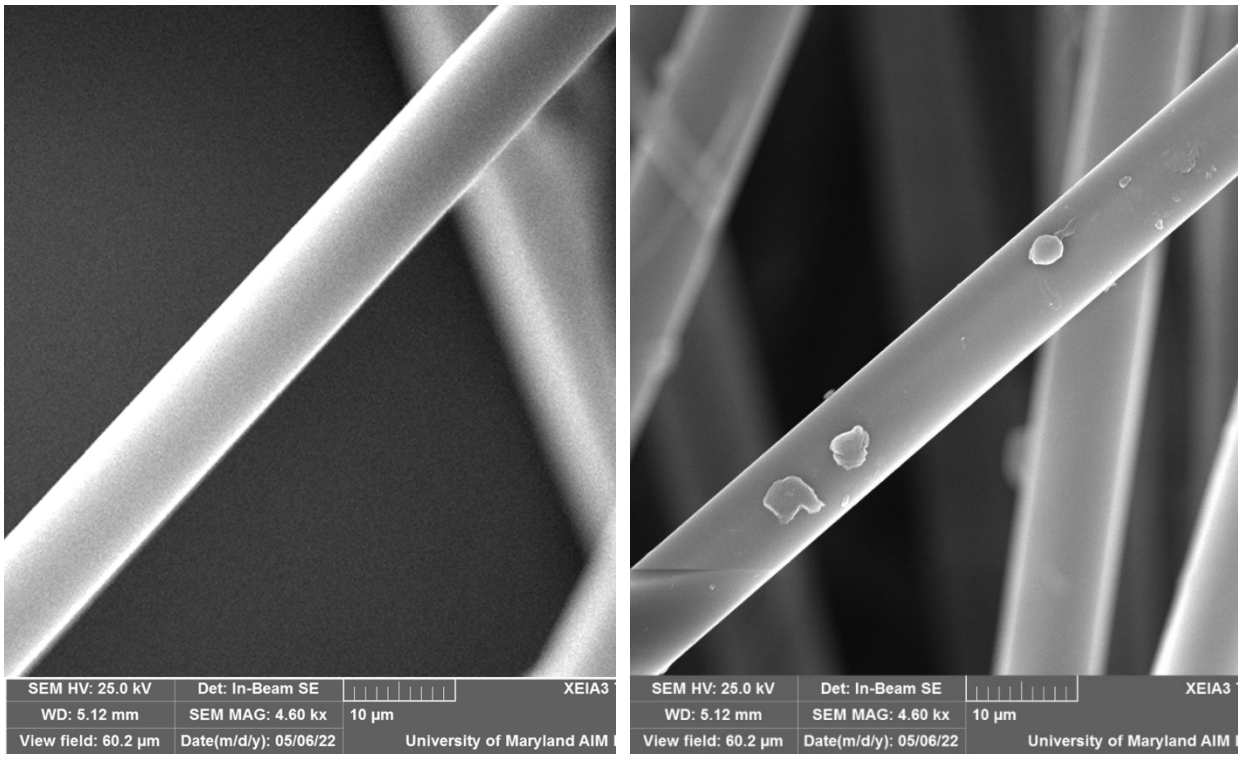

Figure 49. SEM images of aramid fiber before (left) and after (right) grafting.

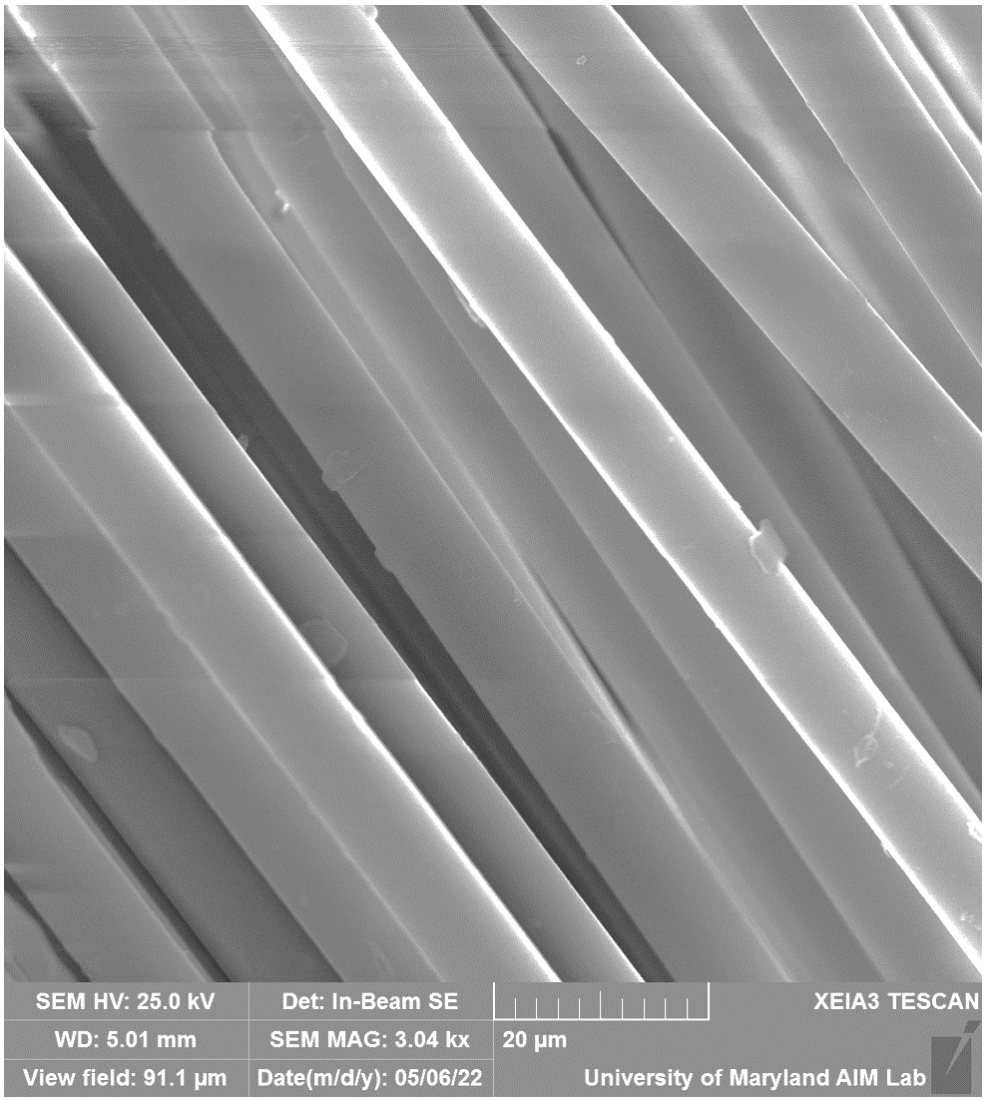

Figure 50. SEM image of nanocellulose-grafted aramid fibers.

3.3.4 Identifying the chemical changes of the aramid fiber using FTIR spectroscopy

FTIR measurements were performed to identify chemical changes in the fibers by comparing the FTIR spectrum of the fibers before and after grafting. The chemical composition of the sample can be determined by FTIR, which measures the energy absorption of its molecules. Each molecule absorbs at a frequency characteristic of its structure and the FTIR spectrum consists of absorption peaks corresponding to the frequencies of vibration between the bonds of atoms in the sample. This technique was used as an initial method for confirming the successful

nanocellulose grafting on the fibers. Figure 51 shows the proposed mechanism of nanocellulose grafting onto the fibers.

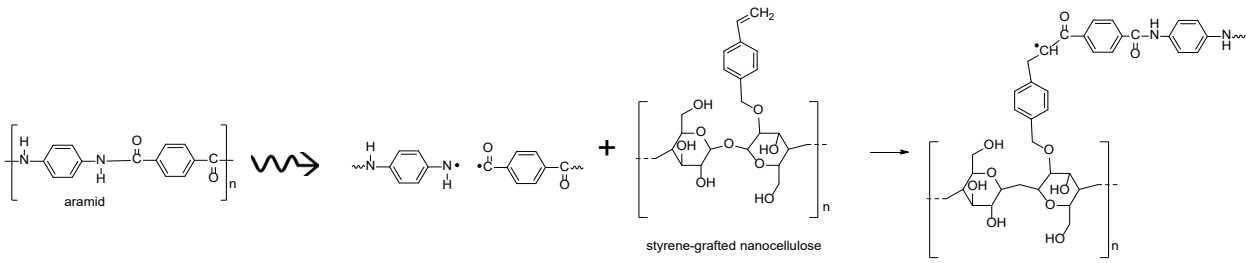

Figure 51. Proposed mechanism for the grafting of styrene-nanocellulose onto the aramid fibers.

The aramid fibers and the nanocellulose share many of the same bonds used to identify their structures by FTIR:

- Broad peak at 3313 cm^{-1} is characteristic of the N-H stretch in the aramid and the O-H stretch in the cellulose
- Peak at 1656 cm^{-1} is characteristic of C=O stretch
- Peak at 827 cm^{-1} is attributed to p-distributed benzene rings present in both aramid and styrene-grafted aramid

The similar structures make it complicated to use the IR spectrum to corroborate grafting. Figure 52 illustrates a comparison between the nontreated aramid fiber and the nanocellulose grafted aramid fiber. The peaks at around 2921 and 2852 cm^{-1} are of importance since these do not appear in the nontreated aramid. These peaks are consistent with the peaks found in the nanocellulose spectrum shown before (Figure 44) and are characteristic of the C-H stretching and bending vibrations present in cellulose.[23,186,189] This peak, not present in the FTIR spectra of the non-treated aramid fiber, is an indication of successful grafting on nanocellulose onto the aramid.

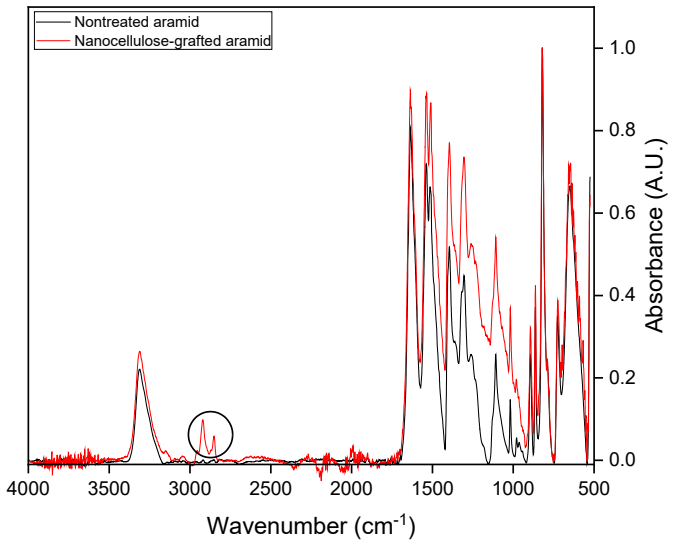

Figure 52. FTIR-ATR spectra of nontreated (black) and nanocellulose-grafted (red) aramid fibers.

As seen in the mechanism proposed, grafting occurs when the unsaturated radicals react with the C-centered radical generated on the aramid, creating a CH_2-C=O bond. Due to the similar chemical bonds present on both materials, it is difficult to reach a definitive conclusion from just the FTIR results. NMR measurements were taken to confirm the successful grafting and bonding between the nanocellulose and the aramid fibers.

3.3.5 Solid state NMR (ss-NMR)

Solid state NMR measurements were conducted on the untreated fibers, the styrene-nanocellulose, and the nanocellulose-grafted fibers to study their molecular structure and confirm proper grafting. ^{13}C NMR spectrum of the untreated aramid fiber is shown in Figure 53. The peaks characteristic to the unirradiated aramid structure are highlighted.[180,190,191]

- Peak at 158 ppm is characteristic to the C=O bond in the aramid

- Peak at 130.5 ppm is characteristic to the quaternary C of the phenyl ring
- Peak at 127.4 ppm is characteristic to the N-phenyl bond
- Peak at 123.9 and 120.9 ppm is characteristic to the ortho resonances of the C atoms in the terephthalamide ring
- Peak at 116.8 ppm is characteristic to the ortho resonances of the C atoms in the phenylenediamine ring

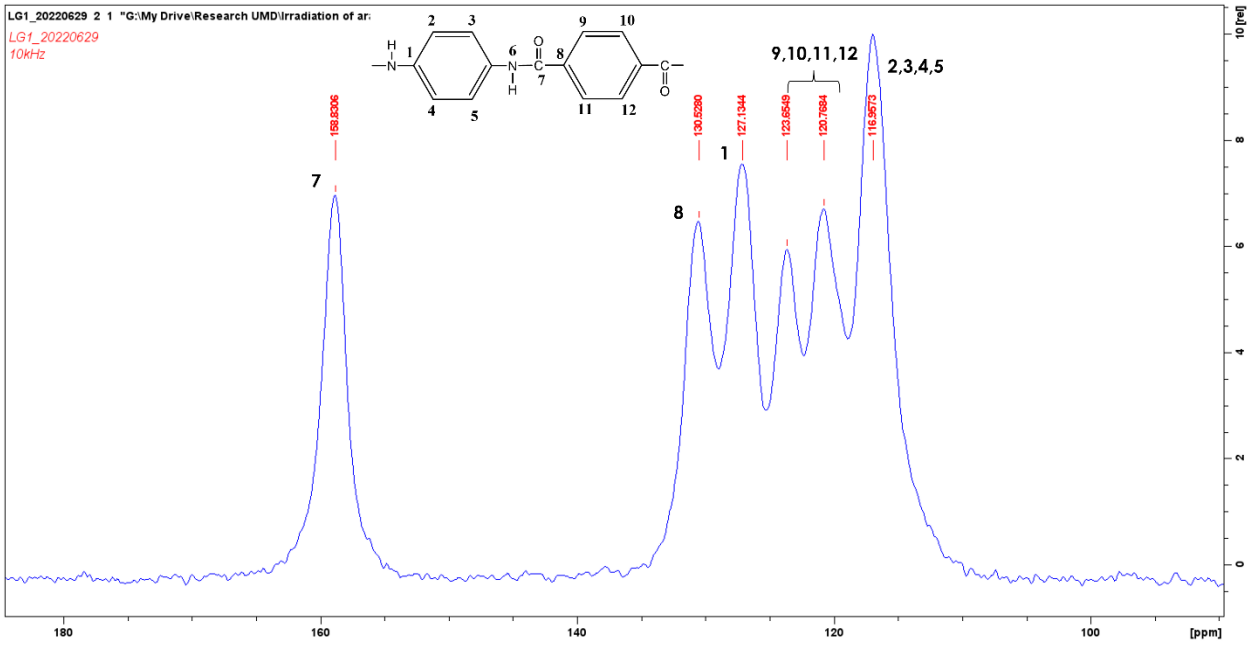

Figure 53. ^{13}C NMR spectrum of untreated aramid fiber. The peaks assigned to the chemical structure of the aramid are highlighted.

The spectrum of the styrene-nanocellulose is shown in Figure 55. For easier identification, the common nomenclature for the C atoms in cellulose will be used as shown in Figure 54.

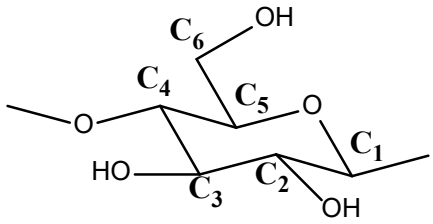

Figure 54. Schematic showing the regular nomenclature for identifying the C-atoms in cellulose.

The peaks have been assigned as follows:[192]

- The peak at 98.1 ppm is characteristic of the C_1 atom
- The peaks at 81.8 and 76.0 ppm are characteristic of the C_4 atom
- The peaks at 68.5 and 65 ppm are characteristic of the C atoms in the ring (C_2, C_3, C_5)
- The peaks at 57.6 and 55.0 ppm are characteristic of the C_6 atom

The structures of the styrene and the nanocellulose were characterized and identified in the spectrum separately because no study of the two together have been published. The absence of the Cl atom in the styrene structure results in a shift of the peaks to lower energy due to the atoms close to it changing from a shielded to a de-shielded state. The peaks of the styrene are as follows:[193]

- The peak at 130.4 ppm is characteristic of the quaternary carbons of the ring and the C at position 12
- The peak at 120 ppm is characteristic of the C atoms in the ring
- The peak at 107.5 ppm is characteristic of the CH_2 atom
- The peak at 35.8 ppm is characteristic of the original C-Cl atom, which becomes a C-O bond when the styrene group is grafted onto the cellulose

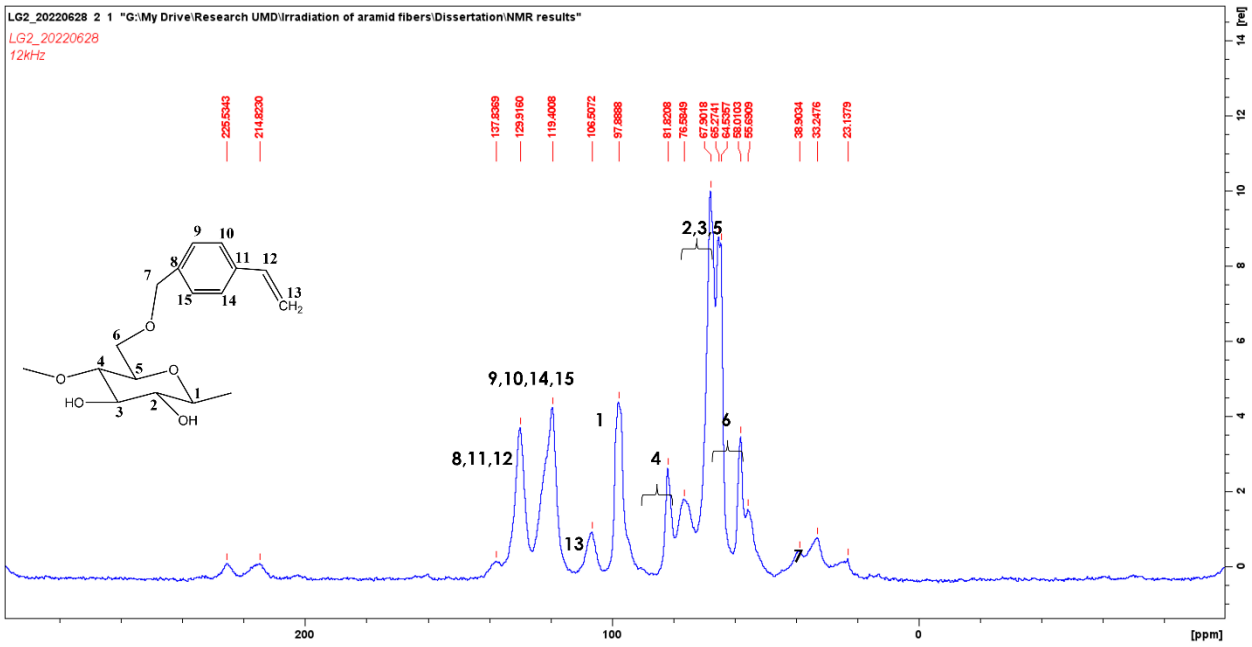

Figure 55. ^{13}C NMR spectrum of styrene-nanocellulose. The peaks assigned to the chemical structure of both the styrene and the cellulose are highlighted.

The ^{13}C NMR spectrum of the nanocellulose-grafted aramid fibers is shown in Figure 56, above the spectra of the aramid fibers and the styrene-nanocellulose for direct comparison. Here, it is important to note the new sharp peak appearing at 23 ppm which is consistent with a C-C bond, expected after grafting the nanocellulose onto the aramid. This C-C bond is expected to appear after grafting, which occurs through addition of the $CH=CH_2$ bond to the free radical. There is a small peak at 105 ppm similar to the one observed in the styrene-nanocellulose spectrum and identified as $CH=CH_2$. However, it also could be the result in a shift due to the grafting. This spectrum will be investigated deeper by looking at the NMR of a similar compound that has the CH_2-C=O bond expected from the grafted aramid.

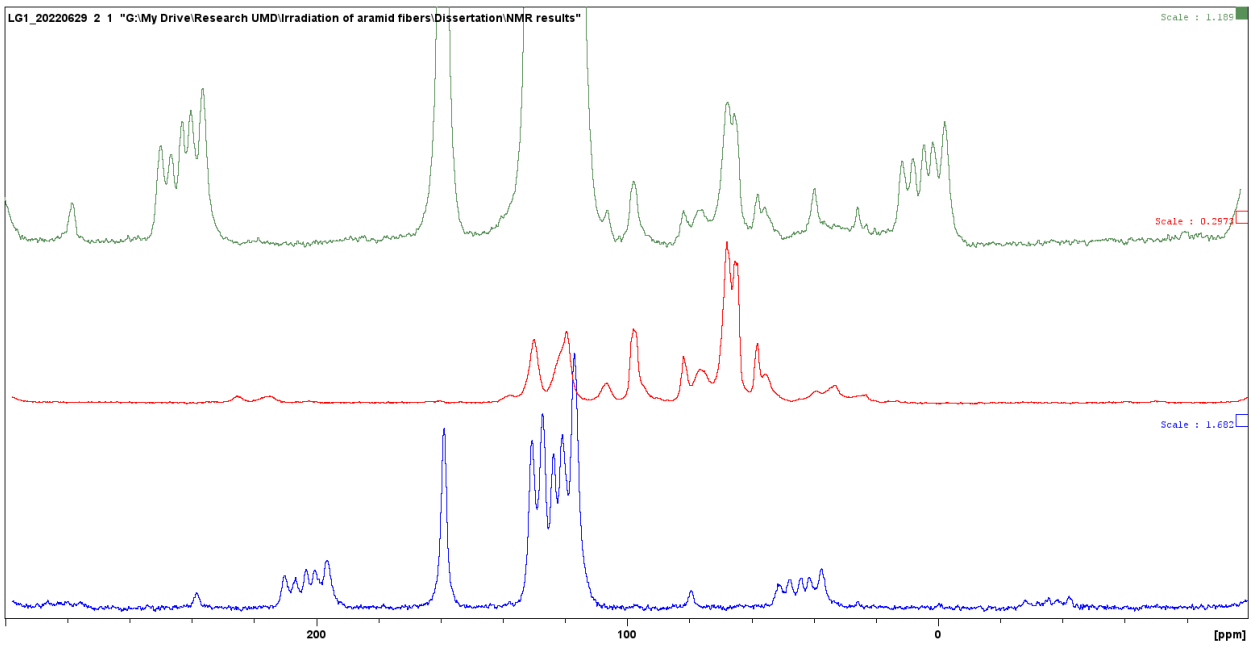

Figure 56. ^{13}C NMR spectra collected from the nanocellulose-grafted aramid fiber (green), styrene-nanocellulose (red), and untreated aramid fibers (blue).

3.4 Radiation grafting of nanocellulose onto UHMWPE fibers

Radiation induced grafting of nanocellulose on UHMWPE fibers studies were also conducted for this project. Both direct and indirect approaches were studied, at lower irradiation doses than for the aramid fibers since UHMWPE fibers are more sensitive to irradiation. Table 10 shows the results for the direct grafting approach. Overall, low DoG was achieved for both nanocellulose and styrene-nanocellulose grafting.

Table 10. Direct radiation grafting results of nanocellulose onto UHMWPE fibers, varying type of nanocellulose and total dose. All samples were purged before irradiation with N_2O.

Sample description	Total Dose (kGy)	Average degree of grafting (%)	Number of samples
UHMW PE fibers suspended in 1 wt% aqueous nanocellulose solution	25	5.86	3
UHMW PE fibers suspended in 1 wt% aqueous styrene-nanocellulose solution	10	2.58	3
	25	1.09	3
	50	0.18	3

In the case of indirect grafting (Table 11) the results were a higher DoG than in the direct approach. However, no significant values were obtained. This could be a combination of the low irradiation dose used, to protect the mechanical properties of the UHMWPE, and homopolymerization of the styrene-nanocellulose when using a grafting temperature of 40 °C.

Table 11. Indirect radiation grafting results of nanocellulose onto UHMW PE fibers varying type of nanocellulose and total dose. All irradiations were done in sub-ambient temperature, and at a grafting temperature of 40 °C.

Sample description	Total Dose (kGy)	Average degree of grafting (%)	Number of samples
Dry UHMW PE, inert atmosphere *Mixed with nanocellulose*	50	0.14	7
Dry UHMW PE, inert atmosphere *Mixed with styrene-nanocellulose*	10	2.16	7
	25	16.92	7
	50	3.56	7

The UHMW PE experiments were not further investigated because complications with the strength measurements for these fibers. Further studies are recommended for the future work of this project.

3.5 Crosslinking of aramid fiber

3.5.1 Crosslinking degree after irradiation in acetylene and triacrylate (TMPTA) environments

The effects of the irradiation of the fibers in the presence of a crosslinker, either acetylene or triacrylate, was first studied by swelling tests. Figure 57 show the results from these studies, with the residual mass of the fibers after swelling is taken as a direct measure of the crosslinking degree of the fibers. An increase in crosslinking degree can be seen as the dose was increased for irradiation in both environments. During the irradiation, the presence of the crosslinking agents

pushes the subsequent reactions to favor crosslinking over chain scission. As more crosslinking occurs, it is harder for the acid to break down the polymer thus leading to an increase in the residual mass.

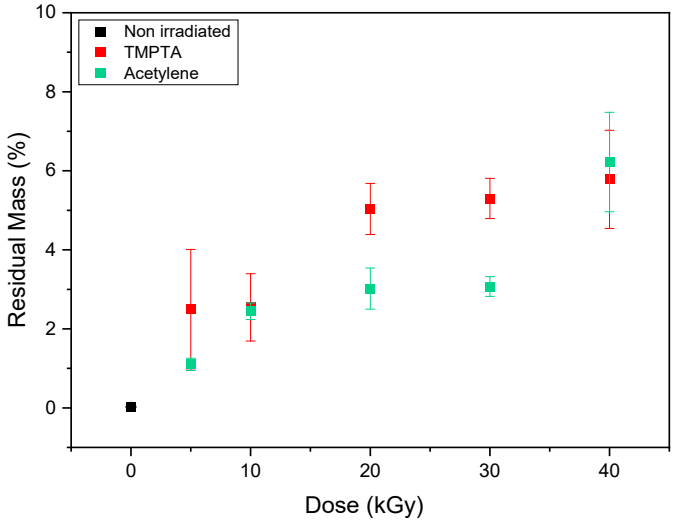

Figure 57. Residual Mass of irradiated fibers as function of dose after dissolving in H_2SO_4.

The proposed crosslinking mechanism for irradiation of aramid in acetylene environments is presented in Figure 58. Similar to the crosslinking mechanism of PE in acetylene environment proposed by Jones, et al, the acetylene molecules are expected to facilitate crosslinking by reducing the distance between the radicals generated during irradiation.[194] As the C-centered radicals are generated on the aramid during irradiation, the acetylene molecule can add to it. This continues happening throughout the surface of the material, and then the acetylene can act as a very short chain, bridging adjacent chains with the fibers resulting in crosslinking and avoiding chain scission.

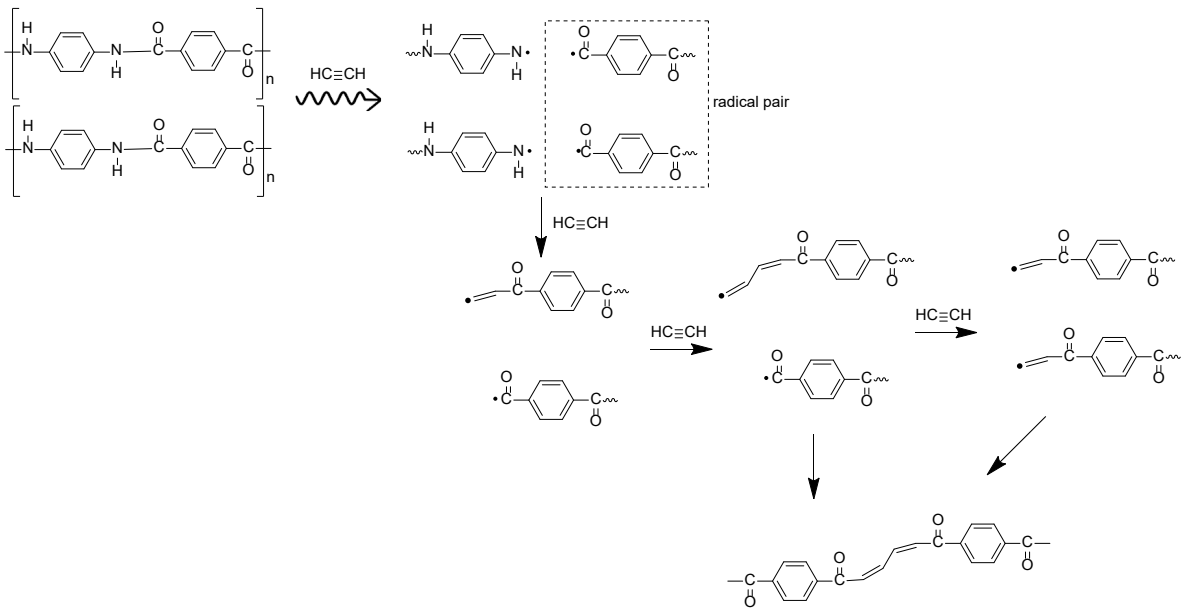

Figure 58. Proposed mechanism for irradiation of aramid in acetylene environment.

3.5.2 Single fiber testing of crosslinked aramid fibers

Aramid fibers in both an acetylene and a triacrylate environment were irradiated at low doses and high dose rates with the goal of increasing their crosslinking degree. The mechanical performance of these fibers was analyzed through single fiber testing, to understand how increasing the degree of crosslinking increases the strength of the fibers. Figure 59 shows the increase in the strength of the fibers as a function of the total dose to which they were irradiated, in an acetylene environment. The strength of the fibers increased as a function of dose and tapered off at around 20 kGy. This is consistent with the theory that most of the crosslinking occurs during the initial irradiation, after which the crosslinking and degradation reactions reach equilibrium. An increase of up to 16% was observed for the fibers after irradiation.

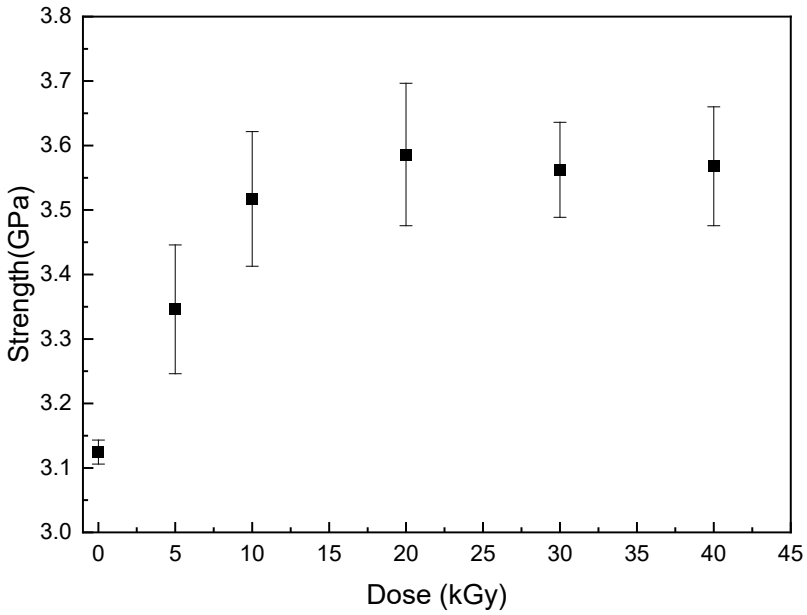

Figure 59. Strength as a function of irradiation dose for the samples irradiated in an acetylene environment.

For the second environment studied for enhanced crosslinking, the fibers were submerged in a TMPTA-glycol solution and excess TMPTA was rinsed with acetone shortly before irradiation. This step was added to the experiments after irradiation of the samples with excess acrylate resulted in the TMPTA solidifying in the irradiation vial. Figure 60 shows the tensile testing of the fibers irradiated in the acrylate environment. Similar to the fibers irradiated in acetylene environment, a quick increase in the strength of the fibers is seen at low total dose. In this case, irradiating the fibers at doses higher than 5 kGy resulted in a slight decrease in their overall strength. Although the issues first encountered with the solidification of the triacrylate were partially resolved by rinsing, some of the remaining triacrylate solidified on the fibers which made it hard to remove from the vials. Precautions were taken to test samples that had not been solidified and to not pull the fibers before the testing. However, this change in the physical properties of the

fibers might have damaged its mechanical properties and the testing could not be done correctly. This resulted in the observed decrease in strength.

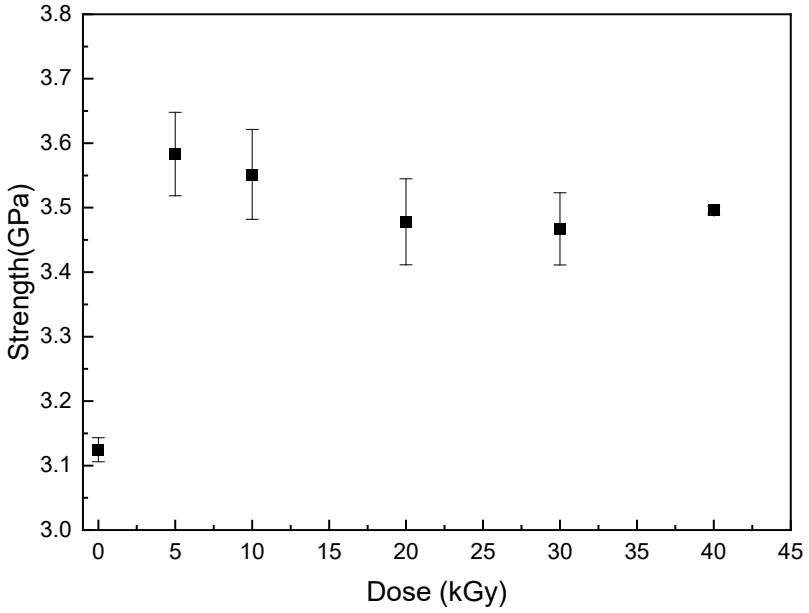

Figure 60. Strength as a function of irradiation dose for the samples irradiated in a triacrylate (TMPTA) environment.

Figure 61 shows the strength of the fibers after irradiation in both acetylene and triacrylate environments as a function of residual mass. In general, higher strength was achieved for the most crosslinked fibers. However, the effects of the solidification of the triacrylate on the tensile tests must be taken into account. From this figure, it can be concluded that lower doses might be most beneficial for increasing the strength of the fibers. This follows the idea that the crosslinkers act immediately as the radicals are generated on the fibers, and are able to create new bonds between the chains.

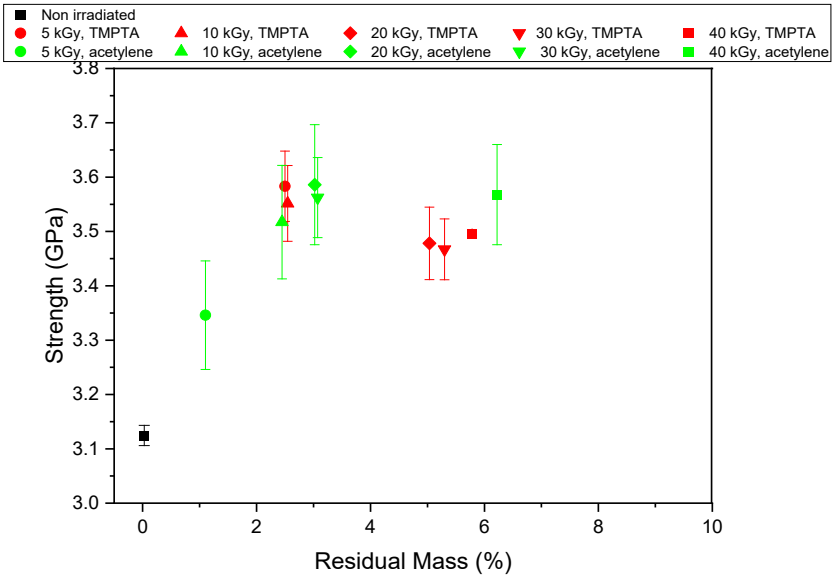

Figure 61. Strength of the fibers after irradiation in TMPTA and acetylene environment as a function of residual mass.

3.6 Radiation degradation of polyester-based resins

The objective of this part of the thesis is to use ionizing radiation, not for grafting or crosslinking, but to degrade and increase the degradability of polyester-based resins for recycling. As mentioned before, the effects of polymer irradiation are determined by the structure of the polymers. In the case of these polyester-based resins, irradiation can lead to degradation through scission of the C-O-C bonds present in their chemical structures. It will be demonstrated that grafting onto polyester-based resins needs to be evaluated differently from the aramid and UHMWPE fibers. Instead of grafting, ionizing radiation can be used to recycle polyester-based resins.

The effects of high dose irradiation on polyester-based resins were studied by EPR and DMA analysis. First, the radicals generated in the irradiated resins were identified and quantified, and their decay was studied. Then DMA analysis provided an insight into changes in the T_g of the

resins, which is an indication of polymer degradation. These results are currently in the review process for a paper that will be published in the next coming months.

3.6.1 Identification of the radiolytically produced free radicals of polyester resins in different environments using EPR spectroscopy

In order to elucidate the radiation impact on the changes in the polyesters' molecular architectures and the associated mechanisms, this dissertation research specifically investigated the roles of the presence of O_2 and of the solvents during electron beam irradiation.

Radiolysis of neat polyester resins (1R, 2R, 3R, 4R) in the absence of solvents

All four resins used in this study comprise the same irradiation-sensitive ester [–(O=)C-O-C] bonds on the backbone of their polymer chains. However, their chemical structures include different functional groups that undergo various radiation-induced reactions and result in varying degrees of backbone scission (Table 4). In addition, the chemical compositions of these resin composites have various compounds such as vinyl toluene in 1R, propylene glycol in 2R and 4R, and high content of styrene in 3R. It is expected that irradiation with the electron beam induces polymerization reactions of these unreacted vinyl monomers.

Figure 62 shows the EPR spectra of the neat 1R, 2R, 3R, 4R resins irradiated by e-beam at a dose-rate of 200 kGy/h and a total dose of 1000 kGy. All samples were irradiated in the presence of atmospheric oxygen to prevent the crosslinking reactions from taking place, thus favoring the radiation-induced scissions of the C-O-C bonds leading to the formation of C-centered and alkoxyl radicals.[109]

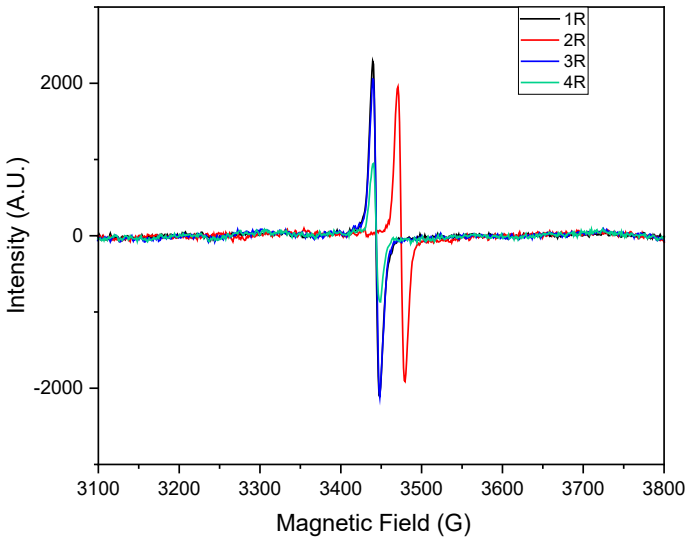

Figure 62. EPR spectra of neat 1R, 2R, 3R, and 4R resins electron beam-irradiated at a dose-rate 200 kGyh^{-1} in the absence of solvent and in the presence of oxygen. The total electron beam dose is 1000 kGy.

Figure 63 shows a typical radiation-induced scission of the C-O-C bonds in polyesters, and Table 12 shows the expected number of hyperfine splitting based on equation 1.18. Thus, it is expected that the EPR spectra of all these polyester resins would exhibit singlets as shown in Figure 63.

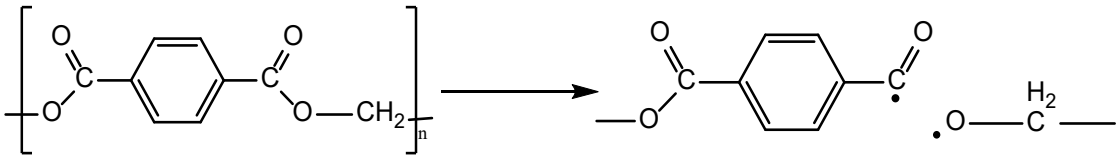

Figure 63. Typical ionizing radiation-induced scission in polyester chains in the presence of O_2.

Table 12. Schematic representation of radical species formed after the radiation-induced scission of polyester chains, and calculation of the number of peaks expected from the hyperfine splitting of each radical.

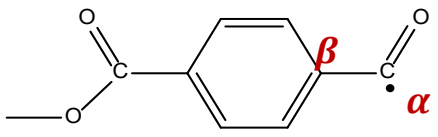 $(2(0)+1)(2(0)+1)=1$ α β	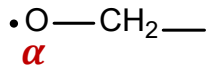 $(2(0)+1)=1$ α

All radiolytically produced alkoxyl radicals in 2R, 3R, and 4R, are unreactive towards dissolved O_2 since they are oxidizing radicals. As can be seen in Figure 62, a singlet is present in all the spectra collected from these irradiated neat resins (no solvents were used). This could be attributed to the effect of the high dose rate on enhancing the disappearance of the C-centered radicals via crosslinking reactions. As a result, the remaining stable alkoxyl radicals exhibit the singlet. It should be mentioned that since these radiolytically-produced alkoxyl radicals have a hydrogen atom at the neighboring carbon, no 1,2 H-shift occurs to produce C-centered radicals. The probability of the alkoxyl radicals abstracting neighboring H atoms, in this case, is much less than the probability of the 1,2 H-shift to occur. [195]

Radiolysis of polyester resins (1R, 2R, 3R, 4R) in the presence of solvents:

The early events of the radiation chemistry of the 1R, 2R, 3R, 4R in solvents are quite different from the radiolysis without solvents. The solvent molecules are also irradiated, and as a result we expect the radiolytically produced free radicals and ions to significantly alter the polyester resin structural procession.

1. Irradiation of 1R, 2R, 3R, and 4R resins in water

Figure 64 shows the EPR spectra of the 1R, 2R, 3R, and 4R resin samples irradiated in water. A singlet is observed in the EPR measurements of each of the different resins (1R, 2R, 3R, and 4R). Slight shifts in the center of the splitting pattern are the result of small variations in the frequency of the instrument at the time of measurement. Having a magnetic field center at 3450 G, the g-factor of the radicals generated is 2.0070.

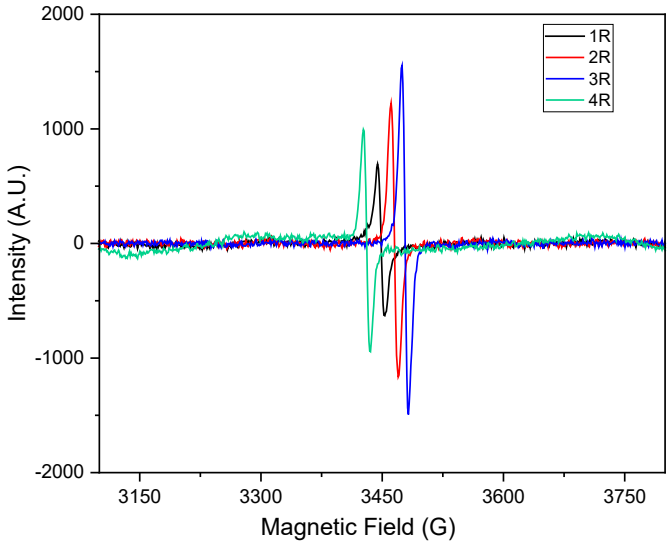

Figure 64. EPR spectra of irradiated 1R, 2R, 3R, and 4R resins in water by electron beam at a dose-rate 200 kGy/h, to a total dose of 1000 kGy.

Water is the best solvent to start with as it is environmentally friendly and does not produce flammable or toxic compounds during irradiation. Adding small amounts of alcohol can facilitate the solubility of other water insoluble monomers in the resin. The radiolysis of water by low linear energy transfer (LET) radiation, such as up to 10 MeV electron beams, produces high yields of the following reactive oxidizing and reducing species:

$$H_2O \xrightarrow{e-} {}^{\bullet}OH,\ e_{aq}^{\bullet-},\ H,\ H_2O_2,\ H_3O^{+},\ H_2$$

The radiation-chemical yield (G), quantified by the amount of species formed or consumed per unit energy, of those products are shown in Table 1. Those products have the following radiation-chemical yield (G), quantified by the amount of the species formed or consumed per unit energy:[100]

The reaction rate constants of hydroxyl radicals ($^{\bullet}OH$) with materials are very high.[175,195] Their reactions with resin materials induce the formation of C-centered radicals, which lead to further degradation of the organic materials. They can induce polymerization reactions of vinyl groups containing monomers through free radical chain-extension reactions and increase the degree of unsaturation via hydrogen abstraction. H-atoms also act in the same way but are generally less oxidizing than $^{\bullet}OH$.

In contrast, $e_{aq}^{\bullet-}$ and H-atoms react rapidly with the dissolved O_2 to produce $O_2^{\bullet-}$. Since the pH of irradiated water is 9.9, the reaction of $O_2^{\bullet-}$ and free H-atoms do not convert to $HO_2^{\bullet}$ (pKa ~ 4.8).[105]

$$HO_2^{\bullet} \rightarrow O_2^{\bullet-} \quad (196)$$

This is also the case in the irradiation of the resins suspended in water, which have a pH of approximately 9.9.

The reaction between two $O_2^{\bullet-}$ radicals is negligible.[105] $O_2^{\bullet-}$ is a reductive species and can transfer electrons to the C(=O)-O-C sites of the chain. It is also expected that the thermal decomposition of H_2O_2 enhances the yield of $^{\bullet}OH$ according to:

$$H_2O_2 \rightarrow 2\ ^{\bullet}OH$$

The mechanism of the $O_2^{\bullet-}$-induced cleavage of esters

Aqueous, or "hydrated", electrons ($e_{aq}^{\bullet-}$) react very rapidly with the carbonyl and phenyl groups through addition reactions, mainly producing anion intermediates. These anions are subsequently converted to C-centered radicals through protonation reactions. $e_{aq}^{\bullet-}$ can also induce dechlorination of chlorinated compounds through the electron-capture mechanism.[197] In this work, the irradiations were performed under aerobic conditions. Therefore, the dissolved O_2 scavenges $e_{aq}^{\bullet-}$ to give rise to the formation of superoxide radicals during the irradiation:

$$e_{aq}^{\bullet-} + O_2 \rightarrow O_2^{\bullet-} \qquad k = 1.9 \times 10^{10}\ LM^{-1}s^{-1}\ (198)$$

$O_2^{\bullet-}$ can also react with the resin and induce degradation. The mechanism of $O_2^{\bullet-}$-induced degradation involves an electron transfer reaction from $O_2^{\bullet-}$ to the resins.

It has been reported that $O_2^{\bullet-}$ induces scissions on the backbone of the polyesters through a S_N2 substitution reaction to the carbonyl group of the esters.[199] S_N2 substitution is a type of nucleophilic substitution reaction where a lone pair of electrons on a nucleophile attacks an electron deficient electrophilic center. These results in the formation of a bond and the expulsion of a leaving group. Figure 65 shows the proposed mechanism of the S_N2 substitution.

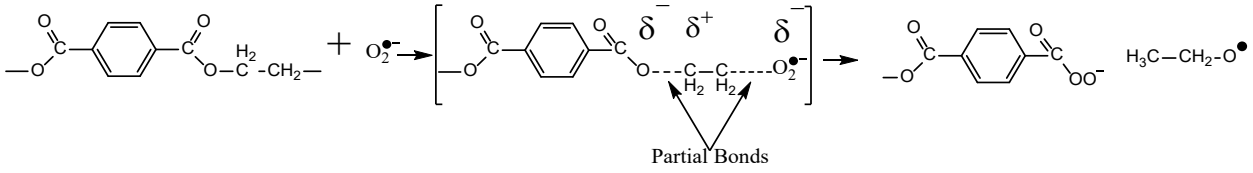

Figure 65. Degradation of the polyester through an S_N2 substitution reaction.

The mechanism of esters' tetroxide formation and their decays

In addition to its reaction with $e_{aq}^{\bullet-}$, O_2 also plays a vital role in enhancing the degradation process through oxidation reactions. Oxygen reacts very rapidly with C-centered radicals,

producing the corresponding peroxyl radicals ($RO_2^{\bullet}$). This is a major step towards oxidation and, eventually, degradation of the resins. These peroxyl radicals undergo various reactions including self-fragmentation.

A high dose rate of 200 kGy per hour was used in this work which favors the bimolecular reaction mode of the peroxyl radicals to produce the intermediate tetroxide as shown in Figure 66:

$$2\ RO_2^{\bullet} \rightarrow ROOOOR \ ^{(200)}$$

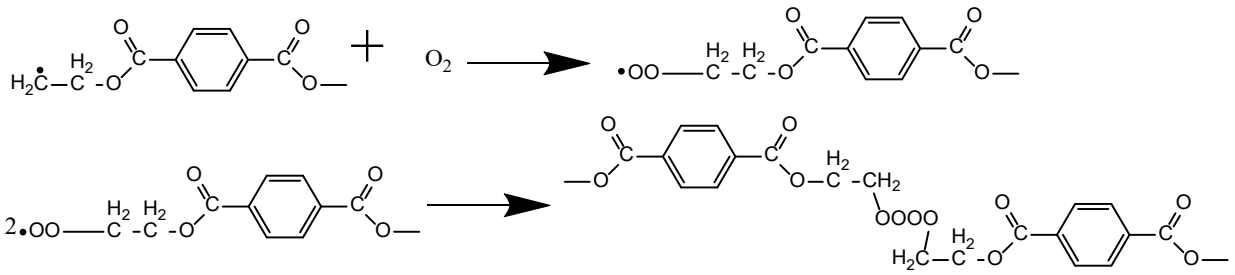

Figure 66. Schematic of the formation of the tetroxide after high-dose irradiation in the presence of oxygen.

The intermediates ROOOOR undergo various decomposition processes leading to degradation of the resins. Figure 67 shows that the tetroxide may decompose through concerted

decay without (a), and with water molecules (b), through the Bennett mechanism.[34,35]

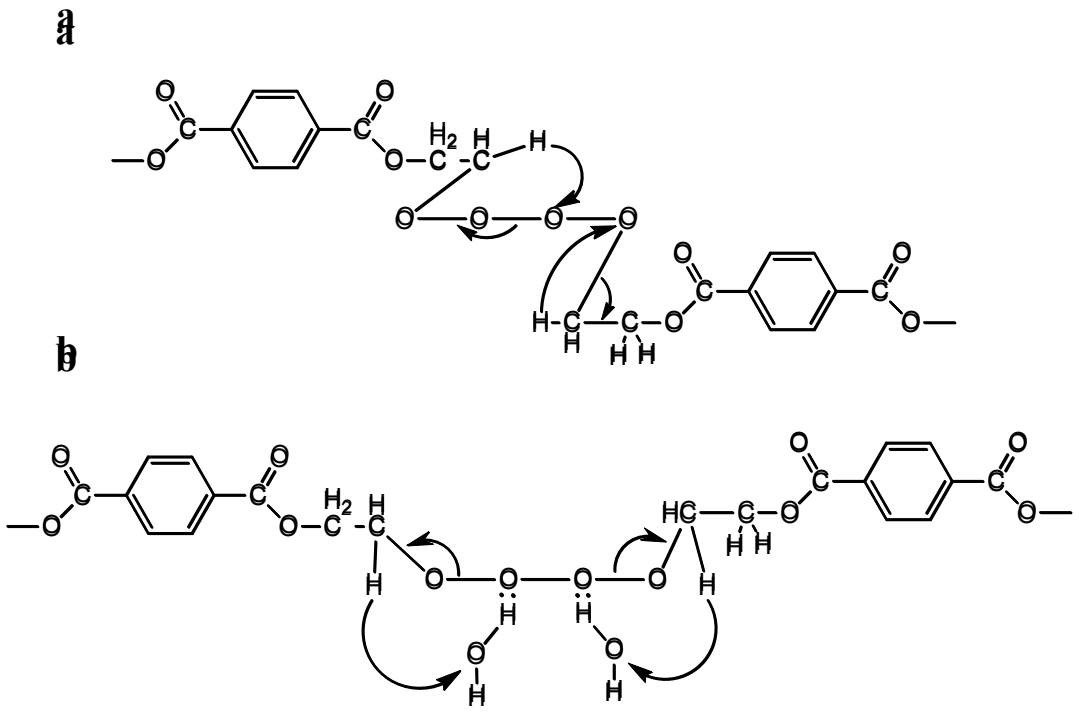

Figure 67. Decomposition of tetroxide formed from the polyester-based resin without (a) and with (b) two water molecules by "Bennet mechanism".[201,202]

Other proposed R1OOOOR2 decay mechanisms are suggested, which involve the production of the aldehyde and ketone.[200] Thus, hydrated radicals induce formation of superoxide radicals that stabilize homolytically cleaved polymer segment free radicals, which subsequently deliver oxidized, decomposed non-radical products.

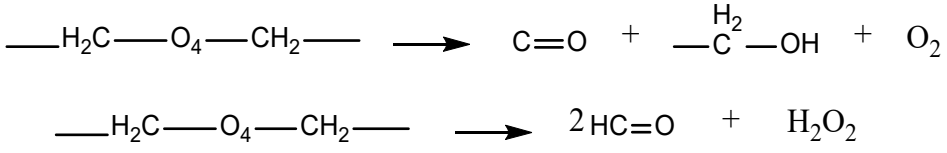

2. Irradiation of 1R, 2R, 3R, and 4R resins in a DMSO/water mixture

Figure 68 shows the EPR spectra of the 1R, 2R, 3R, and 4R resins irradiated in a 50:50 mixture of DMSO and water. Similar to the previous results of the resins irradiated in water, resins 2R, 3R, and 4R exhibit a singlet centered at around 3450 G.

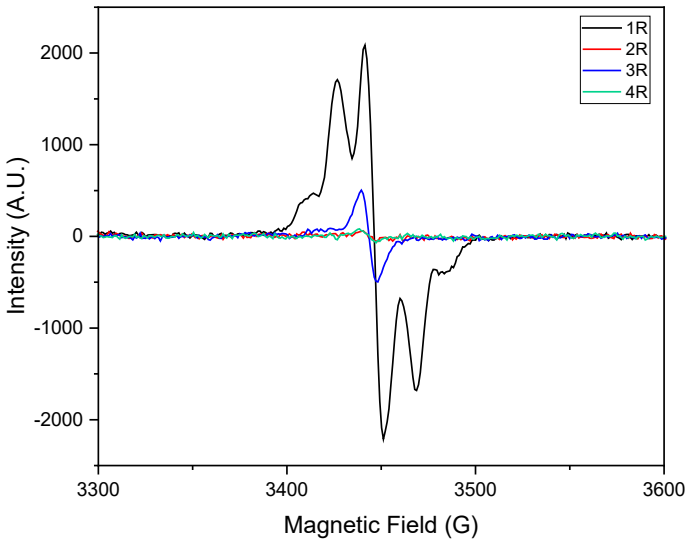

Figure 68. EPR spectra of 1R, 2R, 3R, and 4R resins irradiated in a DMSO-and-water mixture (50:50 ratio) by electron beam. All samples were irradiated to a total dose of 1000 kGy at a dose rate of 200 $kGyh^{-1}$.

The expected reaction from the irradiation of the resins in the DMSO/water solution is shown in Figure 69. Even though DMSO enhances the solubility of the resin in solution, it will scavenge hydroxyl radicals and result in the formation of methyl radicals ($\bullet CH_3$). It is not expected that the $\bullet CH_3$ radical will react with hydrogen peroxide (H_2O_2) since the production of hydrogen peroxide is expected to be very small. However, it should be noted that a quartet only appeared for resin 1R, which contains dicyclopentadiene. This can be explained by a methyl radical abstracting hydrogen from the cyclopentadiene, producing a quartet.

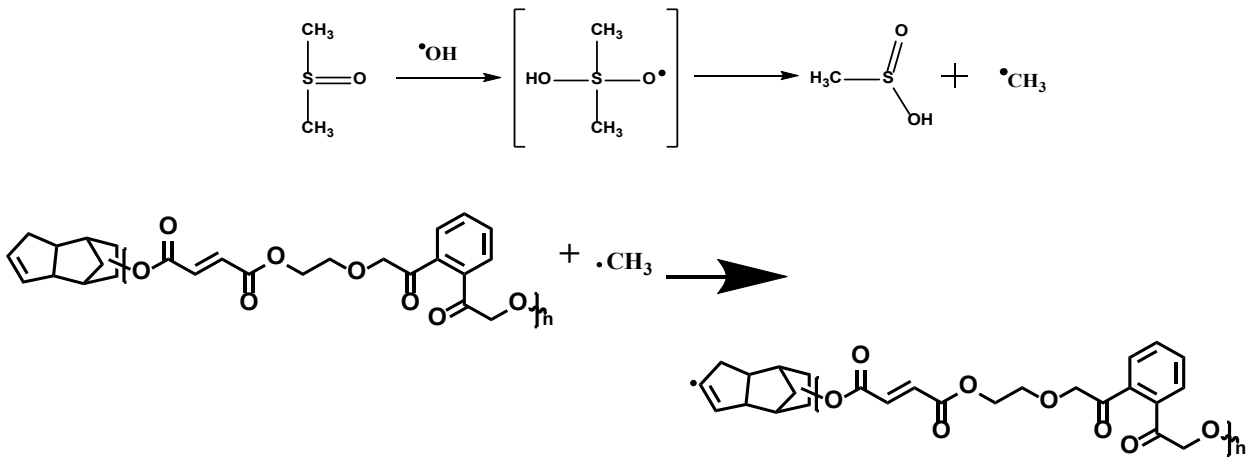

Figure 69. DMSO interaction with •OH radicals[203] (top), and reaction of methyl radical from irradiation in DMSO/water solution with 1R resin (bottom).

The calculation of the number of peaks expected from equation1.18 is shown in Table 13. If both radicals are present, a total of 4 peaks are observed in the EPR as is the case for the resin 1R irradiated in the DMSO/water mixture. Since the alkoxyl radicals are very reactive, as discussed above, the C-centered radical is the most likely to be characterized in the EPR spectrum.

Table 13. Schematic representation of radical species formed after the radiation-induced scission of polyester chains, and calculation of the number of peaks expected from the hyperfine splitting of each radical.

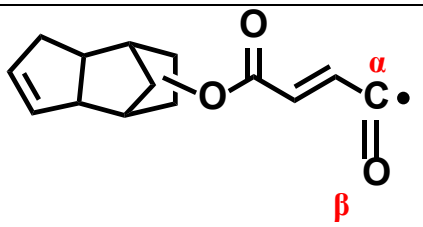	$(2(0)+1)$ $=1$
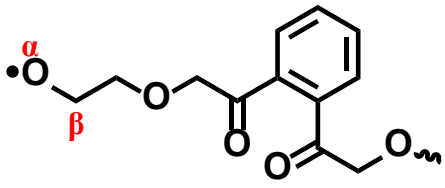	$(2(0)+1)(2(2(1/2)+1)$ $=3$

3. Irradiation of 1R, 2R, 3R, and 4R resins in isopropyl alcohol (IPA)

Figure 70 shows the EPR spectra of the resins after e-beam irradiation in IPA solution, where a singlet for resins 1R, 2R, 3R, and 4R is observed. It should be noted that the IPA molecules in the polyester resins scavenge a portion of the electrons, leading to a decrease in the direct formation of the polyester radicals. Radiolysis of IPA with an electron beam yield reducing species; solvated electrons (e_s^-), hydrogen atoms, and $(CH_3)_2C^{\bullet}OH$. The G(e_s^-) is 0.104 μmolJ-1 to 0.114 μmolJ^{-1} .[105] H-atoms are formed from the dissociation of the $(CH_3)_2COH)^*$ excited state.

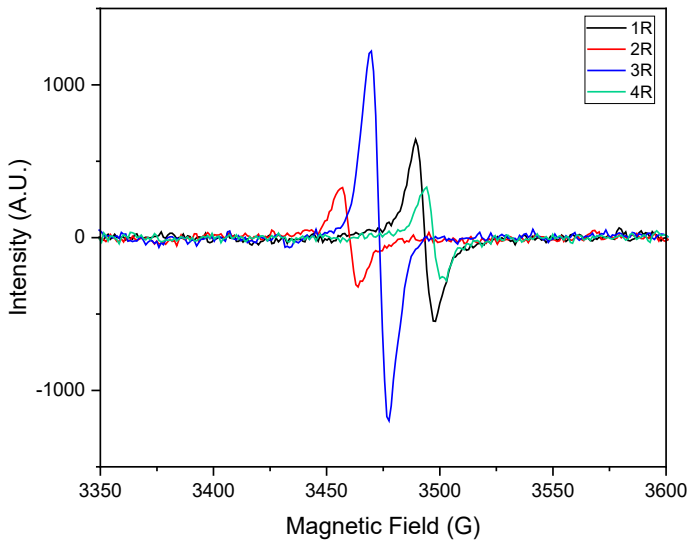

Figure 70. EPR spectra of irradiated 1R, 2R, 3R, and 4R resins in IPA by electron beam at a dose-rate 200 kGy/h, to a total dose of 1000 kGy.

Both e_s^- and H-atoms react very rapidly with dissolved O_2 in the resin-IPA mixtures to produce $O_2^{\bullet-}$, and $HO_2^{\bullet}$, respectively. As mentioned earlier, it is expected that $O_2^{\bullet-}$ reacts with the resins' main constituents, polyesters and the unsaturated (vinyl) monomers, through the SN_2 mechanism. Unlike in the presence of H_2O, it is expected that $HO_2^{\bullet}$ is present in the absence of

H_2O. $HO_2^{\bullet}$ can easily abstract H-atoms from polyesters and the vinyl monomers, leading to the formation of the C-centered radicals.

The stability of polyester alkoxyl radicals

Figure 71 shows the EPR spectra of the irradiated (neat and solvents) polyester resins after 5 months, in the presence of O_2. The EPR results show the presence of polyester alkoxyl radicals even 5 months after the irradiation, but with much smaller concentrations. As mentioned earlier, alkoxyl radicals are very strong oxidizing species, and therefore do not react with O_2. However, they do abstract H atoms from any adjacent C-H groups to produce organic peroxide and alkyl C-centered radicals. Because of the high viscosity of the media, it is expected that the abstraction reactions are relatively slow. The produced C-centered radicals can react with the dissolved O_2 to produce the corresponding peroxyl radicals.

A

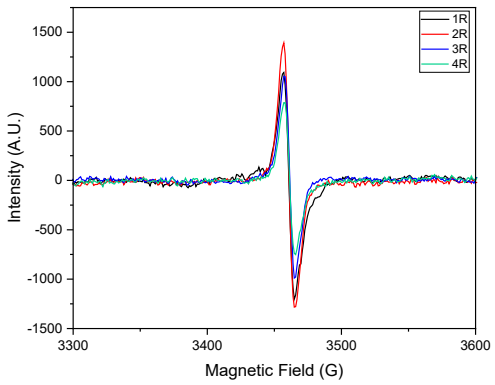

b

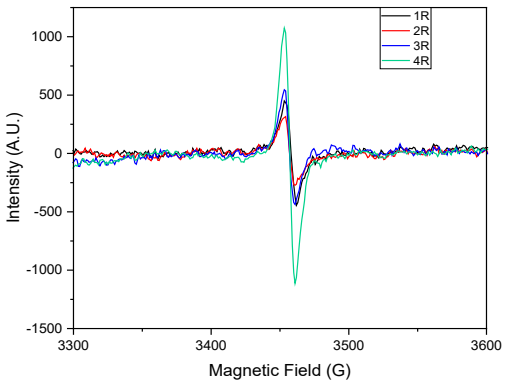

c d

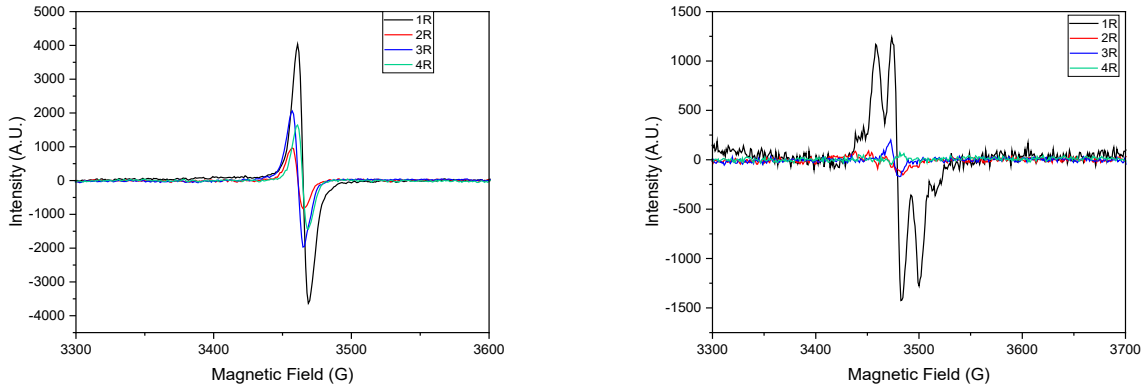

Figure 71. EPR spectra of 1R, 2R, 3R, and 4R resins irradiated in (a) no solvent, (b) water, (c) IPA, and (d) DMSO and water, 5 months after being irradiated by electron beam.

3.6.2 Changes in viscoelastic properties from irradiation in solvent environments

Dynamic mechanical analysis (DMA) is a sensitive technique that is used to assess the dynamic response and the various motional modes present in polymeric materials. Compared to a conventional mechanical test, a sinusoidal stress/strain is applied while varying the frequency and temperature, and the response is measured. DMA was employed in this study as a way of probing the subtle changes in polymer chain architecture as a response to various radiation treatments and solvent environments. At experimental temperatures below T_g, the material is a rigid, glassy solid consistent with low levels of coordinated motion. As the temperature increases, the network's free volume increases and coordinated motions of the polymer chains over larger length scales become possible. The broadness and shape of these transitions lend valuable insight into the distributions of behaviors in the polymer chains that comprise the bulk system. The region of behavior in thermosets for $T > T_g$ is referred to as the rubbery plateau. In the rubbery plateau, the storage modulus (E′) is proportional to the molecular weight between crosslinks (M_c).[204] Another characteristic parameter, tan δ, is the tangent of the phase angle (δ) for viscoelastic materials and is calculated as the ratio between the loss modulus (E″) and E′, which is related to the damping

characteristics of the tested material. Changes in the storage modulus and tan δ responses for the four resin systems are summarized in Table 14. For each resin studied here, the reference values are recorded in Table 14 as absolute units where the various dosing conditions are taken as the relative change from the reference. Resin 1R shows the largest change in T_g (ΔT_g) due to e-beam irradiation of all resin materials, with magnitudes of 50 °C or more in both dry and solvated environments, for all resin systems investigated here. Modulus values in the rubbery plateau (E'_R) also increase concurrently, consistent with increased degrees of cure. Previous studies have distinctly shown that both e-beam and γ-radiation can be used to cross-link resins to high degrees of cure.

Table 14. Summary of key mechanical property changes as a function of treatment environment. Reference samples are recorded as absolute values while the dosed samples are computed as the relative change.

	1R					2R				
	Ref	**Air**	**Water**	**IPA**	**DMSO**	**Ref**	**Air**	**Water**	**IPA**	**DMSO**
Δ T_g	118.1	58.4	59.7	54.0	56.5	124.0	7.30	4.50	6.00	9.00
Δ E'_R (MPa)	12.7	15.1	18.4	10.9	6.9	24.7	1.70	1.00	-0.8	1.80

	3R					4R				
	Ref	**Air**	**Water**	**IPA**	**DMSO**	**Ref**	**Air**	**Water**	**IPA**	**DMSO**
Δ Tg	99.3	14	11.5	14.9	-	158.5	-3.0	-31.7	-5.9	-8.9
Δ E'_R (MPa)	4.99	2.01	1.18	0.87	-	32.8	9.10	-8.10	5.40	7.20

This result suggests that the DCPD-based resin formulation cures more effectively in the e-beam than the other formulations used in this study, likely due to the high degree of residual unsaturation from the DCPD moiety. Isophthalic-based (2R) and BPA-based (3R) compositions

both display relatively narrow increases in T_g, with all relative shift magnitudes occurring between 4 °C to 15 °C. This is again consistent with the expected system behavior associated with improved curing; however, the reduced magnitude of ΔT_g relative to 1R suggest that these systems are comprised of functional groups that are less sensitive to new radiation-induced crosslinking bond formation. Dawes and coworkers showed the radiation resistance of polyester plastics which predominately crosslink in vacuum;[205] however, aromatic polyesters are more resistant to radiation than those with dominant aliphatic segments. Thus, compared to other products, the one with DCPD is expected to be impacted the most. Resin 3R irradiated in DMSO was not able to be tested due to rupture of the sample. We attribute this to the solvent affinity between the BPA based thermoset and DMSO, which was high enough that swelling-induced stress led to catastrophic crack formation that was also apparent for several other formulations in dichloromethane for swelling studies. Despite the limitations the rupture of the 3R sample presents with respect to viscoelastic characterization of the irradiated bulk material, it does show a promising avenue for potential synergistic effects whereby swelling-induced rupture may enhance the delivery of radiation for additional deconstruction. The highly-crosslinked terephthalic acid resin (4R) system exhibits a distinctly different structural change relative to the other compositions. Slight reductions in the T_g are observed for all irradiation conditions, except for the bulk sample irradiated in water where a relative T_g reduction of over 30 °C is observed (Figure 72b, Table 14). As expected, a reduction in E'_R is observed consistent with a reduction in the crosslink density (ν) as shown in Figure 73a. Tan δ also increases in the water-irradiated sample, indicating an increase in the damping character of the material due to higher chain mobility. This result is clear evidence of bond scission in the networked polymer based on the terephthalic acid system.

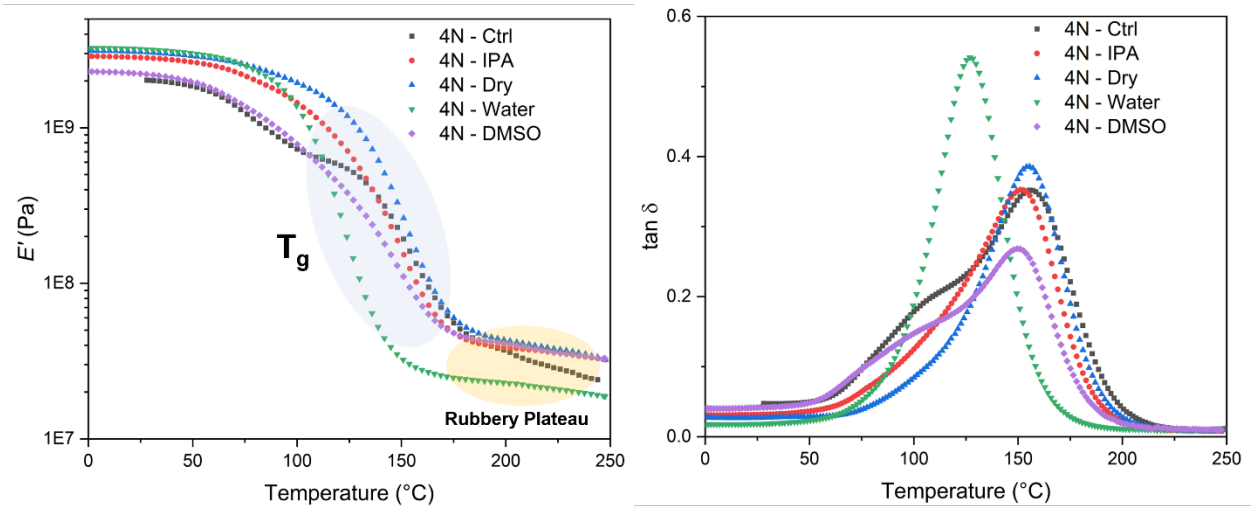

Figure 72. Representative data from dynamic mechanical testing. (a) Resin system 4R (terephthalic acid based) showing changes in G' as a function of temperature and dosing environment. (b)Tanδ as a function of temperature for each resin formulation.

Homopolymer polyesters are known to undergo C(=O)-O-C scission along the backbone of the chains upon irradiation, therefore we would expect their T_g values to decrease as a function of dose.[105] Despite the EPR results, which show clear scissions in all resins in the presence and absence of solvents, their T_g values of 1R, 2R, 3R, and 4R increase upon irradiation. The components of all these resins include maleic anhydride, glycols, small amounts of vinyl monomers (MMA, vinyl toluene), phthalic anhydride, isophthalic acid, propylene glycol and terephthalic acid. All these compounds can undergo ionizing-induced polymerization reactions. In addition, with a dose of 1000 kGy, it is expected that the radiolytically-produced polymers can even undergo crosslinking reactions. These radiolytically-produced crosslinked polymers can lead to the increase in T_g of the irradiated resins.

Table 14 shows that the T_g of O_2-saturated 4R aqueous solutions decreases by 31.7 ˚C. As mentioned in Table 4, 4R resin is a highly cross-linked terephthalic polyester resin. Upon irradiation of the 4R aqueous solutions, •OH radicals abstract H atoms from CH_2 groups, and add to the phenyl groups along the backbone of the of the polyester chains, respectively. The reaction

rate constants are very high; on the order of 10^9 $Lmol^{-1}s^{-1}$ to 10^{10} $Lmol^{-1}s^{-1}$.[105] The addition of the $^{\bullet}OH$ to the phenyl groups along the chain produces cyclohexadienyl systems with unpaired electrons that are not localized on a particular carbon atom in the phenyl ring.[105] It is the abstraction of H-atom from the CH_2 groups that initiates the splitting of the C-O-C bond along the backbones of the polyester chains. The C-centered radicals produced from the H-abstraction undergo very rapid hydrolytic scission at the C-O-C linkage, leading to the production of alkoxyl radicals.[105] These results indicate that radiolytic scission in the presence of solvents can lead to synergistic network breakdown as an alternative to combustion or landfilling. Additional work is needed to fully delineate the effects of repeat unit chemistry and network connectivity on the propensity for deconstruction and re-use of these thermoset formulations.

4. Conclusions:

This dissertation focuses on the design, synthesis, and analysis of novel aramid fibers by covalently incorporating nanocellulose through electron beam irradiation. These synthesized high-performance fibers have higher strength and more surface area, making them ideal for the use in fiber-reinforced composites such as the ones used for body armor applications. Aramid fibers were also modified by inducing crosslinking reactions as a means to avoid scission of the polymeric backbone and resulting in an increase in their strength using electron beam irradiation. Both methods were applied for UHMWPE fibers as part of this thesis. The radiation effects on polymers, which are highly dependent on their chemical structures, were also studied by irradiating epoxy aromatic polyester-based resins. Due to the presence of the π structure of the phenyl groups, and the epoxy groups, both of which scavenge electrons, it is very difficult to produce free radicals on the backbone of the polyester chain. Furthermore, the steric effects of the phenyl groups impede the grafting reactions. In this work we looked at the recycling of the polyester rather than grafting, and we proposed the grafting onto epoxy aromatic polyester-based resins for future work.

4.1 Design, synthesis, and analysis of nanocellulose grafted polymer fibers

Nanocellulose was selected as the ideal filler to increase the strength and improve interactions at the interface of aramid fibers. It is impossible to directly graft cellulose onto the backbone of any polymers because of the absence of C=C double bonds in its structure. Therefore, from the beginning, the strategy has been to introduce unsaturation onto the cellulose molecules. Styrene was chosen as the best candidate to lace the cellulose molecule with a double bond, since styrene undergoes radiation polymerization. Another issue is that the irradiation of nanocellulose leads to the glycosidic scission of the cellulosic chains, i.e., degradation. Thus, it is imperative not to include irradiation of the nanocellulose during any step of the grafting process. Through this thesis,

unmodified and styrene-containing nanocellulose were grafted onto aramid and UHMWPE fibers. Nanocellulose was chosen for its reactive, hydroxyl-full surface and high strength-to-weight ratio. An indirect radiation grafting approach was determined to be the best for incorporating the nanocellulose onto the fibers. This method prevents the degradation of the nanocellulose as just the polymer fibers are irradiated. The vinyl group on the styrene-nanocellulose are then grafted onto the amorphous regions of the fibers by bonding with the radicals generated during the fiber irradiation. It was concluded that the grafting procedure should be conducted at low temperatures in order to avoid homopolymerization of the nanocellulose during the grafting process.

The optimal radiation-grafting parameters were selected after studying the generation of free radicals on the fibers by EPR. Following the irradiation of the fibers at different conditions, the concentration, type, and decay of the radicals generated was analyzed. The availability of these radicals is of outmost importance since they represent the grafting sites to which the nanocellulose would subsequently be grafted to. The radical decay after irradiation of the fibers was also established to assure that there were enough radicals present for the grafting process.

After grafting, a gravimetric analysis was conducted to determine the most favorable parameters for the radiation-induced grafting of nanocellulose onto the fibers. The amount of grafting achieved was measured by calculating the degree of grafting (DoG). Negligible grafting was achieved for the direct grafting experiments, where both the nanocellulose and the fibers were irradiated together. Indirect grafting experiments of unmodified nanocellulose onto the fibers, also resulted in low DoGs, and thus negligible grafting. Successful grafting of styrene-nanocellulose onto the aramid fibers was achieved following an indirect grafting method. After confirming the grafting through the DoG calculations, SEM, FTIR, and NMR analysis of the nanocellulose-grafted fibers was done to look at the uniformity of the grafting and at the chemical changes within

the grafted fibers. NMR results show successful covalent bonding between the styrene-nanocellulose and the aramid fibers. The mechanical properties of the fibers after treatment were also studied. An increase of up to 15% in the tensile strength of the fibers was achieved. In conclusion, grafting was achieved through the addition reactions of the double bond from the styrene-nanocellulose molecules onto the radiolytically produced aramid free radicals, which lead to the formation of covalent bonds.

4.2 Radiation-induced crosslinking of aramid fibers

It is very well known that aramid chains have high resistance to ionizing radiation due the presence of phenyl groups. This made aramid one of the first choice for outer space applications. Therefore, it was the objective of this work to enhance the radiation-induced crosslinking by introducing a link that can covalently connect two aramid chains. Irradiation of the fibers in the presence of two crosslinking agents, acetylene and triacrylate, was explored as a means to crosslink the fibers and increase their strength. It was determined that irradiating the fibers at low doses, in the range of 5 to 40 kGy, and at high dose rates, in the presence of a crosslinker leads to an increase in the tensile strength of the fibers. A mechanism for the crosslinking of aramid fibers, in which the acetylene acts as a bridge between radicals generated on the aramid chain, was proposed. Fibers irradiated in an acetylene environment showed an increase in strength of up to 15%. The success of this approach would have a tremendous potential for radiation-induced crosslinking for radiation resistant polymers.

4.3 The fundamental differences between the radiation chemistry of aromatic polyester and aramid – Radiation-induced degradation of polyester-based resins for upcycling

This work shows that ionizing radiation can also initiate more scission of the C-O-C bond in the aromatic polyester chain as opposed to grafting. These aromatic polyesters are difficult to graft onto due to the presence of bulky phenyl groups on their chemical structure. Thus, instead of using radiation to graft nanomaterials onto polyester-based resins, radiation can be used to aid in their degradation. The recycling of materials can be achieved by either modifying or degrading them. In this thesis, the radiation-induced degradation of various aromatic polyester-based resins was studied.

It was demonstrated that e-beam irradiation induces scissions of the C-O-C bonds along the backbone of the chains of unsaturated polyester thermosets of different compositions based on dicyclopentadiene, isophthalic acid, epoxy vinyl ester, and terephthalic acid. EPR results show the formation of the alkoxyl radicals and C-centered radicals as the primary intermediate products of the C-O-C scissions. While the alkoxyl radicals exhibited great stability five months after the irradiation, the C-centered radicals decayed very rapidly via reactions with oxygen. The oxygen may have been absorbed onto the resin, dissolved in the solvent, or transported from the environment. The radiolytically produced •OH radicals in the unsaturated-ester aqueous solutions play a major role in inducing scissions on the backbone of the polymer chains. Despite the radiation-induced scissions, irradiation of the resins at a dose level of 1000 kGy results in an increase of the glass transition temperature, T_g. This is due to the simultaneous radiation-induced polymerization of the vinyl monomers, toluene, and styrene that are present in the resins. The results also show that radiolysis of 4R, a highly-crosslinked terephtalic acid resin, in aqueous

solutions yields a decrease of 31˚C in T_g which may present an avenue for breakdown of thermosets through radiolytic depolymerization. This work demonstrates that ionizing radiation triggers continuous free radical-chain reactions that lead to the formation of recyclable oligomers.

5. Contribution to Science

This dissertation presents the science of the irradiation effects on various polymeric materials including high-performance fibers, such as aramid and UHMW polyethylene, and polyester-based resins. The effects of radiation on polymers depend greatly on the chemical structure of the irradiated polymer. Radiation-induced grafting was explored in both aramid and UHMWPE fibers which have C-N or C-C bonds (Figure 73) that after radiolysis result in the production of reducing C-centered radicals. On the other hand, aromatic polyesters have bulky structures and phenyl groups which complicate the pathways to achieve radiation-induced grafting. In this case, radiation can be used to degrade the polymer through scission of the C-O-C bonds. Through the methods developed in this thesis, both for the irradiation induced grafting and crosslinking of aramid fibers, patentable novel fibers with an increase in strength of up to 15% were synthesized. The radiation induced degradation of polyester resins in different environments is a significant contribution to the upcycling of these materials.

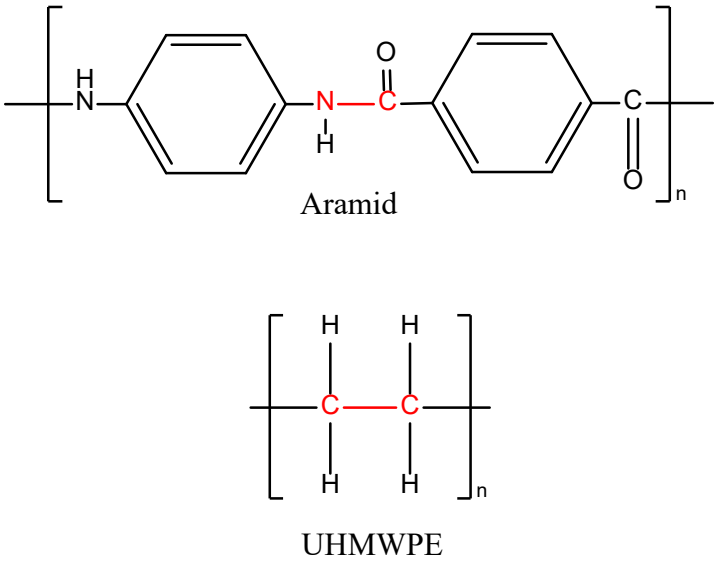

Figure 73. Chemical structure of aramid and UHMWPE showing the C-N and C-C bonds that lead to the formation of C-centered radicals after irradiation.

5.1 Contribution to grafting

Successfully grafting nanomaterials onto polymer fibers through irradiation not only resulted in an increase of the strength of the fiber, which is key for improved performance, but also it added functionality to the previously inert aramid. However, irradiation of nanocellulose leads to scission and degradation of the material due to the presence of glycosidic bonds in its structure. An alternative indirect radiation grafting method was developed to avoid irradiation of nanocellulose (Figure 74).

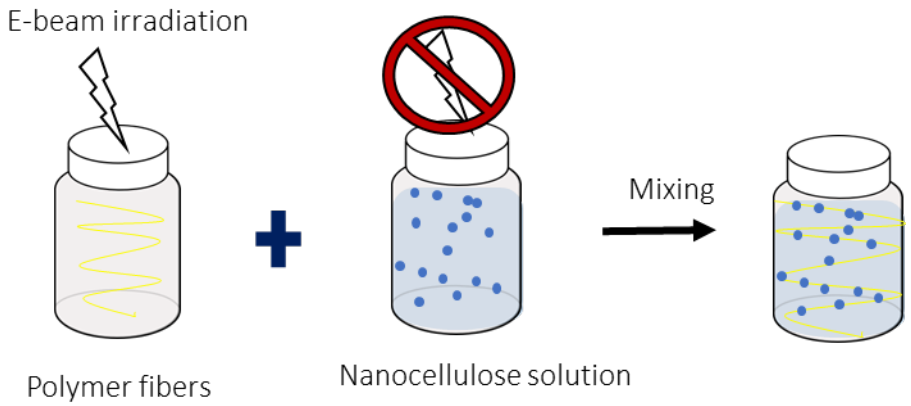

Figure 74. Schematic of the indirect irradiation grafting approach. Only the polymer fibers are irradiated and irradiation of the nanocellulose is avoided.

This indirect grafting method avoided the degradation of the nanocellulose, while generating free radicals all over the polymer fiber surface. A styrene-nanocellulose was also synthesized which contains an unsaturated bond that rapidly reacts with the free radicals on the irradiated fiber surface. Irradiation of the polymer fibers lead to the formation of C-centered radicals, which can add to the double bond of the nanocellulose. This represents a new method of grafting nanocellulose via radiation, which can be applied to a wide variety of polymer fibers. Grafting was achieved without the use of any harsh solvents, and only in the presence of water. The radicals generated on the surface of the aramid fiber were studied by EPR and their kinetics was presented, which has not been studied before.

5.2 Contribution to crosslinking

Aramid fibers have a high crystallinity, in the range of 75-77%. That means that only 25% is amorphous and available for crosslinking. Although the crystalline phase absorbs radiation and may degrade, the goal was to enhance the competing crosslinking reactions in the small amorphous region of the fibers. Acetylene and triacrylate were both used to induce crosslinking during irradiation of the fibers. Acetylene molecules facilitate crosslinking by acting as a bridge between

radicals generated in the fiber chain. The proposed mechanism is shown in Figure 75. An increase of up to 15% in the tensile strength of the fibers was achieved through this method.

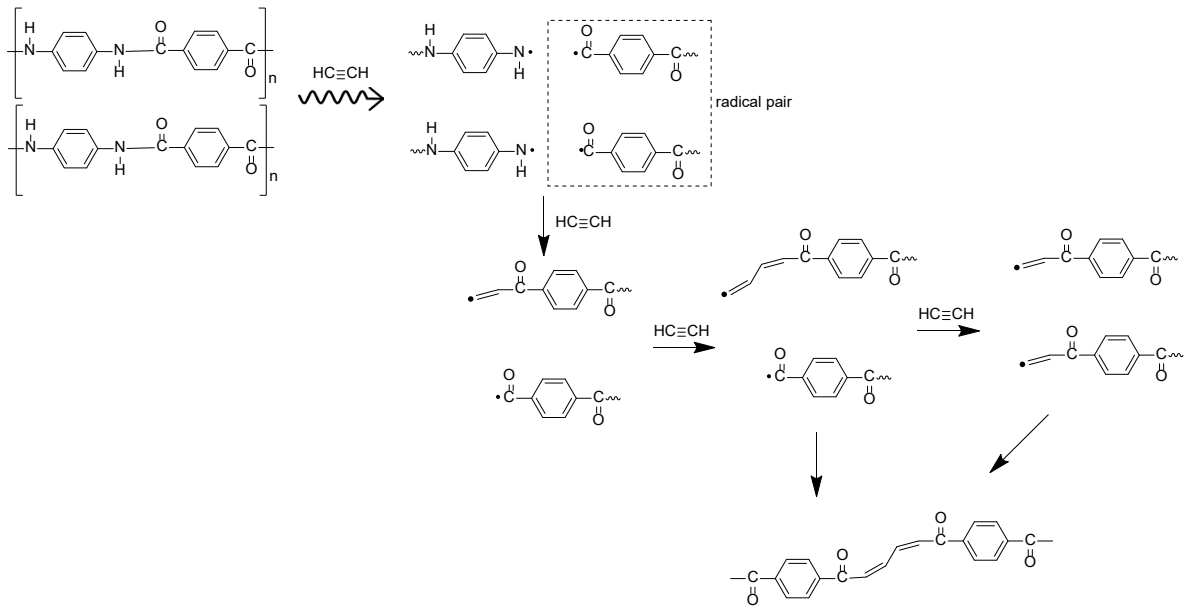

Figure 75. Proposed mechanism for the irradiation of aramid fibers in an acetylene environment. The acetylene molecules react with the C-centered radicals generated on the aramid and brings the chains closer, facilitating crosslinking.

.

5.3 Contribution to polyester-based resin upcycling

Despite the presence of radiation-protective phenyl groups in the polyester backbone, phenyl polyester networks can be scissioned and ultimately degraded by e-beam irradiation. EPR results of the four irradiated resins used in this work show the radiolytic production of the oxidizing and relatively stable alkoxyl radicals. The radiolytic production of the alkoxyl radicals is the result of the e-beam induced scissions of the C-O-C bonds on the backbone of the chains of these phenyl polyesters. Due to the complex multi-component nature of the commercial resins used in this work that contain radiation polymerizable monomers and oligomers, three of the four resins (1R, 2R, 3R) undergo polymerization reactions that lead to an increase in the T_g. In comparison with low

dose rate (gamma) radiolysis, the increase in the T_g of 1R, 2R and 3R was reduced since irradiation with a high dose rate hinders the propagation pathway and enhances the termination pathway during free radical polymerization. The results also show that radiolysis of 4R in aqueous solutions yields a decrease of 31˚C in T_g which may present an avenue for breakdown of thermosets through radiolytic depolymerization. It is concluded that •OH radicals produced from the radiolysis of water play a crucial role in inducing C-O-C scission and, hence, in decreasing the T_g of the 4R resin. The 4R resin formulation also is the most highly crosslinked resin system of the system studied here and, therefore, contains far fewer monomers than the other resins. It is anticipated that a smaller portion of the irradiation dose will be absorbed by the residual monomers and, consequently, unlike the other resins, radiation-induced polymerization, and subsequent crosslinking in 4R is insignificant. Also, a large portion of the irradiation dose is absorbed by water, which leads to the production of •OH. The relatively small value of G(e_s^-) (where e_s^- induces C-O-C scission) from the irradiation of isopropyl alcohol results in a decrease of the alkoxyl radicals.

6. Future Work

- Further NMR studies by looking at the spectrum of a model compound to better identify the peaks that show grafting
- Conduct NMR studies of the crosslinked aramid fibers to corroborate the proposed mechanism
- Fabricate an aramid fiber reinforced composite to test the interfacial shear strength and determine how it's improved
- Optimize resin degradation by the irradiation of all the resins in water, to higher doses, and with a higher concentration of oxygen

The work done on this thesis can be expanded on by fabricating fiber-reinforced polymer composites using the nanocellulose-grafted fibers. For comparison, a composite should also be synthesized with unmodified fibers. The composites can be fabricated following the vacuum assisted resin transfer molding (VARTM) procedure. For this process, nanocellulose should be grafted onto aramid fabric instead of individual fibers. After synthesizing the grafted fabrics, an epoxy resin will be flowed onto the fabrics inside a vacuum bag. It is essential to keep the material under vacuum during the duration of the procedure. Then, the tensile, compressive, and shear strength of the composite can be evaluated by three-point flexural and short beam strength tests, following the ASTM standards for polymer composites. Interfacial shear strength tests should be conducted to determine how the grafting affects the interfacial strength of the composite.

Additionally, the developed grafting methods can be applied on other types of high-performance polymer fibers. Nylon fibers also have a wide range of applications and thus increasing their strength and functionality is of interest. Figure 76 shows the structure for these fibers as potential fibers to graft nanocellulose onto. The effects of irradiation on these fibers should be determined by EPR and mechanical testing before starting the grafting procedure.

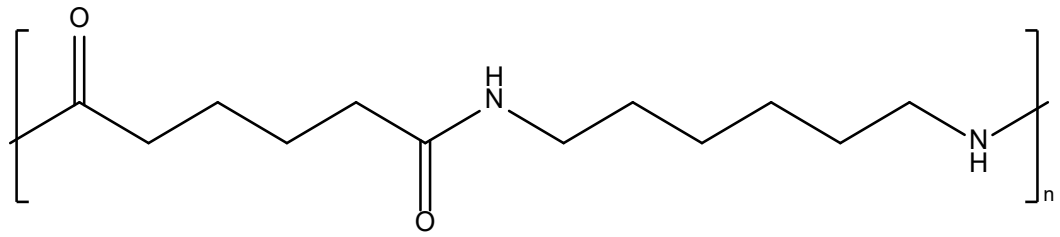

Figure 76. Chemical structure of nylon-6,6 as a potential fiber for future grafting experiments.

The two fiber modifying procedures can be combined by irradiating the fibers in an acetylene environment and utilizing the remaining radicals for grafting. In this thesis, the un-crosslinked radicals were annealed immediately following irradiation to avoid their oxidation

which could lead to fiber degradation. However, these radicals may be used for further grafting of nanocellulose onto the fibers without the need of more irradiation. First steps would be to determine the presence and concentration of these radicals by EPR. Then, nanocellulose can be introduced onto the fibers following the same indirect grafting approach developed in the thesis. Since both of these processes resulted in an increase in the strength of the fibers, an even higher strength may be achieved after applying both.

Although UHMW polyethylene fibers were subjected to the same treatment as the aramid fiber, their mechanical properties were not studied. Future studies should first focus on the issue of entanglement of the UHMWPE fibers during the grafting process. When coming into contact with the nanocellulose solution, the fibers become tangled, making it difficult to perform the gravimetric analysis. It also makes it impossible to conduct the tensile tests. This process can be improved by stretching out the fibers and submerging it in the solution for the grafting process. A set up such as the one shown in Figure 77, in which the fiber is kept taut between the edges of the cardboard window can be tried.

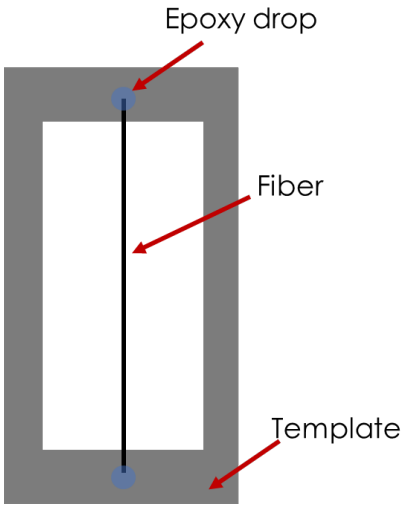

Figure 77. Schematic of the proposed template to keep the fibers taut during the grafting experiments.

As for the polymer degradation part of this thesis, to accomplish greater degradation of the phenyl-unsaturated polyester-based resins, a combination of radiolysis conditions needs to be chosen carefully to maximize the scission of the C-O-C bonds of the polyester chains and to prevent the polymerization reactions of the vinyl monomers that are already present in the resins. This work recommends that water be used as a solvent to take advantage of the production of $^{\bullet}OH$ radicals which lead to higher degrees of scissions. Use of higher O_2 concentrations is advised to prevent the polymerization reactions of the vinyl monomers and to react with the radiolytically-produced C-centered radicals of the polyester chains to prevent the crosslinking reactions between them.

It is of interest to explore the possibility of radiation-induced grafting of these phenyl polyester-based resins as well. Modifying these resins through grafting can also contribute to the polymer upcycling effort. The methods developed for the radiation-induced grafting of nanocellulose onto the aramid can be applied to these resins, while adjusting the necessary parameters to promote grafting over the competing scission reactions. Similar polymers to the phenyl polyester-based resins studied in this work, such as polyethylene terephthalate (PET), have been previously used for grafting.[206] In this case, the first step would be to remove any oxygen from the environment of the material before and during irradiation. As previously mentioned, the presence of oxygen is one of the factors that induce degradation. Another change to the irradiation conditions would be to irradiate the resins at a lower dose. In this work, degradation was induced at a dose of 1000 kGy, to favor grafting a lower dose, up to 300 kGy as was done for the aramid fibers, should be selected. EPR analysis of the irradiated resins is of outmost importance, to identify the formation of reducing C-centered radicals after irradiation.

References

(1) Citation, S. *High-Performance Structural Fibers for Advanced Polymer Matrix Composites*; 2005. https://doi.org/10.17226/11268.

(2) Kotek, R. Recent Advances in Polymer Fibers. *Polym. Rev.* **2008**, *48* (2), 221–229. https://doi.org/10.1080/15583720802020038.

(3) Lane, R. A. High Performance Fibers for Personnel and Vehicle Armor Systems. *AMPTIAC* **2005**, *9* (2).

(4) Nayak, N. V. Composite Materials in Aerospace Applications. *Int. J. Sci. Res. Publ.* **2014**, *4* (9).

(5) Park, J. H.; Rutledge, G. C. 50th Anniversary Perspective : Advanced Polymer Fibers: High Performance and Ultrafine. *Macromolecules* **2017**, *50* (15), 5627–5642. https://doi.org/10.1021/acs.macromol.7b00864.

(6) Singh, T. J.; Samanta, S. Characterization of Kevlar Fiber and Its Composites: A Review. *Mater. Today Proc.* **2015**, *2* (4–5), 1381–1387. https://doi.org/10.1016/j.matpr.2015.07.057.

(7) Zhang, T.; Song, Y.; Zhao, Y.; Zhang, B. Effect of Hybrid Sizing with Nano-SiO2on the Interfacial Adhesion of Carbon Fibers/Nylon 6 Composites. *Colloids Surfaces A Physicochem. Eng. Asp.* **2018**, *553* (37), 125–133. https://doi.org/10.1016/j.colsurfa.2018.05.050.

(8) Bandaru, A. K.; Chavan, V. V; Ahmad, S.; Alagirusamy, R.; Bhatnagar, N. Ballistic Impact Response of Kevlar® Reinforced Thermoplastic Composite Armors. *Int. J. Impact Eng.* **2016**, *89*, 1–13. https://doi.org/10.1016/j.ijimpeng.2015.10.014.

(9) Cline, J.; Moy, P.; Harris, D.; Yu, J.; Wetzel, E. *The Ballistic Response of Woven Kevlar Fabric as a Function of Projectile Sharpness*; 2019.

(10) Jacobs, M. J. N.; Van Dingenen, J. L. J. Ballistic Protection Mechanisms in Personal Armour. *J. Mater. Sci.* **2001**, *36* (13), 3137–3142. https://doi.org/10.1023.

(11) Wang, Y.; Zhupanska, O. I. Lightning Strike Thermal Damage Model for Glass Fiber Reinforced Polymer Matrix Composites and Its Application to Wind Turbine Blades. **2015**. https://doi.org/10.1016/j.compstruct.2015.07.027.

(12) Hollaway, L. C. High Performance Fibre-Reinforced Composites for Sustainable Energy Applications. In *High Performance Textiles and Their Applications*; 2014; pp 366–417. https://doi.org/10.1533/9780857099075.366.

(13) Daynes, S.; Weaver, P. M. Design and Testing of a Deformable Wind Turbine Blade Control Surface. *Smart Mater. Struct.* **2012**, *21* (10). https://doi.org/10.1088/0964-1726/21/10/105019.

(14) Chen, Y. Y. The Application of Carbon Fiber Materials in Sports Equipment. *Appl. Mech. Mater.* **2014**, *687–691* (Emim), 4240–4243.

https://doi.org/10.4028/www.scientific.net/AMM.687-691.4240.

(15) Kaufmann, J. New Materials for Sports Equipment Made of Anisotropic Fiber-Reinforced Plastics with Stiffness Related Coupling Effect. *Procedia Eng.* **2015**, *112*, 140–145. https://doi.org/10.1016/j.proeng.2015.07.189.

(16) Red, C. Market Outlook: Carbon fiber in sporting goods | CompositesWorld https://www.compositesworld.com/articles/market-outlook-carbon-fiber-in-sporting-goods (accessed Feb 1, 2021).

(17) Nasser, J.; Lin, J.; Steinke, K.; Sodano, H. A. Enhanced Interfacial Strength of Aramid Fiber Reinforced Composites through Adsorbed Aramid Nanofiber Coatings. *Compos. Sci. Technol.* **2019**, *174*, 125–133. https://doi.org/10.1016/j.compscitech.2019.02.025.

(18) Ehlert, G. J.; Sodano, H. A. Zinc Oxide Nanowire Interphase for Enhanced Interfacial Strength in Lightweight Polymer Fiber Composites. *ACS Appl. Mater. Interfaces* **2009**, *1* (8), 1827–1833. https://doi.org/10.1021/am900376t.

(19) Fu, S.; Yu, B.; Tang, W.; Fan, M.; Chen, F.; Fu, Q. Mechanical Properties of Polypropylene Composites Reinforced by Hydrolyzed and Microfibrillated Kevlar Fibers. *Compos. Sci. Technol.* **2018**, *163*, 141–150. https://doi.org/10.1016/j.compscitech.2018.03.020.

(20) Maity, J.; Jacob, C.; Singh, R. P. Effect of Surface Fluorination of Poly (p-Phenylene Terephthalamide) Fiber. *Def. Sci. J.* **2014**, *64* (3), 230–235. https://doi.org/10.14429/dsj.64.7321.

(21) Ramasamy, N.; Arumugam, V.; Rajkumar, S. Surface Modification of Kevlar Fibre Fabric and Its Influence on the Properties of Kevlar/Epoxy Composites. *Bull. Mater. Sci.* **2019**, *42* (4), 173. https://doi.org/10.1007/s12034-019-1868-3.

(22) Gonzalez-Chi, P. I.; Rodríguez-Uicab, O.; Martin-Barrera, C.; Uribe-Calderon, J.; Canché-Escamilla, G.; Yazdani-Pedram, M.; May-Pat, A.; Avilés, F. Influence of Aramid Fiber Treatment and Carbon Nanotubes on the Interfacial Strength of Polypropylene Hierarchical Composites. *Compos. Part B Eng.* **2017**, *122*, 16–22. https://doi.org/10.1016/j.compositesb.2017.04.006.

(23) Uribe, B. E. B.; Chiromito, E. M. S.; Carvalho, A. J. F.; Arenal, R.; Tarpani, J. R. TEMPO-Oxidized Cellulose Nanofibers as Interfacial Strengthener in Continuous-Fiber Reinforced Polymer Composites. *Mater. Des.* **2017**, *133*, 340–348. https://doi.org/10.1016/j.matdes.2017.08.004.

(24) Ansari, F.; Galland, S.; Johansson, M.; Plummer, C. J. G.; Berglund, L. A. Cellulose Nanofiber Network for Moisture Stable, Strong and Ductile Biocomposites and Increased Epoxy Curing Rate. *Compos. Part A Appl. Sci. Manuf.* **2014**, *63*, 35–44. https://doi.org/10.1016/j.compositesa.2014.03.017.

(25) Guo, J.; Li, Y.; Wu, S.; Li, W. The Effects of γ-Irradiation Dose on Chemical Modification of Multi-Walled Carbon Nanotubes. *Nanotechnology* **2005**, *16* (10), 2385–2388. https://doi.org/10.1088/0957-4484/16/10/065.

(26) Godara, A.; Gorbatikh, L.; Kalinka, G.; Warrier, A.; Rochez, O.; Mezzo, L.; Luizi, F.; van Vuure, A. W.; Lomov, S. V.; Verpoest, I. Interfacial Shear Strength of a Glass Fiber/Epoxy

Bonding in Composites Modified with Carbon Nanotubes. *Compos. Sci. Technol.* **2010**, *70* (9), 1346–1352. https://doi.org/10.1016/j.compscitech.2010.04.010.

(27) Kalantar, J.; Drzal, L. T. The Bonding Mechanism of Aramid Fibres to Epoxy Matrices - Part 1 A Review of the Literature. *J. Mater. Sci.* **1990**, *25* (10), 4186–4193. https://doi.org/10.1007/BF00581071.

(28) Cheng, Z.; Li, B.; Huang, J.; Chen, T.; Liu, Y.; Wang, X.; Liu, X. Covalent Modification of Aramid Fibers' Surface via Direct Fluorination to Enhance Composite Interfacial Properties. *Mater. Des.* **2016**, *106*, 216–225. https://doi.org/10.1016/j.matdes.2016.05.120.

(29) Andrews, M. C.; Bannister, D. J.; Young, R. J. The Interfacial Properties of Aramid/Epoxy Model Composites. *J. Mater. Sci.* **1996**, *31* (15), 3893–3913. https://doi.org/10.1007/BF00352650.

(30) Uribe, B. E. B.; Chiromito, E. M. S.; Carvalho, A. J. F.; Tarpani, J. R. Low-Cost, Environmentally Friendly Route for Producing CFRP Laminates with Microfibrillated Cellulose Interphase. *Express Polym. Lett.* **2017**, *11* (1), 47–59. https://doi.org/10.3144/expresspolymlett.2017.6.

(31) Ahmed, D.; Hongpeng, Z.; Haijuan, K.; Jing, L.; Yu, M.; Muhuo, Y. Microstructural Developments of Poly (p-Phenylene Terephthalamide) Fibers during Heat Treatment Process: A Review. *Mater. Res.* **2014**, *17* (5), 1180–1200. https://doi.org/10.1590/1516-1439.250313.

(32) Hancox, N. . Kevlar Aramid Fiber. *Mater. Des.* **2017**, *14* (5), 312–313. https://doi.org/10.1016/0261-3069(93)90147-N.

(33) Takayanagi, M.; Ueta, S.; Lei, W.-Y.; Koga, K. A New Chemical Method of Surface-Treatment of Kevlar Fiber for Composites with Epoxy Resin. *Polym. J.* **1987**, *19* (5), 467–474. https://doi.org/10.1295/polymj.19.467.

(34) Kalagi, G. R.; Patil, R.; Nayak, N. *Experimental Study on Mechanical Properties of Natural Fiber Reinforced Polymer Composite Materials for Wind Turbine Blades*; 2018; Vol. 5.

(35) Aerospace Materials with Kevlar® https://www.dupont.com/fabrics-fibers-and-nonwovens/kevlar-for-aerospace.html (accessed Feb 1, 2021).

(36) Mouritz, A. P. Review of Smoke Toxicity of Fiber-Polymer Composites Used in Aircraft. *J. Aircr.* **2009**, *46* (3), 735–745. https://doi.org/10.2514/1.36472.

(37) Fiber Optics https://www.dupont.com/fabrics-fibers-and-nonwovens/fiber-optics.html (accessed Feb 1, 2021).

(38) Inagaki, N.; Tasaka, S.; Kawai, H. Surface Modification of Aromatic Polyamide Film by Oxygen Plasma. *J. Polym. Sci. Part A Polym. Chem.* **1995**, *33* (12), 2001–2011. https://doi.org/10.1002/pola.1995.080331207.

(39) Xi, M.; Li, Y. L.; Shang, S. yong; Li, D. H.; Yin, Y. X.; Dai, X. Y. Surface Modification of Aramid Fiber by Air DBD Plasma at Atmospheric Pressure with Continuous On-Line Processing. *Surf. Coatings Technol.* **2008**, *202* (24), 6029–6033. https://doi.org/10.1016/j.surfcoat.2008.06.181.

(40) Rodríguez-Uicab, O.; Avilés, F.; Gonzalez-Chi, P. .; Canché-Escamilla, G.; Duarte-Aranda, S.; Yazdani-Pedram, M.; Toro, P.; Gamboa, F.; Mazo, M. A.; Nistal, A.; et al. Deposition of Carbon Nanotubes onto Aramid Fibers Using As-Received and Chemically Modified Fibers. *Appl. Surf. Sci.* **2016**, *385*, 379–390. https://doi.org/10.1016/j.apsusc.2016.05.037.

(41) Park, S.-J.; Seo, M.-K.; Ma, T.-J.; Lee, D.-R. Effect of Chemical Treatment of Kevlar Fibers on Mechanical Interfacial Properties of Composites. *J. Colloid Interface Sci.* **2002**, *252* (1), 249–255. https://doi.org/10.1006/jcis.2002.8479.

(42) Liu, T.-M.; Zheng, Y.-S.; Hu, J. Surface Modification of Aramid Fibers with New Chemical Method for Improving Interfacial Bonding Strength with Epoxy Resin. *J. Appl. Polym. Sci.* **2010**, *118* (5), 2541–2552. https://doi.org/10.1002/app.32478.

(43) Cheng, Z.; Zhang, L.; Jiang, C.; Dai, Y.; Meng, C.; Luo, L.; Liu, X. Aramid Fiber with Excellent Interfacial Properties Suitable for Resin Composite in a Wide Polarity Range. *Chem. Eng. J.* **2018**, *347* (February), 483–492. https://doi.org/10.1016/j.cej.2018.04.149.

(44) Zhao, J. Effect of Surface Treatment on the Structure and Properties of Para-Aramid Fibers by Phosphoric Acid. *Fibers Polym.* **2013**, *14* (1), 59–64. https://doi.org/10.1007/s12221-013-0059-x.

(45) Xing, L.; Liu, L.; Huang, Y.; Jiang, D.; Jiang, B.; He, J. Enhanced Interfacial Properties of Domestic Aramid Fiber-12 via High Energy Gamma Ray Irradiation. *Compos. Part B Eng.* **2015**, *69*, 50–57. https://doi.org/10.1016/j.compositesb.2014.09.027.

(46) Zhang, Y. H.; Huang, Y. D.; Liu, L.; Cai, K. L. Effects of γ-Ray Radiation Grafting on Aramid Fibers and Its Composites. *Appl. Surf. Sci.* **2008**, *254* (10), 3153–3161. https://doi.org/10.1016/j.apsusc.2007.10.081.

(47) Zhang, Y.; Huang, Y.; Liu, L.; Wu, L. Surface Modification of Aramid Fibers with γ-Ray Radiation for Improving Interfacial Bonding Strength with Epoxy Resin. *J. Appl. Polym. Sci.* **2007**, *106* (4), 2251–2262. https://doi.org/10.1002/app.26887.

(48) Xie, F.; Xing, L.; Liu, L.; Liu, Y.; Xu, H.; Zhong, Z.; Jia, C.; Huang, Y. A Facile Method to Prepare Nanoscale Polyacrylonitrile Particles Grafted Aramid Fibers for Superior Interfacial and Mechanical Properties of Epoxy Composites. *Polym. Compos.* **2018**, *39* (S4), E2436–E2444. https://doi.org/10.1002/pc.24742.

(49) Xu, L.; Hu, J.; Ma, H.; Wu, G. Electron-Beam-Induced Post-Grafting Polymerization of Acrylic Acid onto the Surface of Kevlar Fibers. *Radiat. Phys. Chem.* **2018**, *145* (August 2017), 74–79. https://doi.org/10.1016/j.radphyschem.2017.12.023.

(50) Chen, F.; Zhai, L.; Yang, H.; Zhao, S.; Wang, Z.; Gao, C.; Zhou, J.; Liu, X.; Yu, Z.; Qin, Y.; et al. Unparalleled Armour for Aramid Fiber with Excellent UV Resistance in Extreme Environment. *Adv. Sci.* **2021**, *8* (12), 2004171. https://doi.org/10.1002/ADVS.202004171.

(51) Yang, X.; Tu, Q.; Shen, X.; Yin, Q.; Pan, M.; Jiang, C.; Hu, C. Enhancing the Interfacial Adhesion with Rubber Matrix by Grafting Polydopamine-Carbon Nanotubes onto Poly(p-Phenylene Terephthalamide) Fibers. *Polymers (Basel).* **2019**, *11* (8), 1231. https://doi.org/10.3390/polym11081231.

(52) Zhang, H.; Liang, G.; Gu, A.; Yuan, L. Facile Preparation of Hyperbranched Polysiloxane-

Grafted Aramid Fibers with Simultaneously Improved UV Resistance, Surface Activity, and Thermal and Mechanical Properties. *Ind. Eng. Chem. Res.* **2014**, *53* (7), 2684–2696. https://doi.org/10.1021/ie403642m.

(53) Atiqullah, M.; Adamu, S.; Emwas, A. H. M. UHMW Ziegler–Natta Polyethylene: Synthesis, Crystallization, and Melt Behavior. *J. Taiwan Inst. Chem. Eng.* **2017**, *76*, 141–155. https://doi.org/10.1016/j.jtice.2017.04.011.

(54) Talebi, S.; Duchateau, R.; Rastogi, S.; Kaschta, J.; Peters, G. W. M.; Lemstra, P. J. Molar Mass and Molecular Weight Distribution Determination of UHMWPE Synthesized Using a Living Homogeneous Catalyst. *Macromolecules* **2010**, *43* (6), 2780–2788. https://doi.org/10.1021/ma902297b.

(55) Gedde, U. W. *Polymer Physics*; Springer Netherlands: Dordrecht, 1999. https://doi.org/10.1007/978-94-011-0543-9.

(56) Lin, S. P.; Han, J. L.; Yeh, J. T.; Chang, F. C.; Hsieh, K. H. Surface Modification and Physical Properties of Various UHMWPE-Fiber-Reinforced Modified Epoxy Composites. *J. Appl. Polym. Sci.* **2007**, *104* (1), 655–665. https://doi.org/10.1002/APP.25735.

(57) Camacho, N.; Gonzalez, J. M.; Espinosa, D.; Mondragón, G.; Stafford, S. UHMWPE IN TOTAL KNEE ARTHROPLASTY: SUCCESSES AND FAILURES. *Rev. Colomb. Mater.* **2021**, No. 16, 3–28. https://doi.org/10.17533/udea.rcm.n16a01.

(58) Zhou, K. Composite Materials and Their Fiber Reinforcement Technology in Aerospace Field. *Sci. Soc. Res.* **2021**, *3* (1), 126–129. https://doi.org/10.36922/ssr.v3i1.1074.

(59) Li, W.; Li, R.; Li, C.; Chen, Z.-R.; Zhang, L. Mechanical Properties of Surface-modified Ultra-high Molecular Weight Polyethylene Fiber Reinforced Natural Rubber Composites. *Polym. Compos.* **2017**, *38* (6), 1215–1220. https://doi.org/10.1002/pc.23685.

(60) Chhetri, S.; Bougherara, H. A Comprehensive Review on Surface Modification of UHMWPE Fiber and Interfacial Properties. *Compos. Part A Appl. Sci. Manuf.* **2021**, *140*, 106146. https://doi.org/10.1016/j.compositesa.2020.106146.

(61) Mohammadalipour, M.; Masoomi, M.; Ahmadi, M.; Kazemi, Z. The Effect of Simultaneous Fiber Surface Treatment and Matrix Modification on Mechanical Properties of Unidirectional Ultra-High Molecular Weight Polyethylene Fiber/Epoxy/Nanoclay Nanocomposites. *J. Compos. Mater.* **2018**, *52* (21), 2961–2972. https://doi.org/10.1177/0021998318755542.

(62) Shanmugam, L.; Kazemi, M. E.; Rao, Z.; Lu, D.; Wang, X.; Wang, B.; Yang, L.; Yang, J. Enhanced Mode I Fracture Toughness of UHMWPE Fabric/Thermoplastic Laminates with Combined Surface Treatments of Polydopamine and Functionalized Carbon Nanotubes. *Compos. Part B Eng.* **2019**, *178*. https://doi.org/10.1016/J.COMPOSITESB.2019.107450.

(63) Ahmadi, M.; Masoomi, M.; Safi, S. Mechanical Property Characterization of Carbon Nanofiber/Epoxy Nanocomposites Reinforced by GMA-Grafted UHMWPE Fibers. *Compos. Part B Eng.* **2015**, *83*, 43–49. https://doi.org/10.1016/j.compositesb.2015.08.006.

(64) Ahmadi, M.; Zabihi, O.; Masoomi, M.; Naebe, M. Synergistic Effect of MWCNTs Functionalization on Interfacial and Mechanical Properties of Multi-Scale UHMWPE Fibre

Reinforced Epoxy Composites. *Compos. Sci. Technol.* **2016**, *134*, 1–11. https://doi.org/10.1016/j.compscitech.2016.07.026.

(65) Wang, H.; Xu, L.; Hu, J.; Wang, M.; Wu, G. Radiation-Induced Oxidation of Ultra-High Molecular Weight Polyethylene (UHMWPE) Powder by Gamma Rays and Electron Beams: A Clear Dependence of Dose Rate. *Radiat. Phys. Chem.* **2015**, *115*, 88–96. https://doi.org/10.1016/j.radphyschem.2015.06.012.

(66) Enomoto, I.; Mishima, K.; Kobayashi, T.; Soeda, S. Functionalization of PE Nonwoven Fabric by Plasma Treatment to Improve Dyeing Affinity. *J. Photopolym. Sci. Technol.* **2010**, *23* (4), 545–548. https://doi.org/10.2494/photopolymer.23.545.

(67) Yakusheva, D. E.; Oshchepkova, T. E.; Yakushev, R. M.; Strel'nikov, V. N. Chemical Structure of Fibers of Ultra-High-Molecular-Weight Polyethylene upon Ion-Beam Treatment and Post-Irradiation Grafting of Acrylic Monomers. *Russ. J. Appl. Chem.* **2010**, *83* (8), 1403–1407. https://doi.org/10.1134/S1070427210080148.

(68) Kondo, Y.; Miyazaki, K.; Yamaguchi, Y.; Sasaki, T.; Irie, S.; Sakurai, K. Mechanical Properties of Fiber Reinforced Styrene–Butadiene Rubbers Using Surface-Modified UHMWPE Fibers under EB Irradiation. *Eur. Polym. J.* **2006**, *42* (5), 1008–1014. https://doi.org/10.1016/j.eurpolymj.2005.11.025.

(69) Xing, Z.; Wang, M.; liu, W.; Hu, J.; Wu, G. Crystal Structure and Mechanical Properties of UHMWPE-g-PMA Fiber Prepared by Radiation Grafting. *Radiat. Phys. Chem.* **2013**, *86*, 84–89. https://doi.org/10.1016/j.radphyschem.2013.01.045.

(70) Patterson, B. A.; Sodano, H. A. Enhanced Interfacial Strength and UV Shielding of Aramid Fiber Composites through ZnO Nanoparticle Sizing. *ACS Appl. Mater. Interfaces* **2016**, *8* (49), 33963–33971. https://doi.org/10.1021/acsami.6b07555.

(71) LaBarre, E. D.; Calderon-Colon, X.; Morris, M.; Tiffany, J.; Wetzel, E.; Merkle, A.; Trexler, M. Effect of a Carbon Nanotube Coating on Friction and Impact Performance of Kevlar. *J. Mater. Sci.* **2015**, *50* (16), 5431–5442. https://doi.org/10.1007/s10853-015-9088-8.

(72) Liu, S.; Luo, G.; Wei, F. Poly(p-Phenylene Terephthalamide)/Carbon Nanotube Composite Membrane: Preparation via Polyanion Solution Method and Mechanical Property Enhancement. *Compos. Sci. Technol.* **2015**, *118*, 135–140. https://doi.org/10.1016/j.compscitech.2015.09.002.

(73) Malakooti, M. H.; Hwang, H. S.; Goulbourne, N. C.; Sodano, H. A. Role of ZnO Nanowire Arrays on the Impact Response of Aramid Fabrics. *Compos. Part B Eng.* **2017**, *127*, 222–231. https://doi.org/10.1016/j.compositesb.2017.05.084.

(74) Gusm¼o, R.; Sofer, Z.; Novµček, M.; Pumera, M.; Gusmão, R.; Sofer, Z.; Nováček, M.; Pumera, M. Contrasts between Mild and Harsh Oxidation of Carbon Nanotubes in Terms of Their Properties and Electrochemical Performance. *ChemElectroChem* **2016**, *3* (10), 1713–1719. https://doi.org/10.1002/celc.201600082.

(75) Sezer, N.; Koç, M. Oxidative Acid Treatment of Carbon Nanotubes. *Surfaces and Interfaces* **2019**, *14*, 1–8. https://doi.org/10.1016/j.surfin.2018.11.001.

(76) Karnati, S. R.; Agbo, P.; Zhang, L. Applications of Silica Nanoparticles in Glass/Carbon Fiber-Reinforced Epoxy Nanocomposite. *Compos. Commun.* **2020**, *17*, 32–41. https://doi.org/10.1016/j.coco.2019.11.003.

(77) Shen, X.-J.; Huang, P.-L.; Chen, J.-H.; Wu, Y.-Y.; Liu, Q.-Y.; Sun, R.-C. Comparison of Acid-Hydrolyzed and TEMPO-Oxidized Nanocellulose for Reinforcing Alginate Fibers. *BioResources* **2017**, *12* (4), 8180–8198. https://doi.org/10.15376/biores.12.4.8180-8198.

(78) Dufresne, A. CHAPTER 1. Nanocellulose: Potential Reinforcement in Composites; 2012; pp 1–32. https://doi.org/10.1039/9781849735315-00001.

(79) Lee, K.-Y.; Aitomäki, Y.; Berglund, L. A.; Oksman, K.; Bismarck, A. On the Use of Nanocellulose as Reinforcement in Polymer Matrix Composites. *Compos. Sci. Technol.* **2014**, *105*, 15–27. https://doi.org/10.1016/j.compscitech.2014.08.032.

(80) Pierre, G.; Punta, C.; Delattre, C.; Melone, L.; Dubessay, P.; Fiorati, A.; Pastori, N.; Galante, Y. M.; Michaud, P. TEMPO-Mediated Oxidation of Polysaccharides: An Ongoing Story. *Carbohydr. Polym.* **2017**, *165*, 71–85. https://doi.org/10.1016/j.carbpol.2017.02.028.

(81) Jacoby, M. Nano From The Forest. *Chemical and engineering new*. July 13, 2014, pp 9–12.

(82) Asadi, A.; Miller, M.; Moon, R. J.; Kalaitzidou, K. Improving the Interfacial and Mechanical Properties of Short Glass Fiber/Epoxy Composites by Coating the Glass Fibers with Cellulose Nanocrystals. *Express Polym. Lett.* **2016**, *10* (7), 587–597. https://doi.org/10.3144/expresspolymlett.2016.54.

(83) Phanthong, P.; Reubroycharoen, P.; Hao, X.; Xu, G.; Abudula, A.; Guan, G. Nanocellulose: Extraction and Application. *Carbon Resour. Convers.* **2018**, *1* (1), 32–43. https://doi.org/10.1016/j.crcon.2018.05.004.

(84) Eyley, S.; Thielemans, W. Imidazolium Grafted Cellulose Nanocrystals for Ion Exchange Applications. *Chem. Commun.* **2011**, *47* (14), 4177–4179. https://doi.org/10.1039/c0cc05359g.

(85) Barsbay, M.; Güven, O. Surface Modification of Cellulose via Conventional and Controlled Radiation-Induced Grafting. *Radiation Physics and Chemistry*. 2019, pp 1–8. https://doi.org/10.1016/j.radphyschem.2019.03.002.

(86) Siró, I.; Plackett, D. Microfibrillated Cellulose and New Nanocomposite Materials: A Review. *Cellulose* **2010**, *17* (3), 459–494. https://doi.org/10.1007/s10570-010-9405-y.

(87) Nechyporchuk, O.; Belgacem, M. N.; Bras, J. Production of Cellulose Nanofibrils: A Review of Recent Advances. *Ind. Crops Prod.* **2016**, *93*, 2–25. https://doi.org/10.1016/j.indcrop.2016.02.016.

(88) Wang, Q. Q.; Zhu, J. Y.; Gleisner, R.; Kuster, T. A.; Baxa, U.; McNeil, S. E. Morphological Development of Cellulose Fibrils of a Bleached Eucalyptus Pulp by Mechanical Fibrillation. *Cellulose* **2012**, *19* (5), 1631–1643. https://doi.org/10.1007/s10570-012-9745-x.

(89) Fujisawa, S.; Ikeuchi, T.; Takeuchi, M.; Saito, T.; Isogai, A. Superior Reinforcement Effect of TEMPO-Oxidized Cellulose Nanofibrils in Polystyrene Matrix: Optical, Thermal, and

Mechanical Studies. *Biomacromolecules* **2012**, *13* (7), 2188–2194. https://doi.org/10.1021/bm300609c.

(90) Yatvin, J.; Sherman, S. A.; Filocamo, S. F.; Locklin, J. Direct Functionalization of Kevlar® with Copolymers Containing Sulfonyl Nitrenes. *Polym. Chem.* **2015**, *6* (16), 3090–3097. https://doi.org/10.1039/C5PY00090D.

(91) Sutter, J. K.; Jensen, B. J.; Gates, T. S.; Morgan, R. J.; Thesken, J. C.; Phoenix, S. L. Material Issues in Space Shuttle Composite Overwrapped Pressure Vessels. **1980**, No. January 2006, 1–13.

(92) Milberg, E. Hinckley Debuts First Carbon Epoxy Performance Boat in Production http://compositesmanufacturingmagazine.com/2018/03/hinckley-debuts-worlds-first-carbon-epoxy-performance-boat-in-production/ (accessed Feb 18, 2021).

(93) Tagawa, S. Radiation Effects of Ion Beams on Polymers; 1993; pp 99–116. https://doi.org/10.1007/BFb0018050.

(94) Ziegelberger, G.; van Rongen, E.; Croft, R.; Feychting, M.; Green, A. C.; Hirata, A.; d'Inzeo, G.; Marino, C.; Miller, S.; Oftedal, G.; et al. Principles for Non-Ionizing Radiation Protection. *Health Phys.* **2020**, *118* (5), 477–482. https://doi.org/10.1097/HP.0000000000001252.

(95) Introduction, A. *Electronic Irradiation of Foods*; 2005. https://doi.org/10.1007/0-387-28386-2.

(96) Ashfaq, A.; Clochard, M.-C.; Coqueret, X.; Dispenza, C.; Driscoll, M. S.; Ulański, P.; Al-Sheikhly, M. Polymerization Reactions and Modifications of Polymers by Ionizing Radiation. *Polymers (Basel).* **2020**, *12* (12), 2877. https://doi.org/10.3390/polym12122877.

(97) Andrew, W. *Ionizing Radiation and Polymers*; Elsevier, 2013. https://doi.org/10.1016/C2011-0-05010-X.

(98) Martins, M. N.; Silva, T. F. Electron Accelerators: History, Applications, and Perspectives. *Radiat. Phys. Chem.* **2014**, *95* (March 2018), 78–85. https://doi.org/10.1016/j.radphyschem.2012.12.008.

(99) Hamm, R. W.; Hamm, M. E. Industrial Accelerators and Their Applications. In *Industrial Accelerators and Their Applications*; WORLD SCIENTIFIC, 2012; pp 59–60. https://doi.org/10.1142/7745.

(100) Gehringer, P. Radiation Processing of Aqueous Systems Radiation Processing of Aqueous Systems Lecture given at the IAEA's Interregional Training Course on Developments in The. **1997**, No. September.

(101) Baldacchino, G.; Hickel, B. Chapter 4 Water Radiolysis under Extreme Conditions. Application to the Nuclear Industry. *Radiat. Chem.* **2021**, 53–64. https://doi.org/10.1051/978-2-7598-0317-0.c007.

(102) Schuler, R. H.; Patterson, L. K.; Janata, E. Yield for the Scavenging of Hydroxyl Radicals in the Radiolysis of Nitrous Oxide-Saturated Aqueous Solutions. *J. Phys. Chem.* **1980**, *84* (16), 2088–2089. https://doi.org/10.1021/j100453a020.

(103) Buxton, G. V; Greenstock, C. L.; Helman, W. P.; Ross, A. B. Critical Review of Rate Constants for Reactions of Hydrated Electrons, Hydrogen Atoms and Hydroxyl Radicals (·OH/·O − in Aqueous Solution. *J. Phys. Chem. Ref. Data* **1988**, *17* (2), 513–886. https://doi.org/10.1063/1.555805.

(104) DAINTON, F. S.; PETERSON, D. B. Use of Nitrous Oxide to Discriminate between the Forms of Hydrogen Atoms (H• and H2 + ?) Produced by γ-Irradiation of Aqueous Solutions. *Nature* **1960**, *186* (4728), 878–879. https://doi.org/10.1038/186878a0.

(105) Spinks, J. W. T.; Woods, R. J. *An Introduction to Radiation Chemistry*, 3rd ed.; 1991; Vol. 95. https://doi.org/10.1002/bbpc.19910950346.

(106) *Crosslinking and Scission in Polymers*; Güven, O., Ed.; Springer Netherlands: Dordrecht, 1990. https://doi.org/10.1007/978-94-009-1924-2.

(107) Manas, D.; Ovsik, M.; Mizera, A.; Manas, M.; Hylova, L.; Bednarik, M.; Stanek, M. The Effect of Irradiation on Mechanical and Thermal Properties of Selected Types of Polymers. *Polymers (Basel).* **2018**, *10* (2), 158. https://doi.org/10.3390/polym10020158.

(108) Kerry Thomas, J. Fundamental Aspects of the Radiolysis of Solid Polymers, Crosslinking and Degradation. *Nucl. Instruments Methods Phys. Res. Sect. B Beam Interact. with Mater. Atoms* **2007**, *265* (1), 1–7. https://doi.org/10.1016/J.NIMB.2007.08.021.

(109) Ashfaq, A.; Clochard, M. C.; Coqueret, X.; Dispenza, C.; Driscoll, M. S.; Ulański, P.; Al-Sheikhly, M. Polymerization Reactions and Modifications of Polymers by Ionizing Radiation. *Polymers (Basel).* **2020**, *12* (12), 1–67. https://doi.org/10.3390/polym12122877.

(110) Al-Assaf, S.; Phillips, G. O.; Williams, P. A.; du Plessis, T. A. Application of Ionizing Radiations to Produce New Polysaccharides and Proteins with Enhanced Functionality. *Nucl. Instruments Methods Phys. Res. Sect. B Beam Interact. with Mater. Atoms* **2007**, *265* (1), 37–43. https://doi.org/10.1016/j.nimb.2007.08.015.

(111) Han, D. H.; Shin, S.-H.; Petrov, S. Crosslinking and Degradation of Polypropylene by Electron Beam Irradiation in the Presence of Trifunctional Monomers. *Radiat. Phys. Chem.* **2004**, *69* (3), 239–244. https://doi.org/10.1016/S0969-806X(03)00458-4.

(112) Nagasawa, N.; Kaneda, A.; Kanazawa, S.; Yagi, T.; Mitomo, H.; Yoshii, F.; Tamada, M. Application of Poly(Lactic Acid) Modified by Radiation Crosslinking. *Nucl. Instruments Methods Phys. Res. Sect. B Beam Interact. with Mater. Atoms* **2005**, *236* (1–4), 611–616. https://doi.org/10.1016/J.NIMB.2005.04.052.

(113) Klein, P. G.; Gonzalez-Orozco, J. A.; Ward, I. M. Effect of Draw Ratio on the Structure and Properties of Electron Beam Crosslinked Polyethylene. *Polymer (Guildf).* **1994**, *35* (10), 2044–2048. https://doi.org/10.1016/0032-3861(94)90226-7.

(114) Deng, M.; Shalaby, S. W. Effects of Gamma Irradiation, Gas Environments, and Postirradiation Aging on Ultrahigh Molecular Weight Polyethylene. *J. Appl. Polym. Sci.* **1995**, *58* (11), 2111–2119. https://doi.org/10.1002/app.1995.070581123.

(115) Forster, A. L. LONG TERM STABILITY AND IMPLICATIONS FOR PERFORMANCE OF HIGH STRENGTH FIBERS USED IN BODY ARMOR, University of Maryland, 2012.

(116) Van Ooij, W. J.; Luo, S.; Datta, S. Surface Modification of Textile Fibers and Cords by Plasma Polymerization. *Plasmas Polym.* **1999**, *4* (1), 33–55. https://doi.org/10.1023/A:1021851531645.

(117) Kang, H. M.; Yoon, T. H.; van Ooij, W. J. Enhanced Adhesion of Aramid Tire Cords via Argon Plasma Etching and Acetylene Plasma Polymerization. *J. Adhes. Sci. Technol.* **2006**, *20* (11), 1155–1169. https://doi.org/10.1163/156856106777920802.

(118) Dai, Y.; Meng, C.; Cheng, Z.; Luo, L.; Liu, X. Nondestructive Modification of Aramid Fiber Based on Selective Reaction of External Cross-Linker to Improve Interfacial Shear Strength and Compressive Strength. *Compos. Part A Appl. Sci. Manuf.* **2019**, *119*, 217–224. https://doi.org/10.1016/j.compositesa.2019.02.007.

(119) Chae, Y.; An, Y. J. Current Research Trends on Plastic Pollution and Ecological Impacts on the Soil Ecosystem: A Review. *Environ. Pollut.* **2018**, *240*, 387–395. https://doi.org/10.1016/J.ENVPOL.2018.05.008.

(120) Fink, J. K. *Polymer Waste Management*; John Wiley & Sons, Inc.: Hoboken, NJ, USA, 2018. https://doi.org/10.1002/9781119536376.

(121) Martínez-López, M.; Martínez-Barrera, G.; del Coz-Díaz, J. J.; Martínez-Martínez, J. E.; Gencel, O.; Ribeiro, M. C. S.; Varela-Guerrero, V. Polymer Waste Materials as Fillers in Polymer Mortars: Experimental and Finite Elements Simulation. *Case Stud. Constr. Mater.* **2018**, *9*, e00178. https://doi.org/10.1016/j.cscm.2018.e00178.

(122) *Advancing Sustainable Materials Management: Facts and Figures Report*; Washington, D.C., 2020.

(123) *Recycled Polyester*; Muthu, S. S., Ed.; Textile Science and Clothing Technology; Springer Singapore: Singapore, 2020. https://doi.org/10.1007/978-981-32-9559-9.

(124) Burillo, G.; Clough, R. L.; Czvikovszky, T.; Guven, O.; Le Moel, A.; Liu, W.; Singh, A.; Yang, J.; Zaharescu, T. Polymer Recycling: Potential Application of Radiation Technology. *Radiat. Phys. Chem.* **2002**, *64* (1), 41–51. https://doi.org/10.1016/S0969-806X(01)00443-1.

(125) González-López, L.; Kearney, L.; Janke, C. J.; Wishart, J.; Kanbargi, N.; Al-Sheikhly, M. On the Mechanism of the Steady-State Gamma Radiolysis-Induced Scissions of the Phenyl-Vinyl Polyester-Based Resins. *Front. Chem.* **2022**, *9*, 1218. https://doi.org/10.3389/fchem.2021.803347.

(126) Guillet, J. E.; Huber, H. X.; Scott, J. A. Synthesis and Applications of Photodegradable Poly(Ethylene Terephthalate). *J. Macromol. Sci. Part A* **1995**, *32* (4), 823–833. https://doi.org/10.1080/10601329508010292.

(127) Dalai, S.; Wenxiu, C. Investigation of Radiation-Crosslinked Foam of LDPE/EVA Blends. *J. Appl. Polym. Sci.* **1996**, *62* (1), 75–80. https://doi.org/10.1002/(SICI)1097-4628(19961003)62:1<75::AID-APP10>3.0.CO;2-7.

(128) Zhao, W.; Hasegawa, S.; Fujita, J.; Yoshii, F.; Sasaki, T.; Makuuchi, K.; Sun, J.; Nishimoto, S. I. Effect of Irradiation on Pyrolysis of Polypropylene in the Presence of Zeolites. *Polym. Degrad. Stab.* **1996**, *53* (2), 199–206. https://doi.org/10.1016/0141-3910(96)00084-5.

(129) Schnabel, W.; Levchik, G. F.; Wilkie, C. A.; Jiang, D. D.; Levchik, S. V. Thermal Degradation of Polystyrene, Poly(1,4-Butadiene) and Copolymers of Styrene and 1,4-Butadiene Irradiated under Air or Argon with 60Co-γ-Rays. *Polym. Degrad. Stab.* **1999**, *63* (3), 365–375. https://doi.org/10.1016/S0141-3910(98)00114-1.

(130) Navratil, J.; Manas, M.; Mizera, A.; Bednarik, M.; Stanek, M.; Danek, M. Recycling of Irradiated High-Density Polyethylene. *Radiat. Phys. Chem.* **2015**, *106*, 68–72. https://doi.org/10.1016/j.radphyschem.2014.06.025.

(131) Vignon, A.; Ayoub, A.; Massardier, V. The Effect of γ-Irradiation and Reactive Extrusion on the Structure and Properties of Polycarbonate and Starch Blends: A Work Oriented to the Recycling of Thermoplastic Wastes. *J. Appl. Polym. Sci.* **2013**, *127* (5), 4168–4176. https://doi.org/10.1002/app.38024.

(132) Dodiuk, H.; Goodman, S. H. Handbook of Thermoset Plastics. *Handb. Thermoset Plast.* **2013**, 1–768. https://doi.org/10.1016/C2011-0-09694-1.

(133) Liu, C.; Lei, W.; Cai, Z.; Chen, J.; Hu, L.; Dai, Y.; Zhou, Y. Use of Tung Oil as a Reactive Toughening Agent in Dicyclopentadiene-Terminated Unsaturated Polyester Resins. *Ind. Crops Prod.* **2013**, *49*, 412–418. https://doi.org/10.1016/j.indcrop.2013.05.023.

(134) Thostenson, E. T.; Chou, T.-W. Processing-Structure-Multi-Functional Property Relationship in Carbon Nanotube/Epoxy Composites. *Carbon N. Y.* **2006**, *44* (14), 3022–3029. https://doi.org/10.1016/j.carbon.2006.05.014.

(135) He, S.; Petkovich, N. D.; Liu, K.; Qian, Y.; Macosko, C. W.; Stein, A. Unsaturated Polyester Resin Toughening with Very Low Loadings of GO Derivatives. *Polymer (Guildf).* **2017**, *110*, 149–157. https://doi.org/10.1016/j.polymer.2016.12.057.

(136) Global Unsaturated Polyester Resins Market by Type (Orthophthalic, Isophthalic, DCPD), End-use Industry (Building & Construction, Marine, Transportation, Pipes & Tanks, Artificial Stone, Wind Energy, Electrical & Electronics) & Region - Forecast to 2026 https://www.researchandmarkets.com/reports/5437954/global-unsaturated-polyester-resins-market-by?utm_source=BW&utm_medium=PressRelease&utm_code=j93mtr&utm_campaign=1592894+-+Unsaturated+Polyester+Resins+Market+by+Type%2C+End-use+Industry+%26+Region+-+Glob (accessed Nov 1, 2021).

(137) Yoon, K. H.; DiBenedetto, A. T.; Huang, S. J. Recycling of Unsaturated Polyester Resin Using Propylene Glycol. *Polymer (Guildf).* **1997**, *38* (9), 2281–2285. https://doi.org/10.1016/S0032-3861(96)00951-2.

(138) Spyros, A. Quantitative Determination of the Distribution of Free Hydroxylic and Carboxylic Groups in Unsaturated Polyester and Alkyd Resins by 31P-NMR Spectroscopy. *J. Appl. Polym. Sci.* **2002**, *83* (8), 1635–1642. https://doi.org/10.1002/APP.10069.

(139) Jung, S.-J.; Lee, S.-J.; Cho, W.-J.; Ha, C.-S. Synthesis and Properties of UV-Curable Waterborne Unsaturated Polyester for Wood Coating. *J. Appl. Polym. Sci.* **1998**, *69* (4), 695–708. https://doi.org/10.1002/(SICI)1097-4628(19980725)69:4<695::AID-APP8>3.0.CO;2-E.

(140) Ahamad, A.; C, M. L.; Mohan, A.; Safeer, M.; Thachil, E. T. Synthesis of Unsaturated Polyester Resin — Effect of Anhydride Composition. *Des. Monomers Polym.* **2001**, *4* (3), 260–267. https://doi.org/10.1163/156855501750536242.

(141) Hu, L.-F.; Zhang, C.-J.; Chen, D.-J.; Cao, X.-H.; Yang, J.-L.; Zhang, X.-H. Synthesis of High-Molecular-Weight Maleic Anhydride-Based Polyesters with Enhanced Properties. *ACS Appl. Polym. Mater.* **2020**, *2* (12), 5817–5823. https://doi.org/10.1021/acsapm.0c01075.

(142) Perrot, A.; Hyršl, J.; Bandžuch, J.; Waňousová, S.; Hájek, J.; Jenčík, J.; Herink, T. Use of Dicyclopentadiene and Methyl Dicyclopentadiene for the Synthesis of Unsaturated Polyester Resins. *Polymers (Basel).* **2021**, *13* (18). https://doi.org/10.3390/POLYM13183135.

(143) Wang, Y.; Cui, X.; Yang, Q.; Deng, T.; Wang, Y.; Yang, Y.; Jia, S.; Qin, Z.; Hou, X. Chemical Recycling of Unsaturated Polyester Resin and Its Composites via Selective Cleavage of the Ester Bond. *Green Chem.* **2015**, *17* (9), 4527–4532. https://doi.org/10.1039/C5GC01048A.

(144) Oliveux, G.; Dandy, L. O.; Leeke, G. A. Current Status of Recycling of Fibre Reinforced Polymers: Review of Technologies, Reuse and Resulting Properties. *Prog. Mater. Sci.* **2015**, *72*, 61–99. https://doi.org/10.1016/j.pmatsci.2015.01.004.

(145) Mativenga, P. T.; Shuaib, N. A.; Howarth, J.; Pestalozzi, F.; Woidasky, J. High Voltage Fragmentation and Mechanical Recycling of Glass Fibre Thermoset Composite. *CIRP Ann.* **2016**, *65* (1), 45–48. https://doi.org/10.1016/J.CIRP.2016.04.107.

(146) Jiang, J.; Deng, G.; Chen, X.; Gao, X.; Guo, Q.; Xu, C.; Zhou, L. On the Successful Chemical Recycling of Carbon Fiber/Epoxy Resin Composites under the Mild Condition. *Compos. Sci. Technol.* **2017**, *151*, 243–251. https://doi.org/10.1016/J.COMPSCITECH.2017.08.007.

(147) Pickering, S. J. Recycling Technologies for Thermoset Composite Materials—Current Status. *Compos. Part A Appl. Sci. Manuf.* **2006**, *37* (8), 1206–1215. https://doi.org/10.1016/j.compositesa.2005.05.030.

(148) Martínez-Barrera, G.; Martínez-López, A.; Vigueras-Santiago, E.; Martínez-López, M. Effects of Gamma Radiation on the Physicochemical Properties of Polyester Resin and Its Use in Composite Materials; 2020; pp 15–28. https://doi.org/10.1007/978-981-32-9559-9_2.

(149) O'Donnell, J. H. Chemistry of Radiation Degradation of Polymers; 1991; pp 402–413. https://doi.org/10.1021/bk-1991-0475.ch024.

(150) Coqueret, X. Radiation-Induced Polymerization. In *Applications of ionizing radiation in materials processing*; Sun, Y., Chmeliewski, A., Eds.; 2016; pp 143–165.

(151) Stannett, V. T. Radiation Grafting - State-of-the-Art. *Int. J. Radiat. Appl. Instrumentation. Part* **1990**, *35* (1–3), 82–87. https://doi.org/10.1016/1359-0197(90)90062-M.

(152) Kornacka, E. M. RADIATION-INDUCED OXIDATION OF POLYMERS. In *Applications of ionizing radiation in materials processing. Vol. 1*; Institute of Nuclear

Chemistry and Technology, 2017.

(153) Janata, E.; Schuler, R. H. Rate Constant for Scavenging Eaq- in N2O-Saturated Solutions. *J. Phys. Chem.* **1982**, *86* (11), 2078–2084. https://doi.org/10.1021/j100208a035.

(154) Labarbe, R.; Hotoiu, L.; Barbier, J.; Favaudon, V. A Physicochemical Model of Reaction Kinetics Supports Peroxyl Radical Recombination as the Main Determinant of the FLASH Effect. *Radiother. Oncol.* **2020**, *153*, 303–310. https://doi.org/10.1016/j.radonc.2020.06.001.

(155) Gabr, M. H.; Elrahman, M. A.; Okubo, K.; Fujii, T. Effect of Microfibrillated Cellulose on Mechanical Properties of Plain-Woven CFRP Reinforced Epoxy. *Compos. Struct.* **2010**, *92* (9), 1999–2006. https://doi.org/10.1016/j.compstruct.2009.12.009.

(156) Walo, M. Radiation Induced Grafting. *Radiat. Phys. Chem.* **1977**, *9* (1–3), 55–67. https://doi.org/10.1016/0146-5724(77)90072-3.

(157) Lappan, U.; Geißler, U.; Gohs, U.; Uhlmann, S. Influence of Irradiation Temperature on Grafting of Styrene into Poly(Tetrafluoroethylene -Co- Hexafluoropropylene) Films. *Macromol. Mater. Eng.* **2009**, *294* (8), 510–515. https://doi.org/10.1002/mame.200900077.

(158) Gueven, O. An Overview of Current Developments in Applied Radiation Chemistry of Polymers. *Adv. Radiat. Chem. Polym. IAEA-TECDOC-1420* **2004**, No. November, 33–39.

(159) Oral, E.; Neils, A. L.; Rowell, S. L.; Lozynsky, A. J.; Muratoglu, O. K. Increasing Irradiation Temperature Maximizes Vitamin E Grafting and Wear Resistance of Ultrahigh Molecular Weight Polyethylene. *J Biomed Mater Res Part B Appl Biomater* **2012**, *101*, 436–440. https://doi.org/10.1002/jbm.b.32807.

(160) Wang, L.; Brink, J. J.; Liu, Y.; Herring, A. M.; Ponce-González, J.; Whelligan, D. K.; Varcoe, J. R. Non-Fluorinated Pre-Irradiation-Grafted (Peroxidated) LDPE-Based Anion-Exchange Membranes with High Performance and Stability. *Energy Environ. Sci.* **2017**, *10* (10), 2154–2167. https://doi.org/10.1039/C7EE02053H.

(161) Dong, L. C.; Hoffman, A. S. A New Method for Immobilization of Biomolecules Using Preirradiation Grafting at Low Temperature. *Int. J. Radiat. Appl. Instrumentation. Part* **1986**, *28* (2), 177–182. https://doi.org/10.1016/1359-0197(86)90124-4.

(162) Tiesinga, E.; Mohr, P. J.; Newell, D. B.; Taylor, B. N. *The 2018 CODATA Recommended Values of the Fundamental Physical Constants*; Gaithersburg, 2019.

(163) Eaton, G. R.; Eaton, S. S.; Barr, D. P.; Weber, R. T. *Quantitative EPR*; Springer Vienna: Vienna, 2010. https://doi.org/10.1007/978-3-211-92948-3.

(164) Jeschke, G. *Physical Chemistry IV Part 2: Electron Paramagnetic Resonance*; Gunnar Jeschke, 2016.

(165) Phoenix, S. L.; Beyerlein, I. J. Statistical Strength Theory for Fibrous Composite Materials. In *Comprehensive Composite Materials*; Elsevier, 2000; pp 559–639. https://doi.org/10.1016/B0-08-042993-9/00056-5.

(166) Zok, F. W. On Weakest Link Theory and Weibull Statistics. *J. Am. Ceram. Soc.* **2017**, *100*

(4), 1265–1268. https://doi.org/10.1111/jace.14665.

(167) Brown, I. M.; Sandreczki, T. C.; Morgan, R. J. Electron Paramagnetic Resonance Studies of Kevlar 49 Fibres: Stress-Induced Free Radicals. *Polymer (Guildf).* **1984**, *25* (6), 759–765. https://doi.org/10.1016/0032-3861(84)90003-X.

(168) Brown, J. R.; Hodgeman, D. K. C. An e.s.r. Study of the Thermal Degradation of Kevlar 49 Aramid. *Polymer (Guildf).* **1982**, *23* (3), 365–368. https://doi.org/10.1016/0032-3861(82)90336-6.

(169) M Jetten, M. S.; Pierik, A. J.; Hagen, W. R.; Hagen, W. R. EPR Characterization of a High-Spin System in Carbon Monoxide Dehydrogenase from Methanothrix Soehngenii. **1991**, *202*, 1291–1297.

(170) Dellinger, B.; Lomnicki, S.; Khachatryan, L.; Maskos, Z.; Hall, R. W.; Adounkpe, J.; McFerrin, C.; Truong, H. Formation and Stabilization of Persistent Free Radicals. *Proc. Combust. Inst.* **2007**, *31* (1), 521–528. https://doi.org/10.1016/j.proci.2006.07.172.

(171) Ross, M. M.; Chedekel, M. R.; Risby, T. H.; Lestz, S. S.; Yasbin, R. E. Electron Paramagnetic Resonance Spectrometry of Diesel Particulate Matter. *Environ. Int.* **1982**, *7* (5), 325–329. https://doi.org/10.1016/0160-4120(82)90124-6.

(172) ANTHOLINE, W. E.; KASTRAU, D. H. W.; STEFFENS, G. C. M.; BUSE, G.; ZUMFT, W. G.; KRONECK, P. M. H. A Comparative EPR Investigation of the Multicopper Proteins Nitrous-Oxide Reductase and Cytochrome c Oxidase. *Eur. J. Biochem.* **1992**, *209* (3), 875–881. https://doi.org/10.1111/j.1432-1033.1992.tb17360.x.

(173) Poncin-Epaillard, F.; Chevet, B.; Brosse, J.-C. Study of an Aramid Surface Reactivity: Modification with a Cold Plasma or an Electron Beam Followed by a Postgrafting Reaction. *J. Appl. Polym. Sci.* **1994**, *52* (8), 1047–1061. https://doi.org/10.1002/app.1994.070520806.

(174) Carlsson, D. J.; Gan, L. H.; Wiles, D. M. Photodegradation of Aramids. I. Irradiation in the Absence of Oxygen. *J. Polym. Sci. Polym. Chem. Ed.* **1978**, *16* (9), 2353–2363. https://doi.org/10.1002/pol.1978.170160922.

(175) Xie, H.; Xie, X.; Hu, G.; Prabhakaran, V.; Saha, S.; Gonzalez-Lopez, L.; Phakatkar, A. H.; Hong, M.; Wu, M.; Shahbazian-Yassar, R.; et al. Ta–TiOx Nanoparticles as Radical Scavengers to Improve the Durability of Fe–N–C Oxygen Reduction Catalysts. *Nat. Energy* **2022**, *7* (3), 281–289. https://doi.org/10.1038/s41560-022-00988-w.

(176) Dorfman, L. M.; Adams, G. E. *Reactivity of the Hydroxyl Radical in Aqueous Solutions*; Gaithersburg, MD, 1973. https://doi.org/10.6028/NBS.NSRDS.46.

(177) Yang, Z.; Peng, H.; Wang, W.; Liu, T. Crystallization Behavior of Poly(ε-Caprolactone)/Layered Double Hydroxide Nanocomposites. *J. Appl. Polym. Sci.* **2010**, *116* (5), 2658–2667. https://doi.org/10.1002/app.

(178) Derombise, G.; Vouyovitch Van Schoors, L.; Messou, M.-F.; Davies, P. Influence of Finish Treatment on the Durability of Aramid Fibers Aged under an Alkaline Environment. *J. Appl. Polym. Sci.* **2010**, *117* (2), 888–898. https://doi.org/10.1002/app.31534.

(179) Shebanov, S. M.; Novikov, I. K.; Pavlikov, A. V.; Anańin, O. B.; Gerasimov, I. A. IR and

Raman Spectra of Modern Aramid Fibers. *Fibre Chem.* **2016**, *48* (2), 1–7. https://doi.org/10.1007/s10692-016-9761-y.

(180) Cai, G. M.; Yu, W. D. Study on the Thermal Degradation of High Performance Fibers by TG/FTIR and Py-GC/MS. *J. Therm. Anal. Calorim.* **2011**, *104* (2), 757–763. https://doi.org/10.1007/s10973-010-1211-0.

(181) Mori, M.; Uyama, Y.; Ikada, Y. Surface Modification of Aramid Fibre by Graft Polymerization. *Polymer (Guildf).* **1994**, *35* (24), 5336–5341. https://doi.org/10.1016/0032-3861(94)90487-1.

(182) Engelbrecht-Wiggans, A.; Burni, F.; Krishnamurthy, A.; Forster, A. L. Tensile Testing of Aged Flexible Unidirectional Composite Laminates for Body Armor. *J. Mater. Sci.* **2020**, *55* (3), 1035–1048. https://doi.org/10.1007/s10853-019-04063-w.

(183) Pang, S. W. Radiation Damage in Dry Etching. *Microelectron. Eng.* **1986**, *5* (1–4), 351–361. https://doi.org/10.1016/0167-9317(86)90064-X.

(184) Roeder, R. D.; Garcia-Valdez, O.; Whitney, R. A.; Champagne, P.; Cunningham, M. F. Graft Modification of Cellulose Nanocrystals via Nitroxide-Mediated Polymerisation. *Polym. Chem.* **2016**, *7* (41), 6383–6390. https://doi.org/10.1039/C6PY01515H.

(185) Yu, T.; Liu, S.; Xu, M.; Peng, J.; Li, J.; Zhai, M. Synthesis of Novel Aminated Cellulose Microsphere Adsorbent for Efficient Cr(VI) Removal. *Radiat. Phys. Chem.* **2016**, *125*, 94–101. https://doi.org/10.1016/j.radphyschem.2016.03.019.

(186) Liu, S.; Xu, M.; Yu, T.; Han, D.; Peng, J.; Li, J.; Zhai, M. Radiation Synthesis and Performance of Novel Cellulose-Based Microsphere Adsorbents for Efficient Removal of Boron (III). *Carbohydr. Polym.* **2017**, *174*, 273–281. https://doi.org/10.1016/j.carbpol.2017.06.012.

(187) Sirvï, J. A.; Visanko, M.; Heiskanen, J. P.; Liimatainen, H. UV-Absorbing Cellulose Nanocrystals as Functional Reinforcing Fillers in Polymer Nanocomposite Films. **2016**. https://doi.org/10.1039/c6ta00900j.

(188) Kim, D. Y.; Lee, B. M.; Koo, D. H.; Kang, P. H.; Jeun, J. P. Preparation of Nanocellulose from a Kenaf Core Using E-Beam Irradiation and Acid Hydrolysis. *Cellulose* **2016**, *23* (5), 3039–3049. https://doi.org/10.1007/s10570-016-1037-4.

(189) Romanzini, D.; Ornaghi Junior, H. L.; Amico, S. C.; Zattera, A. J. Preparation and Characterization of Ramie-Glass Fiber Reinforced Polymer Matrix Hybrid Composites. *Mater. Res.* **2012**, *15* (3), 415–420. https://doi.org/10.1590/S1516-14392012005000050.

(190) Brauckmann, J. O.; Zolfaghari, P.; Verhoef, R.; Klop, E. A.; De Wijs, G. A.; Kentgens, A. P. M. Structural Studies of Polyaramid Fibers: Solid-State NMR and First-Principles Modeling. *Macromolecules* **2016**, *49* (15), 5548–5560. https://doi.org/10.1021/acs.macromol.6b01051.

(191) Yeager, M. P.; Hoffman, C. M.; Xia, Z.; Trexler, M. M. Method for the Synthesis of Para-Aramid Nanofibers. *J. Appl. Polym. Sci.* **2016**, *133* (42), 1–8. https://doi.org/10.1002/app.44082.

(192) Foston, M. Advances in Solid-State NMR of Cellulose. *Curr. Opin. Biotechnol.* **2014**, *27*, 176–184. https://doi.org/10.1016/j.copbio.2014.02.002.

(193) 4-Vinylbenzyl chloride 1592-20-7 https://www.guidechem.com/dictionary/en/1592-20-7.html (accessed Jan 9, 2022).

(194) Jones, R. A.; Salmon, G. A.; Ward, I. M. Radiation-induced Crosslinking of Polyethylene in the Presence of Acetylene: A Gel Fraction, UV-visible, and ESR Spectroscopy Study. *J. Polym. Sci. Part B Polym. Phys.* **1993**, *31* (7), 807–819. https://doi.org/10.1002/polb.1993.090310709.

(195) von Sonntag, C. *Free-Radical-Induced DNA Damage and Its Repair*; Springer Berlin Heidelberg: Berlin, Heidelberg, 2006. https://doi.org/10.1007/3-540-30592-0.

(196) Bielski, B. H. J.; Cabelli, D. E.; Arudi, R. L.; Ross, A. B. Reactivity of HO 2 /O − 2 Radicals in Aqueous Solution. *J. Phys. Chem. Ref. Data* **1985**, *14* (4), 1041–1100. https://doi.org/10.1063/1.555739.

(197) Jones, C. G.; Silverman, J.; Al-Sheikhly, M.; Neta, P.; Poster, D. L. Dechlorination of Polychlorinated Biphenyls in Industrial Transformer Oil by Radiolytic and Photolytic Methods. *Environ. Sci. Technol.* **2003**, *37* (24), 5773–5777. https://doi.org/10.1021/es030412i.

(198) Adams, G. E.; Willson, R. L. On the Mechanism of BUdR Sensitization: A Pulse Radiolysis Study of One Electron Transfe in Nucleic-Acid Derivatives. *Int. J. Radiat. Biol. Relat. Stud. Physics, Chem. Med.* **1972**, *22* (6), 589–597. https://doi.org/10.1080/09553007214551481.

(199) Hamlin, T. A.; Swart, M.; Bickelhaupt, F. M.; Vch, W. Nucleophilic Substitution (S N 2): Dependence on Nucleophile, Leaving Group, Central Atom, Substituents, and Solvent. *ChemPhysChem* **2018**, *19*, 1315–1330. https://doi.org/10.1002/cphc.201701363.

(200) Neta, P.; Huie, R. E.; Ross, A. B. Rate Constants for Reactions of Peroxyl Radicals in Fluid Solutions. *J. Phys. Chem. Ref. Data* **1990**, *19* (2), 413–513. https://doi.org/10.1063/1.555854.

(201) Bennett, J. E.; Brown, D. M.; Mile, B. Studies by Electron Spin Resonance of the Reactions of Alkylperoxy Radicals. Part 1.—Absolute Rate Constants for the Termination Reactions of Alkylperoxy Radicals. *Trans. Faraday Soc.* **1970**, *66*, 386–396. https://doi.org/10.1039/TF9706600386.

(202) Bennett, J. E.; Summers, R. Product Studies of the Mutual Termination Reactions of Sec - Alkylperoxy Radicals: Evidence for Non-Cyclic Termination. *Can. J. Chem.* **1974**, *52* (8), 1377–1379. https://doi.org/10.1139/v74-209.

(203) Norman, R. O. C.; Gilbert, B. C. Electron-Spin Resonance Studies of Short-Lived Organic Radicals; 1967; pp 53–119. https://doi.org/10.1016/S0065-3160(08)60309-3.

(204) Menard, K. P.; Menard, N. R. Dynamic Mechanical Analysis in the Analysis of Polymers and Rubbers. In *Encyclopedia of Polymer Science and Technology*; Wiley, 2015; pp 1–33. https://doi.org/10.1002/0471440264.pst102.pub2.

(205) Dawes, K.; Glover, L. C.; Vroom, D. A. The Effects of Electron Beam and G-Irradiation on

Polymeric Materials. In *Physical Properties of Polymers Handbook*; Springer New York: New York, NY, 2007; pp 867–887. https://doi.org/10.1007/978-0-387-69002-5_52.

(206) Chumakov, M. K.; Shahamat, L.; Weaver, A.; LeBlanc, J.; Chaychian, M.; Silverman, J.; Benjamin Richter, K.; Weiss, D.; Al-Sheikhly, M. Electron Beam Induced Grafting of N-Isopropylacrylamide to a Poly(Ethylene-Terephthalate) Membrane for Rapid Cell Sheet Detachment. *Radiat. Phys. Chem.* **2011**, *80* (2), 182–189. https://doi.org/10.1016/j.radphyschem.2010.07.030.